

2011

## LOCAL BUCKLING IN CORRODED STEEL BRIDGE COMPRESSION MEMBERS

Andrew R. Krisciunas

Follow this and additional works at: <https://ir.lib.uwo.ca/digitizedtheses>

---

### Recommended Citation

Krisciunas, Andrew R., "LOCAL BUCKLING IN CORRODED STEEL BRIDGE COMPRESSION MEMBERS" (2011). *Digitized Theses*. 3405.  
<https://ir.lib.uwo.ca/digitizedtheses/3405>

This Thesis is brought to you for free and open access by the Digitized Special Collections at Scholarship@Western. It has been accepted for inclusion in Digitized Theses by an authorized administrator of Scholarship@Western. For more information, please contact [wlsadmin@uwo.ca](mailto:wlsadmin@uwo.ca).

**LOCAL BUCKLING IN CORRODED  
STEEL BRIDGE COMPRESSION MEMBERS**

(Thesis Format: Monograph)

by

Andrew R. Krisciunas

Graduate Program in  
Civil and Environmental Engineering

A thesis submitted in partial fulfillment  
of the requirements for the degree of  
Master of Engineering Science

The School of Graduate and Postdoctoral Studies  
The University of Western Ontario  
London, Ontario, Canada  
August 2011

© Andrew R. Krisciunas, 2011

**LOCAL BUCKLING IN CORRODED  
STEEL BRIDGE COMPRESSION MEMBERS**

(Thesis Format: Monograph)

by

Andrew R. Krisciunas

Graduate Program in  
Civil and Environmental Engineering

A thesis submitted in partial fulfillment  
of the requirements for the degree of  
Master of Engineering Science

The School of Graduate and Postdoctoral Studies  
The University of Western Ontario  
London, Ontario, Canada  
August 2011

© Andrew R. Krisciunas, 2011

THE UNIVERSITY OF WESTERN ONTARIO  
SCHOOL OF GRADUATE AND POSTDOCTORAL STUDIES

**CERTIFICATE OF EXAMINATION**

Supervisor

\_\_\_\_\_  
Dr. F.M. Bartlett

Examiners

\_\_\_\_\_  
Dr. Wenxing Zhou

\_\_\_\_\_  
Dr. Maged Youssef

\_\_\_\_\_  
Dr. Ralph Buchal

The thesis by

**Andrew R. Krisciunas**

entitled:

**Local Buckling in Corroded Steel Bridge Compression Members**

is accepted in partial fulfillment of the  
requirements for the degree of  
Master of Engineering Science

Date \_\_\_\_\_

\_\_\_\_\_  
Chair of the Thesis Examination Board



## **ABSTRACT**

Corrosion in steel bridge members is common in Northern climates and can occur uniformly in the vehicle splash zone or locally near connections. The analysis of corroded compression members in steel bridges is often uncertain due to a lack of experimentally verified theoretical knowledge of their underlying mechanics. Code criteria for analyzing compression members with section loss may be overly conservative because the effect of localized deterioration on local and Euler buckling is not well understood.

The research reported in this thesis clarifies the local buckling susceptibility of corroded steel bridge compression members. A finite element analysis model was developed to predict the critical load causing local buckling of a W-shape given a predetermined flange cross sectional loss. The finite element analysis model was validated experimentally with five full-scale column tests with idealized corrosive patterns. A robust sensitivity analysis was conducted to determine the sensitivity of the axial capacity to geometric variables that affect local buckling for a range of slenderness ratios. A simplified assessment method, based on data obtained in the sensitivity study, is presented that accounts for both localized and uniform deterioration in steel bridge compression members with corroded flanges. This method provides engineers with a means to quickly and conservatively assess the reduced capacity of such members.

**Keywords:** buckling; corrosion; design; deterioration; finite element analysis; column tests; steel.

*For my wife, Cammie.*

*Thank you for all your support, patience and encouragement.*

## **ACKNOWLEDGEMENTS**

First and foremost, I offer my sincerest gratitude to my supervisor, Dr. Mike Bartlett. His infectious optimism, perpetual energy, dedication and guidance has been instrumental in the completion of my thesis. Dr. Bartlett has been a brilliant mentor and a sincere friend.

Thank you to Wilbert Logan and Graeme Johnston for their assistance in the UWO Structures Lab and to Clayton Cook and the gentlemen at the University Machine Shop for their quality workmanship and efficiency. My thanks also to Dr. Michael Tait at McMaster University for graciously facilitating the stub columns to be tested at Applied Dynamics Laboratory.

Financial support from the Natural Sciences and Engineering Research Council (NSERC) of Canada's Discovery Grants Program is gratefully acknowledged.

A very special thank you to my wife, Cammie, who has stood by and encouraged me all these years. To my son, Jack, for being such a ball of light after long days at the office and giving me the motivation to finish my thesis and get a real job. To my father, Ray, for his encouragement and practical advice. And finally, to my mother, Judy, for always being a phone call away when things were tough.

# TABLE OF CONTENTS

	PAGE
Certificate of Examination.....	ii
Abstract and Keywords.....	iii
Dedication Page.....	iv
Acknowledgements.....	v
Table of Contents.....	vi
List of Figures.....	ix
List of Tables.....	xii
List of Appendices.....	xiii
Nomenclature.....	xiv
<b>Chapter 1: Introduction.....</b>	<b>1</b>
1.1: Introduction.....	1
1.2: Limits for Local Buckling.....	2
1.3: Literature Review.....	6
1.4: Research Objectives.....	9
1.5: Outline of Thesis.....	10
<b>Chapter 2: Finite Element Analysis Using Solidworks Simulation.....</b>	<b>16</b>
2.1: Introduction.....	16
2.2: Column Buckling and Finite Element Analysis.....	16
2.3: Solidworks Simulation.....	17
2.4: Modeling of Imperfections.....	19
2.4.1: Residual Stress.....	20
2.4.2: Out-of-Straightness.....	21
2.5: Mesh Size.....	22
2.6: Buckle Geometry.....	23
2.7: Summary of Model.....	24
2.7.1: Assumptions.....	25
2.8: Summary.....	26
<b>Chapter 3: Experimental Validation of Solidworks FEA Model.....</b>	<b>34</b>
3.1: Introduction.....	34
3.2: Specimen Descriptions.....	34
3.2.1: Initial Geometric Imperfections.....	36
3.2.2: Material Properties and Residual Stresses.....	37
3.3: Test Apparatus.....	38
3.3.1: Numerical Analysis of Column End Supports.....	39
3.3.2: Load Frame and Actuator.....	40
3.3.3: Instrumentation.....	41
3.4: Test Procedure.....	42
3.5: Test Results.....	44
3.5.1: Column 1: Control.....	45

3.5.2: Column 2 .....	45
3.5.3: Column 3 .....	46
3.5.4: Column 4 .....	47
3.5.5: Column 5 .....	47
3.5.6: Strain Gauge Readings.....	48
3.6: Comparison to FEA .....	49
3.6.1: Column 1: Control.....	50
3.6.2: Column 2 .....	51
3.6.3: Column 3 .....	52
3.6.4: Column 4 .....	53
3.6.5: Column 5 .....	53
3.7: Summary .....	54
<b>Chapter 4: Sensitivity Analysis .....</b>	<b>74</b>
4.1: Introduction.....	74
4.2: Sensitivity Analysis Results.....	75
4.2.1: Extent of Flange Section Loss.....	75
4.2.2: Symmetry of Flange Section Loss.....	80
4.2.3: Length of Deterioration .....	81
4.2.4: Distance from Corroded Region to Column Midpoint.....	82
4.2.5: Initial Out-of-Straightness .....	82
4.2.6: Cross-Section Aspect Ratio.....	83
4.2.7: Ratio of Flange Area to Web Area .....	84
4.3: Summary .....	86
<b>Chapter 5: Simplified Assessment of Corroded Steel Compression Members.....</b>	<b>104</b>
5.1: Introduction.....	104
5.2: Simplified Assessment Method .....	105
5.2.1: Identification of Key Parameters.....	105
5.2.2: Proposed Method.....	106
5.2.3: Design Charts .....	107
5.2.4: Assessment Procedure .....	108
5.2.5: Example Calculations.....	109
5.3: CAN/CSA S16-09 Procedure for Evaluating Columns with Class 4 Flanges.....	112
5.4: Comparison with Finite Element Analysis Results .....	114
5.4.1: Realistic Maximum Flange Section Loss in Bridge Compression Members .....	115
5.4.2: Comparison of Columns Sensitive to Corrosion .....	116
5.5: Summary .....	118
<b>Chapter 6: Summary, Conclusions, and Recommendations for Future Work....</b>	<b>128</b>
6.1: Summary .....	128
6.2: Conclusions .....	130
6.3: Recommendations for Future Work.....	132

<b>References .....</b>	<b>134</b>
<b>Appendices.....</b>	<b>136</b>
<b>Curriculum Vitae.....</b>	<b>162</b>

## LIST OF FIGURES

	PAGE
<b>Figure 1-1:</b> Typical Corrosion Locations in Steel Through-Truss .....	12
<b>Figure 1-2:</b> Corrosion in Salt Spray Zone of East Brough's Bridge (London, ON) ...	12
<b>Figure 1-3:</b> Width-to-Thickness Ratios in Corroded W-Shapes.....	13
<b>Figure 1-4:</b> Typical Differences in CAN/CSA S16-09 Provisions.....	13
<b>Figure 1-5:</b> Steps Given in NCHRP 333 to Assess Local Buckling in Corroded Steel Compression Members .....	14
<b>Figure 2-1:</b> Inadequacy of Built-in Fixities .....	28
<b>Figure 2-2:</b> Column Rocker Assembly .....	28
<b>Figure 2-3:</b> Residual Stress in Cross Section.....	29
<b>Figure 2-4:</b> Thermal Analysis Used to Develop Residual Stresses .....	29
<b>Figure 2-5:</b> Residual Stress Distribution due to Thermal Loading .....	30
<b>Figure 2-6:</b> Mesh Control in Deteriorated Region.....	30
<b>Figure 2-7:</b> Second-Order Tetrahedral Element Used Throughout FEA.....	31
<b>Figure 2-8:</b> Local Buckle from a 4-Point Bending Test .....	31
<b>Figure 2-9:</b> Local Buckle from a W150x30 Column with Localized Deterioration at Mid-Height .....	32
<b>Figure 2-10:</b> Time Depending Loading Scheme .....	32
<b>Figure 2-11:</b> Solidworks FEA Results Compared with CSA S6-06 (CSA 2006) for a W150x30 Column .....	33
<b>Figure 3-1:</b> FEA Predicted Local Buckle Shapes .....	56
<b>Figure 3-2:</b> Determination of Camber and Sweep .....	56
<b>Figure 3-3:</b> Column End Support Assembly.....	57
<b>Figure 3-4:</b> FEA of Column End Supports Prior to Fabrication.....	58
<b>Figure 3-5:</b> Load Frame General Arrangement .....	59
<b>Figure 3-6:</b> Lateral Deformations Observed in Load Frame .....	59
<b>Figure 3-7:</b> Implementation of Load Frame Bracing.....	60
<b>Figure 3-8:</b> Displacement Transducer Locations.....	61
<b>Figure 3-9:</b> Strain Gauge Locations for Column 2 .....	61
<b>Figure 3-10:</b> Strain Gauge Locations for Column 3 .....	62
<b>Figure 3-11:</b> Strain Gauge Locations for Columns 4 and 5 .....	62
<b>Figure 3-12:</b> Actuator Loading Rate Used during Column Tests.....	63
<b>Figure 3-13:</b> Comparison of Overall Column Buckling Deformation for Column Tests 1, 2, 3 and 5.....	63
<b>Figure 3-14:</b> Comparison of Weak Axis Midheight Deformation Predicted by FEA to Test Data (Column 1).....	64
<b>Figure 3-15:</b> Yielding in Flange of Column 1 .....	64
<b>Figure 3-16:</b> Plastic Hinge at Midheight (Column 2).....	65
<b>Figure 3-17:</b> Web Displacement in Direction of Weak Axis Buckling Over Time of Test Column 2.....	65

<b>Figure 3-18:</b>	Failure Progression in Column 3 .....	66
<b>Figure 3-19:</b>	Comparison of Curvature Predicted by FEA to Test Data (Column 3) .....	67
<b>Figure 3-20:</b>	Comparison of Weak Axis Midheight Deformation Predicted by FEA to Test Data (Column 5).....	67
<b>Figure 3-21:</b>	Strain Gauge Locations on Column 2 Relative to Failed Shape.....	68
<b>Figure 3-22:</b>	Strain Gauge Data for Column 2 (Left Flange) .....	68
<b>Figure 3-23:</b>	Strain Gauge Data for Column 2 (Right Flange).....	69
<b>Figure 3-24:</b>	Comparison of Weak Axis Midheight Deformation Predicted by FEA to Test Data (Column 2).....	69
<b>Figure 3-25:</b>	Comparison of Weak Axis Midheight Deformation Predicted by FEA to Test Data (Column 3).....	70
<b>Figure 4-1:</b>	Variables in Sensitivity Analysis.....	89
<b>Figure 4-2:</b>	Sensitivity of Axial Capacity to Flange Loss (W150x30, Symmetric Deterioration, $L^*=200\text{mm}$ , $y^*=0\text{mm}$ , $L$ , $\delta=L/1000$ ) .....	90
<b>Figure 4-3:</b>	Percent Difference between Axial Capacity Determined Using FEA ( $P_{FEA}$ ) and the Theoretical Crushing Capacity ( $C_y$ ) for Stocky Columns with Varying Flange Loss .....	91
<b>Figure 4-4:</b>	Ratio of the Maximum Displacement of the Local Buckle ( $\delta_{max}$ ) to the Thickness of the Reduced Flange ( $t^*$ ) for Varying Flange Loss .....	91
<b>Figure 4-5:</b>	Method for Determining $\delta_{max}$ .....	92
<b>Figure 4-6:</b>	Sensitivity of Axial Capacity to Symmetric and Non-Symmetric Flange Deterioration (W150x30, $t^*/t_o=0.5$ , $L^*=200\text{ mm}$ , $y^*=0$ , $\delta=L/1000$ ) .....	92
<b>Figure 4-7:</b>	Torsional Rotation Caused by Non-Symmetric Corrosion.....	93
<b>Figure 4-8:</b>	Sensitivity of Axial Capacity to $L^*$ (W150x30, Symmetric Deterioration, $t^*/t_o=0.5$ , $y^*=0L$ , $\delta=L/1000$ ).....	93
<b>Figure 4-9:</b>	Sensitivity of Axial Capacity to $y^*$ (W150x30, Symmetric Deterioration, $t^*/t_o=0.5$ , $L^*=200\text{ mm}$ , $\delta=L/1000$ ).....	94
<b>Figure 4-10:</b>	Sensitivity of Axial Capacity to $\delta$ (W150x30, Symmetric Deterioration, $t^*/t_o=0.5$ , $L^*=200\text{ mm}$ , $y^*=0L$ ) .....	94
<b>Figure 4-11:</b>	Cross-sectional Properties Used in Aspect Ratio Sensitivity Analysis ...	95
<b>Figure 4-12:</b>	Sensitivity of Axial Capacity to Aspect Ratio of the Column Cross Section (Symmetric Deterioration, $t^*/t_o=0.5$ , $L^*=200\text{ mm}$ , $y^*=0L$ , $\delta=L/1000$ ) .....	95
<b>Figure 4-13:</b>	Ratio of Flange to Web Area for W-Shape Columns Prone to Local Buckling.....	96
<b>Figure 4-14:</b>	Sensitivity of the Axial Capacity of Stocky Columns to $A_f/A_w$ (W150x30, Symmetric Deterioration, $L^*=200\text{ mm}$ , $y^*=0L$ , $kL/r=15$ ).....	96
<b>Figure 4-15:</b>	Sensitivity of the Axial Capacity of Slender Columns to $A_f/A_w$ (W150x30, Symmetric Deterioration, $L^*=200\text{ mm}$ , $y^*=0L$ , $kL/r=159$ ).....	97
<b>Figure 5-1:</b>	Deterioration Factor for Flange Loss ( $t^*$ ).....	120



<b>Figure 5-2:</b>	Deterioration Factor for Length of Deterioration ( $L^*$ ) Relative to Benchmark Case ( $t^*/t_o=0.5, L^*/b=1.3$ ) .....	120
<b>Figure 5-3:</b>	Design Chart for Determining $t^*$ Deterioration Factor, $\Psi$ .....	121
<b>Figure 5-4:</b>	Design Chart for Determining $L^*$ Deterioration Factor, $\Omega$ .....	122
<b>Figure 5-5:</b>	Deteriorated Columns for Example Calculations .....	123
<b>Figure 5-6:</b>	Comparison of Methods in CAN/CSA S16-09 (W150x30, $t^*/t_o=0.5$ , Symmetric Deterioration) .....	124
<b>Figure 5-7:</b>	Conservatism of CAN/CSA S16-09 with Respect to FEA (W150x30, $L^*=200$ mm, Symmetric Deterioration).....	124

## LIST OF TABLES

	PAGE
<b>Table 1-1:</b> Likely Consequences of Corrosion Type and Location in Bridge W-Shape Compression Members .....	15
<b>Table 3-1:</b> Summary of Test Specimen Geometry and Flange Deterioration (dimensions in mm) .....	71
<b>Table 3-2:</b> Summary of Test Data .....	72
<b>Table 3-3:</b> Material Data from Tensile Coupon and Stub Column Tests.....	72
<b>Table 3-4:</b> Comparison of Local Buckle Geometry Observed in Failed Test Specimens and Predicted by FEA.....	73
<b>Table 4-1:</b> Parameter Matrix .....	98
<b>Table 4-2:</b> Flange Section Loss as a Function of Yield Strength.....	99
<b>Table 4-3:</b> Variation of Failure Mode with Slenderness Ratio.....	100
<b>Table 4-4:</b> Deformed Shapes of Slender Columns ( $kL/r=159$ ) with Varying $t^*/t_o$ after Failure .....	101
<b>Table 4-5:</b> Development of Failure Mode for Intermediate Columns ( $kL/r=80.5$ , $t^*/t_o=0.25$ ) .....	102
<b>Table 4-6:</b> Summary of Sensitivity Variables to Include in Analysis.....	103
<b>Table 5-1:</b> W-Shape Columns Subject to Local Flange Buckling given 25% Flange Thickness Loss.....	125
<b>Table 5-2:</b> Analysis of Columns Sensitive to Corrosion (Realistic Cases).....	126
<b>Table 5-3:</b> Analysis of Columns Sensitive to Corrosion (Extreme Cases) .....	127

## LIST OF APPENDICES

	PAGE
<b>Appendix A1: Steel Properties of Test Columns.....</b>	<b>136</b>
<b>A1.1:</b> Introduction.....	137
<b>A1.2:</b> Tensile Coupon Data.....	137
<b>A1.3:</b> Stub Column Test Data.....	138
<b>Figure A1-1:</b> Tensile Coupon Test A for Columns 1 and 4 .....	140
<b>Figure A1-2:</b> Tensile Coupon Test B for Columns 1 and 4.....	140
<b>Figure A1-3:</b> Tensile Coupon Test C for Column 5 .....	141
<b>Figure A1-4:</b> Stub Column Test A for Columns 1 and 4.....	141
<b>Figure A1-5:</b> Stub Column Test B for Columns 2 and 3.....	142
<b>Figure A1-6:</b> Stub Column Test C for Columns 5.....	142
<b>Appendix A2: Drawing Set of Column End Supports.....</b>	<b>143</b>
<b>Appendix A3: Equations for Design Charts.....</b>	<b>149</b>
<b>A3.1:</b> Introduction.....	150
<b>Table A3-1:</b> Design Curve Equations for $\Psi$ .....	151
<b>Table A3-1:</b> Design Curve Equations for $\Omega$ .....	152
<b>Appendix A3: Derivation of the Critical Length .....</b>	<b>153</b>
<b>A4.1:</b> Introduction.....	154
<b>A4.2:</b> Cross Sectional Properties .....	155
<b>A4.3:</b> Weak-Axis Critical Length.....	156
<b>A4.4:</b> Strong-Axis Critical Length.....	158
<b>Figure A4-1:</b> Idealized Cross-Sectional Dimensions for a W-Shape .....	161

## NOMENCLATURE

$A$	gross-cross sectional area
$A_d$	area of the reduced cross section
$A_f$	cross-sectional area of flange
$A_w$	cross-sectional area of web
$b$	flange width
$b^*$	width of deteriorated flange
$b_{eq}$	reduced equivalent Class 3 flange width
$C_{FEA}$	nominal compressive capacity calculated using finite element analysis
$C_d$	reduced nominal compressive capacity of the deteriorated column
$C_{S6}$	nominal compressive capacity calculated using CAN/CSA S6-06
$C_{S16}$	nominal compressive capacity of the deteriorated Class 4 cross section using the methods given in CAN/CSA S16-09
$C_o$	nominal compressive capacity of the undeteriorated column
$C_y$	yield capacity of the reduced cross section
$d$	overall depth of wide-flange section
$E$	modulus of elasticity (200 000 MPa for structural steel)
$F_y$	specified minimum yield strength
$(F_y)_{eq}$	reduced equivalent Class 3 yield strength
$h$	web height
$I$	second moment of area
$k$	effective length factor
$L$	column length
$L_c$	critical length
$L^*$	length of deterioration
$n$	parameter for compressive resistance (n=1.34 for hot-rolled W-shapes)
$P$	professional factor
$P_{cr}$	critical Euler buckling load
$P_{FEA}$	failure load predicted by finite element analysis
$P_t$	failure load from experimental testing
$P_u$	ultimate applied load
$R$	radius of curvature
$r$	radius of gyration
$t$	flange thickness
$t_c$	time required to achieve the maximum compressive load
$t_o$	thickness of undeteriorated flange
$t^*$	thickness of deteriorated flange
$w$	web thickness
$w^*$	thickness of deteriorated web
$x$	horizontal offset
$y^*$	distance of the corroded region from the column midpoint

### **Greek Symbols**

$\alpha_l$	coefficient of thermal expansion ( $12 \times 10^{-6} / ^\circ\text{C}$ for structural steel)
$\Delta$	deflection
$\Delta T$	temperature differential
$\delta$	initial out-of-straightness in the direction of weak-axis buckling
$\delta_c$	camber
$\delta_{max}$	maximum local buckling displacement at failure perpendicular to the flange
$\delta_s$	sweep
$\varepsilon$	strain
$\lambda$	slenderness parameter
$\sigma_{cr}$	critical local buckling stress
$\sigma_r$	maximum magnitude of residual stress
$\Psi$	capacity reduction factor accounting for the thickness of deterioration
$\psi$	curvature
$\Omega$	capacity reduction factor accounting for the length of deterioration

## **CHAPTER 1: INTRODUCTION**

### **1.1 INTRODUCTION**

A large number of bridges in Canada and the United States are nearing the end of their service lives and are in need of rehabilitation or replacement. In steel bridges, corrosion can lead to cross-sectional losses and reduced live-load capacity. Aging steel truss bridges in northern climates are particularly prone to corrosion because they are typically exposed to chlorides in the form of deicing media (Kayser and Nowak 1989). Figure 1-1 shows the likely locations where section loss due to corrosion may occur in a typical steel through truss. Corrosion often occurs uniformly within the splash zone and locally (in the form of pitting) at gusset plates, hand rails, or where the concrete deck is cast against web members (Kulicki et al. 1990). Such corrosion resulting from vehicular spray is clearly visible across a 3m high region of the interior truss members of the East Brough's Bridge in London, as shown in Figure 1-2 (Jelinek 2002), that was replaced in 2000. The research presented in this thesis concentrates on assessing the axial capacity of corroded compression members in steel truss bridges, specifically, those fabricated using W-shapes.

The analysis of corroded compression members in steel bridges is often uncertain due to a lack of experimentally verified knowledge of their underlying mechanics. In bending and tension members, local yielding results in a redistribution of stresses and is associated with plastic deformations that provide warning of an impending structural

failure. In compression members, corrosion may reduce axial capacity of W-shape columns in the following three ways:

1. For stocky members, a loss in cross-sectional area can lead to premature yielding.
2. For intermediate and slender members, deterioration can lead to a reduced second moment of area which may initiate a premature instability failure.
3. For all column lengths, deterioration that increases the width-to-thickness ratio of the flange or web elements may lead to local buckling.

Case 1 is readily calculated theoretically by computing the axial capacity using the reduced cross-sectional area,  $A_d$ . Case 2 has been studied by others (e.g., Jelinek 2002) and theoretical models have also been developed to assess the capacity of columns with second moments of area that vary over the length of the member (e.g., Timoshenko and Gere 1961). Case 3, however, has not been investigated in detail by previous researchers and the effect of localized deterioration on local buckling needs to be investigated further.

## **1.2 LIMITS FOR LOCAL BUCKLING**

Corrosion can initiate local buckling by reducing the flange or web thickness, or by the build-up of pack rust between elements that bulge locally and so induce out-of-plane eccentricities. The research herein will focus on cross-sectional area losses causing local buckling. As shown in Figure 1-3, corrosion typically reduces the thickness of a flange from  $t$  to  $t^*$  or the thickness of a web from  $w$  to  $w^*$ . As the flange width is not significantly reduced, i.e.,  $b^* \approx b$ , the width-to-thickness ratio of the corroded flange,  $b^*/t^*$ , can be markedly greater than that of the uncorroded flange,  $b/t$ . Similarly, for the web,  $h/w^*$  can be markedly greater than the original  $h/w$ .

The flanges of W-shape compression members are prone to local buckling when the flange width-to-thickness ratio exceeds the limit (Kulak 2006):

$$[1.1] \quad \frac{b}{2t} = \frac{277}{\sqrt{\sigma_{cr}}}$$

where:  $b$  = flange width [mm]

$t$  = flange thickness [mm]

$\sigma_{cr}$  = critical local buckling stress [MPa]

The factor of 1/2 on the left side of Eq. [1.1] is necessary because in this thesis, local buckling is described in terms of the full flange width  $b$  whereas in CAN/CSA S16-09 (CSA 2009) and other standards, it is described in terms of the half-flange width. To account for the adverse effects of residual stresses and out-of-straightness, the design provisions of the Canadian Highway Bridge Design Code (CHBDC) (CSA 2006) and CSA S16-09 (CSA 2009) require that, if the flange is required to resist the specified minimum yield strength  $F_y$ , in MPa:

$$[1.2] \quad \frac{b}{2t} \leq \frac{200}{\sqrt{F_y}}$$

The CHBDC commentary (CSA 2006a) to Clause C14.14.3 states that deterioration in compression members can reduce the net cross-sectional area, reduce the second moment of area, and cause distortion that may cause local buckling. It emphasizes the need to quantify the extent and distribution of corrosion along the length of a member accurately in the field. While the CHBDC effectively limits width-to-thickness ratios in the design



of new bridge compression members to prevent local buckling, it provides little guidance for evaluating the capacity of existing corroded compression members with flanges that may not satisfy Eq. [1.2]. Despite this shortcoming, Clause 10.6.2 of the CHBDC still requires that: "...deterioration mechanisms considered for steel components shall include corrosion."

CSA Standard S16-09 "Limit States Design of Steel Structures" (CSA 2009), however, gives some general guidance for the analysis of compression members with flanges that do not satisfy Eq. [1.2] and so are Class 4 cross sections. Clause 13.3.5 states that the capacity of a Class 4 section in compression shall be calculated using reduced values of either  $F_y$  or  $b$  such that the Class 3 limits are met. Thus the capacity of the member can be computed based on a reduced yield strength,  $(F_y)_{eq}$ :

$$[1.3] \quad (F_y)_{eq} = \left( \frac{400}{b/t} \right)^2$$

or based on cross-section properties computed using a reduced flange width,  $b_{eq}$ :

$$[1.4] \quad b_{eq} = \frac{400t}{\sqrt{F_y}}$$

As shown in Figure 1-4, the compressive resistances determined using these two methods are rarely equivalent. The figure shows, for a Grade 350W W610x153 with 65% section loss on both flanges causing  $t^*=0.35t$ , the variation of the nominal compressive resistance of the corroded section,  $C_{S16}$ , expressed as a fraction of the nominal compressive resistance of the original uncorroded section,  $C_o$ , with the slenderness ratio  $kL/r$ . The

reduced flange width method, Eq. [1.4], makes the shape more susceptible to weak-axis buckling at long unsupported lengths and so markedly reduces the capacity at high slenderness ratios. The reduced yield strength method, Eq. [1.3], is more severe for low slenderness ratios but gives a greater capacity at higher slenderness ratios,  $kL/r \gtrsim 70$ , where the member capacity is more dominated by buckling. Both methods conservatively assume that the reduced material thickness is present over the entire length of the column, whereas in practice corrosion is usually localized in relatively short regions along the member. Typically, in practice the evaluator will compute capacities using both methods and adopt the larger of the two for subsequent assessment, however, the conservatism inherent in both methods may lead to unrealistic predictions.

To prevent local buckling of the webs of W-shape compression members, the CHBDC (CSA 2006) limits the height to width ratio:

$$[1.5] \quad \frac{h}{w} \leq \frac{670}{\sqrt{F_y}}$$

where:  $h$  = web height [mm]

$w$  = web width [mm]

Most available W-shapes meet this requirement, however, web corrosion may also cause this limit to be exceeded. In steel bridge truss members, typically flanges are more prone to corrosion because they are more exposed to airborne spray and are susceptible to crevice corrosion due to their direct contact with gusset plates. Therefore, any effect of web deterioration will be outside the scope of this research study.

Table 1-1 presents the likely structural consequences for corrosion at different locations in bridge compression members, previously identified in Figure 1-1. Local buckling may develop at any of these locations provided the deterioration is severe enough. It is logical that compression members would be more susceptible to local buckling if the deterioration is located near the midheight because bending stresses due to initial out-of-straightness and subsequent second-order response are typically higher in this region, so the distance of the deterioration from the column midpoint should be investigated further.

### **1.3 LITERATURE REVIEW**

Previous research has demonstrated that even non-corroded compression members in older steel bridges may be deficient by modern codes, particularly if their slenderness ratio exceeds 70 (Shek 2006). During a full-scale destructive bridge test to validate in-plane buckling prediction methods, Bakht witnessed premature local buckling of a steel compression chord that resulted in a significantly reduced structural capacity (Bakht et al. 1996). These studies demonstrate the need for a greater knowledge of the effects corrosion can have on the local stability of steel bridge compression members.

The effect of corrosion on the behavior of steel bridge members is currently an inactive subfield in structural engineering. The most significant contribution is the National Cooperative Highway Research Program (NCHRP) Report 333 (Kulicki et al. 1990), a comprehensive guideline intended to be a practical reference for design engineers and bridge inspectors. Detailed inspection guidelines and evaluation procedures are presented to help the engineer predict capacity and failure modes of corroded bridge members.

Figure 1-5 summarizes the guidance given in NCHRP 333, concerning local buckling initiated by corrosion of steel compression members. The report addresses all forms of bridge corrosion and thus is extremely useful for general diagnostic problems. However, its provisions concerning local buckling in truss compression members are insufficient. Specifically, accurate guidelines to account for localized deterioration where the primary failure mode is local buckling are not given. A method is proposed to account for varying column slenderness, but it may be overly simplistic and can only be used to determine the global column buckling load. The provisions of Appendix C of the 1978 AISC specifications (AISC 1978) are recommended to account for premature local buckling but, like the similar provisions in CAN/CSA S16-09, the results are conservative because uniform section loss over the entire length of the column is assumed. Finally, these procedures do not account for the complex interaction between local and global buckling. Several subsequent papers [e.g. (Prucz and Kulicki 1998), (Van De Lindt and Pei 2006)] cite NCHRP 333 as a key reference, but the methodology it recommends does little to address local buckling instability.

More recently, a study in Japan investigated the effects of pitting corrosion on the local stability of structural bending members in marine bulk carriers (Nakai et al. 2004). The study yielded somewhat inconclusive results, though a general trend of reduced capacity with increased corrosion was established. As the nature of pitting corrosion in such environments is generally quite uniform compared to bridges, the effects of more localized deterioration on local buckling was not investigated.

Research investigating the general capacity loss of corroded steel bridge girders found that buckling of the web in bearing was the critical mode of failure (Kayser and Nowak

1989). The study concluded that the addition of bearing stiffeners significantly increases the capacity of deteriorated steel girder webs and therefore results in a “more corrosion-tolerant structure”. A similar study that focused on the web crippling capacity of corroded steel girder ends in Michigan has suggested that assumptions made by engineers are often overly conservative and can lead to the premature load posting, rehabilitation or closure of a bridge (van de Lindt and Ahlborn 2005). It was shown that design equations provided by the state transportation department assumed that web loss occurred over the entire web height and so ignored much of the uncorroded web steel. While these two studies are superficially related to the present study, they consider only girder webs subjected to local bearing loads and the resulting equations, recommendations, and design aids are not applicable to corroding steel bridge compression members. Van de Lindt and Ahlborn (2005) do effectively demonstrate how the results of their complex finite-element analysis can be presented in simple design chart form for use by practitioners.

The lack of literature addressing the effect of deterioration on local buckling highlights the need for a greater understanding of this phenomenon. There is a need to define, and recognize the structural impact of common corrosion geometry and patterns in bridge truss members. A clear relationship between corrosion intensity and the local buckling resistance of steel compression members must be quantified and the findings must be presented in a simplified form, so bridge evaluators can rapidly and accurately assess the likelihood of a brittle structural failure of steel W-shape compression members with corroded flanges due to local buckling.

## 1.4 RESEARCH OBJECTIVES

This objective of the research reported in this thesis is to clarify the local buckling susceptibility of corroded flanges in steel W-shape bridge compression members. Both uniform and localized pitting corrosion patterns will be considered as they commonly occur in practice. Due to the high variability of corrosion patterns, intensity, and location, a realistically bounded sensitivity analysis will be conducted to identify the corrosion geometry most critical to local buckling.

The specific objectives of this research are as follows:

1. Develop a 3-D finite element analysis (FEA) model that can accurately predict the reduced axial capacity of deteriorated columns that are prone to local buckling.
2. Validate the model experimentally through full-scale laboratory tests of W-shapes in axial compression with simulated corrosion.
3. Conduct a robust sensitivity analysis to determine the variables that are most critical to local buckling instability.
4. Examine the accuracy of the current method for evaluating steel compression members with Class 4 flanges, as given in CAN/CSA S16-09 (CSA 2009).
5. Produce a simplified assessment method that can provide a quick and accurate technique for conservatively estimating the remaining capacity of steel bridge compression members with flange deterioration.

## 1.5 OUTLINE OF THESIS

Chapter 2 presents the finite element modeling techniques that were developed to analyze deteriorated steel compression members using Solidworks Simulation (Dassault Systèmes 2010). It is demonstrated that typical column imperfections, including residual stress and initial out-of-straightness, can be readily and realistically simulated using thermal loads. The analysis of undeteriorated columns is then calibrated using the conventional empirical equations given in the CHBDC (CSA 2006). Practical challenges with idealizing flange corrosion in the finite element analysis model, such as mesh sizes and time-dependent loading schemes, are presented.

Chapter 3 summarizes the testing of five full-scale columns at the Structures Laboratory at The University of Western Ontario in 2011. The testing program was undertaken to validate the finite element analysis model presented in Chapter 2. The selection of test specimens and the design of the test apparatus are described in detail, the test procedure is outlined, and results are presented. The test results are then compared to FEA predictions and conclusions regarding the adequacy of the model are given.

Chapter 4 presents an in-depth sensitivity analysis that was conducted using the finite element model validated in Chapter 3. The objective of the analysis presented in this chapter is to rank, by order of importance, dimensional variables that affect local buckling in column flanges with localized deterioration. Each variable is examined over the range of slenderness ratios permitted for bridge compression members by CAN/CSA S6-06 (CSA 2006). Recommendations concerning critical variables that should be

considered in the any simplified assessment method to assess the compressive resistance of such columns are proposed.

Chapter 5 presents a simplified method that can be used to quickly and accurately assess the capacity of steel W-shape compression members with corroded flanges. Two design charts are given which allow the evaluator to determine rapidly strength loss factors that account for the increased width-to-thickness ratio of the deteriorated flange and the length of deterioration. The accuracy of current methods in S16-09 (CSA 2009) analyzing compression members with Class 4 flanges is examined and compared to that of the proposed simplified method.

Chapter 6 summarizes the research program and presents the conclusions of this research. Recommendations for future work are also presented.



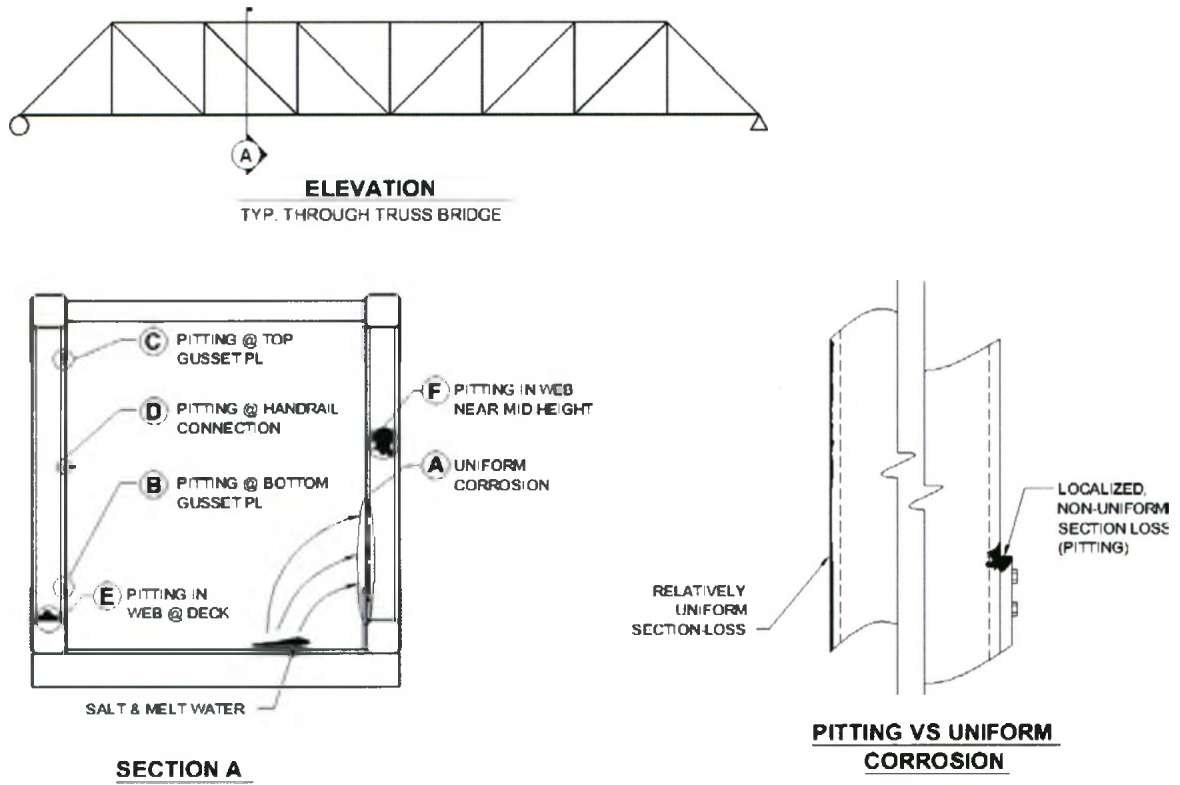


Figure 1-1: Typical Corrosion Locations in Steel Through-Truss



Figure 1-2: Corrosion in Salt Spray Zone of East Brough's Bridge (London, ON) (Jelinek 2002)

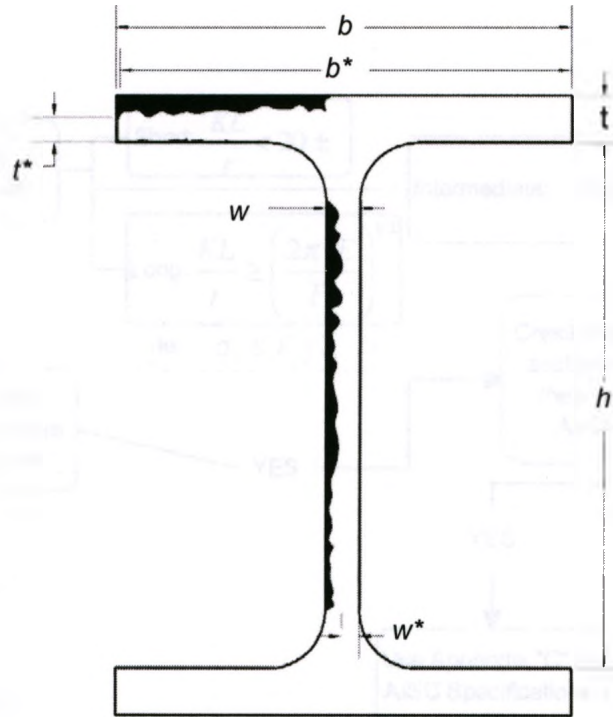


Figure 1-3 : Width-to-Thickness Ratios in Corroded W-Shapes

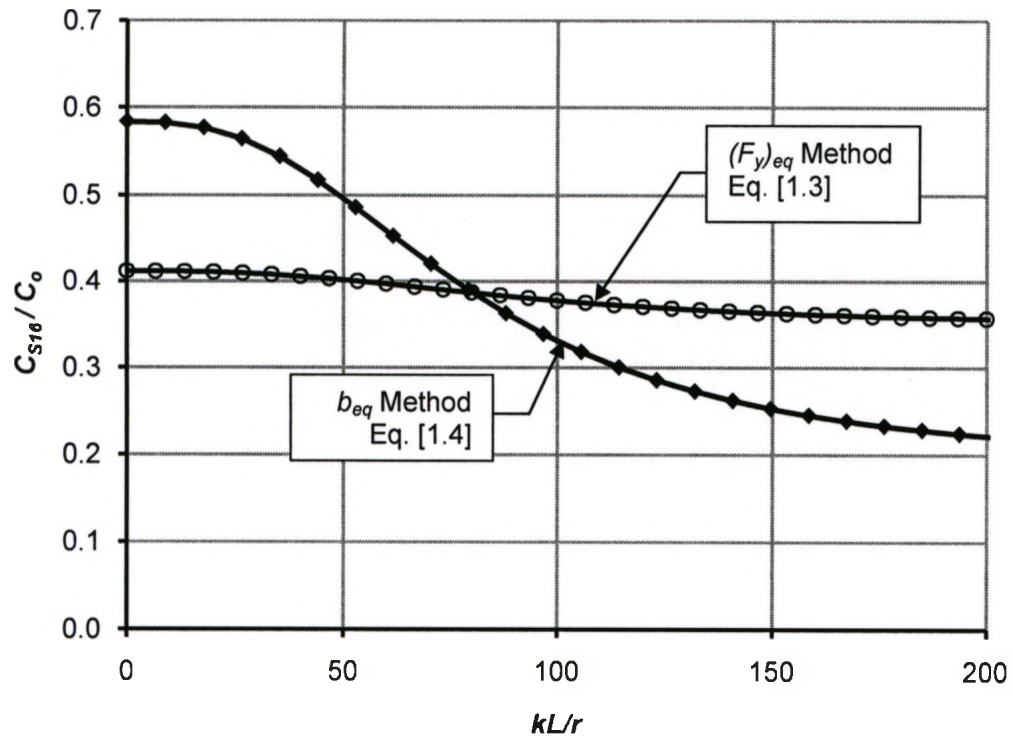


Figure 1-4: Typical Differences in CAN/CSA S16-09 Provisions

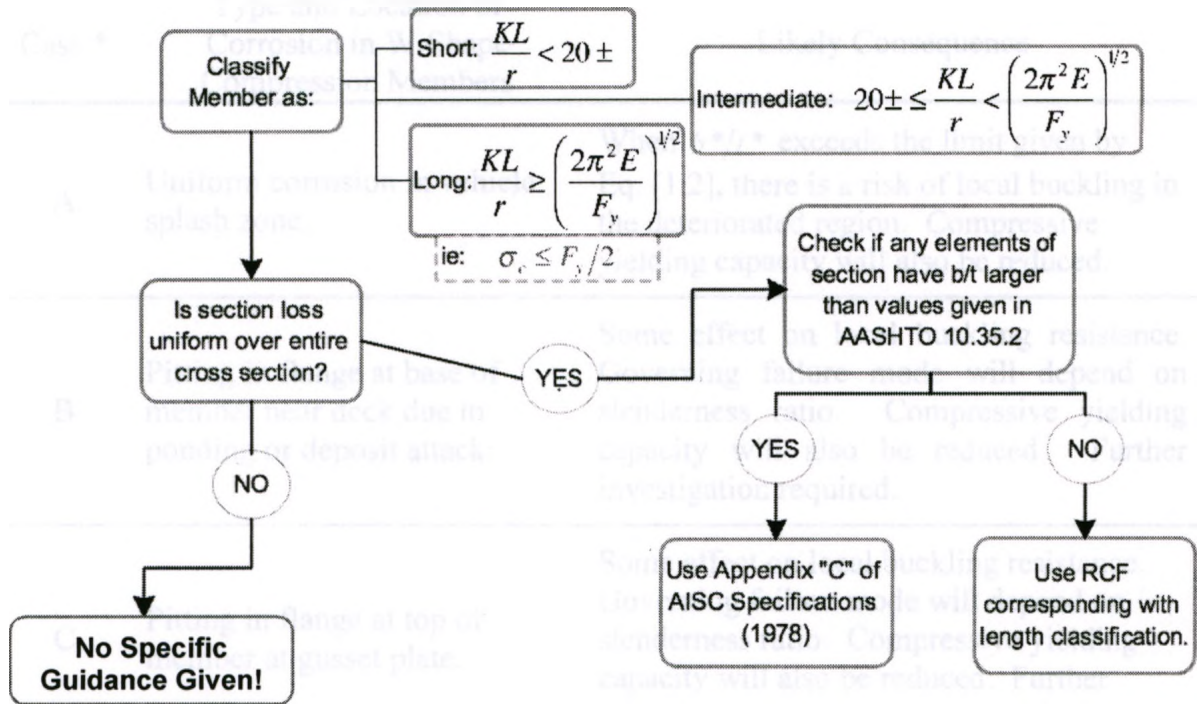


Figure 1-5: Steps Given in NCHRP 333 to Assess Local Buckling in Corroded Steel Compression Members

Table 1-1: Likely Consequences of Corrosion Type and Location in Bridge W-Shape Compression Members

Case *	Type and Location of Corrosion in W-Shape Compression Members	Likely Consequence
A	Uniform corrosion in vehicle splash zone.	When $b^*/t^*$ exceeds the limit given by Eq. [1.2], there is a risk of local buckling in the deteriorated region. Compressive yielding capacity will also be reduced.
B	Pitting in flange at base of member near deck due to ponding or deposit attack.	Some effect on local buckling resistance. Governing failure mode will depend on slenderness ratio. Compressive yielding capacity will also be reduced. Further investigation required.
C	Pitting in flange at top of member at gusset plate.	Some effect on local buckling resistance. Governing failure mode will depend on slenderness ratio. Compressive yielding capacity will also be reduced. Further investigation required.
D	Localized uniform corrosion, pitting or holes in flange in the middle of the member at handrail or bracing connections.	Localized deterioration may attract local buckle and change governing failure mode provided the limit given by Eq. [1.2] is exceeded. Compressive yielding capacity will also be reduced. Complex interaction between global buckling, yielding, and local buckling requires further investigation.
E	Localized corrosion of web near deck.	Localized deterioration may attract local buckle and change governing failure mode provided the limit given by Eq. [1.5] is exceeded. Compressive yielding capacity will also be reduced.
F	Localized corrosion of web in the middle of the member due to ponding or debris buildup.	Localized deterioration may attract local buckle and change governing failure mode provided the limit given by Eq. [1.5] is exceeded. Compressive yielding capacity will also be reduced.

\* See Figure 1-3



## **CHAPTER 2:FINITE ELEMENT ANALYSIS**

### **USING SOLIDWORKS SIMULATION**

#### **2.1 INTRODUCTION**

This chapter presents justification for using Solidworks Simulation Finite Element Analysis (FEA) to investigate the research objectives set out in Chapter 1. Section 2.2 outlines the benefits of a FEA study in the previously defined research scope. Section 2.3 discusses the modeling capabilities of Solidworks Simulation and validates its use for basic buckling problems. Section 2.4 discusses the incorporation of imperfections inherent in rolled structural steel shapes into the model, and investigates the adequacy of the program to predict intermediate column buckling accurately. Finally, meshing parameters are discussed in Section 2.5 and the buckle geometry is examined at a preliminary level in Section 2.6.

#### **2.2 COLUMN BUCKLING AND FINITE ELEMENT ANALYSIS**

The interaction between localized deterioration, local buckling, and Euler buckling is complex and therefore not easily investigated by manual calculations. To fully understand and accurately predict the effect of localized deterioration on local buckling instability using physical experimentation, a large number of column tests would be required. Using FEA, a large number of tests can be simulated rapidly and validated using a few select physical tests. Furthermore, the investigation is not limited by experimental constraints such as actuator capacity restrictions as FEA can be easily

applied to large cross sections. Finally, input variables including material strength, stress-strain relationships, initial column imperfections, location and intensity of deterioration, end-fixity, and column dimensions can be easily and accurately controlled throughout the course of a FEA-based sensitivity analysis.

### **2.3 SOLIDWORKS SIMULATION**

Solidworks, a solid modeling design suite used primarily for mechanical engineering applications, has been integrated with a robust finite element analysis engine: Solidworks Simulation (Dassault Systèmes 2010). The software is written and distributed by Dassault Systèmes Simulia Corp. This company also developed Abaqus, which is widely used by structural engineering researchers. Additionally, Solidworks includes a full-featured Computer Aided Design (CAD) package that allows for quick and intuitive model manipulation without having to resort to cumbersome programming languages.

Solidworks was originally adopted in the present investigation as a drawing tool but, because steel columns are readily idealized, it was decided to investigate Solidworks as an analysis tool. Other more robust FEA software packages (such as Ansys) were considered, but the additional cost and added complexity could not be justified. Before fully committing to Solidworks as the primary research analysis package, however, preliminary validation was conducted to ensure that the software could accurately analyze steel columns with intermediate slenderness ratios that fail by inelastic buckling.

The first step was to ensure Solidworks could accurately model simple Euler buckling. This required the development of purely pinned end conditions that provide no resistance to rotation (i.e., and so idealize a column with an effective length factor,  $k$ , of 1.0). The

use of fixities built into the program was not satisfactory. As shown in Figure 2-1, Solidworks applies deformation constraints over the entire element face, Fig. 2-1a, causing unintended fixity at the bottom of the column when it was restrained in the  $x$ ,  $y$  and  $z$  directions, Fig. 2-1b. To solve this problem, the rocker assembly shown in Fig. 2-2a was created for the analysis to allow free rotation at the lower end of the column. Once fixity was relieved at both ends, Fig. 2-2b, the model accurately predicted the Euler buckling loads computed using the familiar equation (e.g. Timoshenko and Gere 1961):

$$[2.1] \quad P_{cr} = \frac{\pi^2 EI}{(kL)^2}$$

where:  $P_{cr}$  = critical Euler buckling load [N]

$E$  = Young's modulus (200 000 MPa for structural steel)

$I$  = second moment of area about the weak axis [ $mm^4$ ]

$k$  = effective length factor (1.0 for pin/pin)

$L$  = column length [ $mm$ ]

For a W150x30 column of Grade 350W steel with  $I = 5.56 \times 10^6 \text{ mm}^4$  about the weak axis and  $L = 7000 \text{ mm}$ , the buckling load predicted by Solidworks of 210.2 kN was within 6.2% of the theoretical value obtained using Eq. [2.1]. To ensure buckling would occur, a small out-of-straightness was created using a lateral load of 0.5 kN distributed evenly over the web. If the out-of-straightness is induced by thermal gradients the Solidworks prediction would more closely approximate the Euler Buckling load.

## 2.4 MODELING OF IMPERFECTIONS

Current steel column design criteria are not limited to Euler buckling but must also address inelastic buckling of intermediate columns initiated by imperfections. CAN/CSA S6-06 (CSA 2006) computes this nominal resistance as:

$$[2.2] \quad C_{S6} = AF_y (1 + \lambda^{2n})^{1/n}$$

where:  $C_{S6}$  = nominal compressive capacity [N]

$A$  = gross cross sectional area [ $mm^2$ ]

$F_y$  = yield strength of steel [MPa]

$n = 1.34$  for rolled W-shapes

and the slenderness parameter,  $\lambda$ , is:

$$[2.3] \quad \lambda = \frac{kL}{r} \sqrt{\frac{F_y}{\pi^2 E}}$$

where:  $r$  = radius of gyration ( $= \sqrt{I/A}$ ) [mm]

Column imperfections must be included for the accurate computation of inelastic buckling failure loads. The two principal imperfections that contribute to the buckling strength of hot-rolled steel cross sections are residual stress and initial out-of-straightness (Galambos 1998). There is currently no built-in routine in Solidworks to simulate these imperfections, so the available features had to be manipulated to suit.



### 2.4.1 Residual Stress

Residual stresses develop in hot-rolled steel sections and plates due to uneven cooling after rolling, and are a primary cause of reduced buckling strength in intermediate columns (Galambos 1998). The flange tips are generally first to cool and can develop significant residual compressive stresses and so also may reduce the load corresponding to local flange buckling.

Previous research has indicated the simplified linear residual stress pattern shown in Figure 2-3, with a maximum stress magnitude of  $0.3F_y$ , is acceptable for wide flange cross sections in compression (ASCE 1971). The validity of this residual stress idealization to generate a column curve numerically that closely resembles Eq. [2.2] was confirmed by Shek (2006). The applicability of this residual stress idealization when local buckling is the primary failure mode will be confirmed through calibration with physical testing, and modifications will be made if necessary.

Solidworks Simulation offers no direct way to simulate initial residual stresses, but because residual stresses are related to thermal dissipation, it is logical to simulate them using thermal gradients. Fig. 2-4a shows the thermal loading used, selected by trial and error, to create compressive stresses at the flange tips and centre of the web and tension stresses at the web/flange interfaces of a W150x30 shape. The flange tips and centre of the web are uniformly heated to  $+50\text{ }^\circ\text{C}$  and the web/flange interfaces are uniformly cooled to  $-33\text{ }^\circ\text{C}$ . The thermal loads are allowed to distribute evenly throughout the model during the thermal analysis thus ensuring even stress distribution after the resulting strains are resolved, as shown in Fig 2-4b.

Figure 2-5 shows the resulting normalized stresses approaching  $\pm 0.3F_y$  in the flange and web of a W150x30 column (compression positive, tension negative) with  $F_y = 350 \text{ MPa}$ . The stress variations across the half width of the flange and half depth of the web are linear.

#### 2.4.2 Out-of-Straightness

Column sweep or camber causes bending to occur from the onset of loading, and is the primary reason buckling manifests as a failure mode (Galambos 1998). Without initial out-of-straightness, concentrically loaded columns could, at least theoretically, crush uniformly. Current specifications permit hot-rolled steel W shapes to vary in straightness up to  $L/1000$ , provided the flange widths equal or exceed  $150 \text{ mm}$  (ASTM 2010). Initially, out-of-straightness was simulated by applying a lateral load to the web face normal to the weak axis. In stockier columns (i.e.,  $kL/r < 50$ ), however, the lateral force required to create the target sweep induced large internal moments that lead to premature failure.

To alleviate undesirable moments and minimize model variability, a thermal gradient causing constant curvature about the weak axis was instead applied. The magnitude of the gradient was determined using Eq. [2.4], and then calibrated using linear interpolation:

$$[2.4] \quad \Delta T = \frac{\varepsilon}{\alpha_t} = \frac{\left(\frac{b}{2}\right)}{R\alpha_t}$$

where:  $\Delta T =$  required thermal gradient [ $^{\circ}\text{C}$ ]

$\varepsilon$  = cross-sectional strain in the direction of weak-axis bending

$\alpha_t$  = coefficient of thermal expansion ( $12 \times 10^{-6} / ^\circ\text{C}$  for structural steel)

$R$  = radius of curvature [ $mm$ ]

$b$  = flange width [ $mm$ ]

No additional internal stresses are generated due to the additional thermal loading because there is no fixity at the column ends and the temperature gradient varies uniformly across the cross section. The shape of the deformed member is therefore an arc of a circle.

## 2.5 MESH SIZE

Balancing mesh size with model performance and solution time was an iterative process. Increasing the overall element size decreases the solution time but results in a less accurate analysis. Using an extremely fine mesh, however, is computationally inefficient and so results in an unreasonably long solution time. Figure 2-6 shows the two primary mesh controls applied to the model: 1) an overall minimum global mesh size with a maximum element size of 30  $mm$  and 2) a finer local mesh in the deteriorated regions. A transition zone exists between the two controlled regions which eliminates undesirable stress concentrations due to abrupt changes in element size. It was found through trial and error that the global mesh size of 30  $mm$  was sufficiently fine to capture Euler buckling. In the deteriorated regions, the maximum mesh size was set equal to the thickness of the deteriorated flange,  $t^*$ , to accurately capture local buckling.

Solidworks offers the user several meshing options each comprised of different element types: solid mesh, shell mesh, beam mesh and mixed mesh (Dassault Systèmes 2010). Shell elements are 2-dimensional and are meant to idealize thin plates with a uniform thickness (e.g. sheet metal in plane stress conditions), and beam elements idealize extruded structural members with uniform cross-sectional properties. While beam elements are capable of resisting axial, bending, shear and torsion, they are not able to simulate complex buckling phenomena and thus a solid mesh consisting of 3-dimensional elements was used throughout the model. Figure 2-7 shows the default parabolic tetrahedral element used to mesh solid bodies. This particular element type is defined by 10 nodes: four corner nodes and six mid-side nodes. During the thermal analysis, each node has one degree of freedom, and during the nonlinear stress analysis, each node has three degrees of freedom.

## **2.6 BUCKLE GEOMETRY**

The geometry of buckled slender plates is well-understood when the edges are pinned and the plate is subjected to uniform compression, however, deteriorated flanges of W-shapes are difficult to idealize.

In an attempt to verify that the buckle geometry obtained with FEA were realistic, an approximate comparison was made with the flange of a W150x30 that failed due to local buckling in a 4-point bending test. Figure 2-8 shows the local buckle that occurred in the 4-point bending test and Figure 2-9 shows the simulated local buckling failure of a W150x30 column with localized deterioration at mid-height. Clearly the distance between inflection points in both buckled shapes is approximately half the flange width.

While the accuracy of buckling geometry in the model will be examined in-depth after physical testing, the present comparison indicates that results are reasonable and provides further justification for continuing with the proposed analysis approach.

## 2.7 SUMMARY OF MODEL

Like most FEA software packages, Solidworks requires the user to apply loading using pre-defined time steps. However, before stresses can be resolved, a thermal analysis was necessary to ensure temperatures are linearly distributed throughout the cross section. After the thermal analysis, resulting temperatures are automatically input as thermal loads in the primary analysis. Figure 2-10 summarizes the three-step approach adopted in the primary analysis:

- i. In the first step, stresses caused by the linear variation temperature are resolved to generate and simulate residual stresses across the cross section.
- ii. In the second step, column sweep is created by applying an additional uniform thermal gradient to cause bending about the weak axis.
- iii. In the third step, the column is loaded axially until failure occurs.

Figure 2-11 compares the nominal axial capacity of a W150x30 column calculated using FEA with those calculated using S6-06 (Eq. [2.2]). The W150x30 has an overall depth,  $d$ , of 157 mm, a flange width,  $b$ , and thickness,  $t$ , of 153 mm and 9.3 mm, respectively, and a web width,  $w$ , of 6.6 mm. It is made from steel with  $F_y = 350$  MPa. Clearly the FEA results conform extremely well to the empirically based code equation: the 15 FEA



values shown are on average 0.7% greater than the values computed using Eq. [2.2], and the ratios of  $C_{FEA}/C_{S6}$  have a coefficient of variation of 1.8%.

The time required for Solidworks Simulation to fully analyze columns with localized deterioration ranged from approximately fifteen minutes to three hours depending on the slenderness ratio and geometry of the localized deterioration. The hardware of the analysis PC exceeded all minimum and recommended system requirements specified by the Dassault Systèmes help database (2010). For a typical intermediate column, W150x30x4500 ( $kL/r = 120$ ), with 50% section loss on both flanges, the finite element analysis model consisted of approximately 54000 elements, 94000 nodes, 281000 degrees of freedom, and took one hour and fifteen minutes to run the full analysis.

### 2.7.1 Assumptions

The finite element model is based on the following assumptions:

- Column ends have no fixity to prevent rotation (i.e.,  $k = 1.0$ ).
- Columns are concentrically loaded.
- Modulus of elasticity for steel is 200 000 MPa.
- Steel stress-strain curve is bilinear: linear elastic-perfectly plastic.
- Residual stress distribution is linear with a maximum magnitude of  $\pm 0.3F_y$ .
- Columns are not perfectly straight and have a maximum mid-height sweep of  $L/1000$ .

## 2.8 SUMMARY

In this chapter, the feasibility of finite element analysis using Solidworks Simulation for the previously discussed study has been investigated. Specifically, the failure of undeteriorated columns was examined in detail by comparing results obtained from FEA to Eq. [2.2], the empirically derived equation given in CAN/CSA S6-06 (CSA 2006).

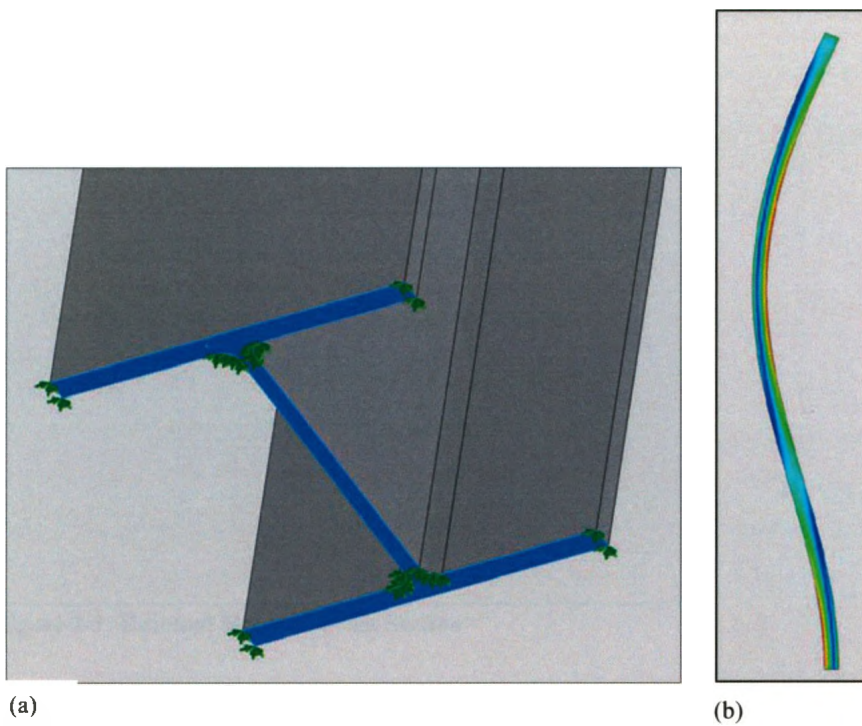
It has been determined that Solidworks Simulation can very accurately predict the failure load and buckled shape of undeteriorated W-shape columns provided that the following conditions are met:

1. End fixity is relieved at both ends of the column ( $k = 1.0$ ) by restraining one face in the  $x$  and  $y$  directions and creating a rocker-assembly at the other end of the column.
2. Residual stress is simulated using thermal loads that are allowed to redistribute prior to axial loading.
3. The resulting residual stress has a linear distribution with a maximum stress magnitude of  $0.3F_y$ , as shown in Figure 2-3.
4. The column is not perfectly straight and an initial sweep of  $L/1000$  is created prior to axial loading using a thermal gradient in the direction of free rotation about the weak axis. The magnitude of the thermal gradient can be determined using Eq. [2.4] and calibrated using linear interpolation.
5. The overall mesh size should be a maximum 30 mm for a W150x30 column.
6. A finer mesh control should be defined in the region of local deterioration so that the maximum element size is less than the thickness of deterioration ( $t^*$ ).

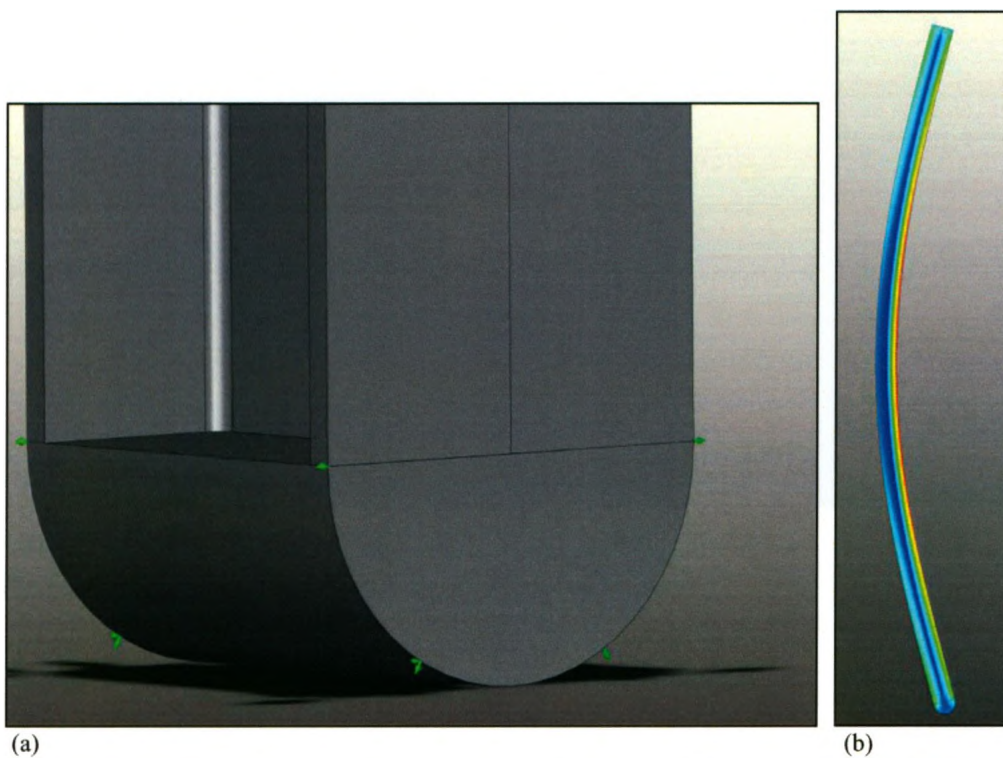
7. The stress-strain curve for the column steel is bilinear: linear elastic-perfectly plastic.

The ability of Solidworks Simulation to analyze columns having local flange deterioration was also investigated and validated at a preliminary level. However, due to the complex interaction between local buckling, global buckling, and yielding and the lack of an accurate theoretical model, additional experimental testing is necessary to fully validate FEA results.





(a)  
**Figure 2-1: Inadequacy of Built-in Fixities**  
 (a) End constraint over column end face  
 (b) Associated undesirable end fixity, ( $k < 1.0$ )



(a)  
**Figure 2-2: Column Rocker Assembly**  
 (a) Rocker at column bottom  
 (b) No end fixity ( $k = 1.0$ )

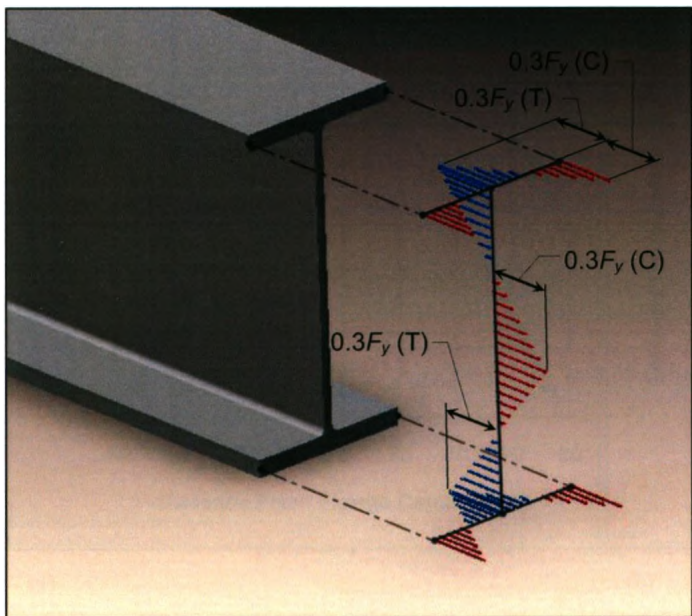


Figure 2-3: Residual Stress in Cross Section

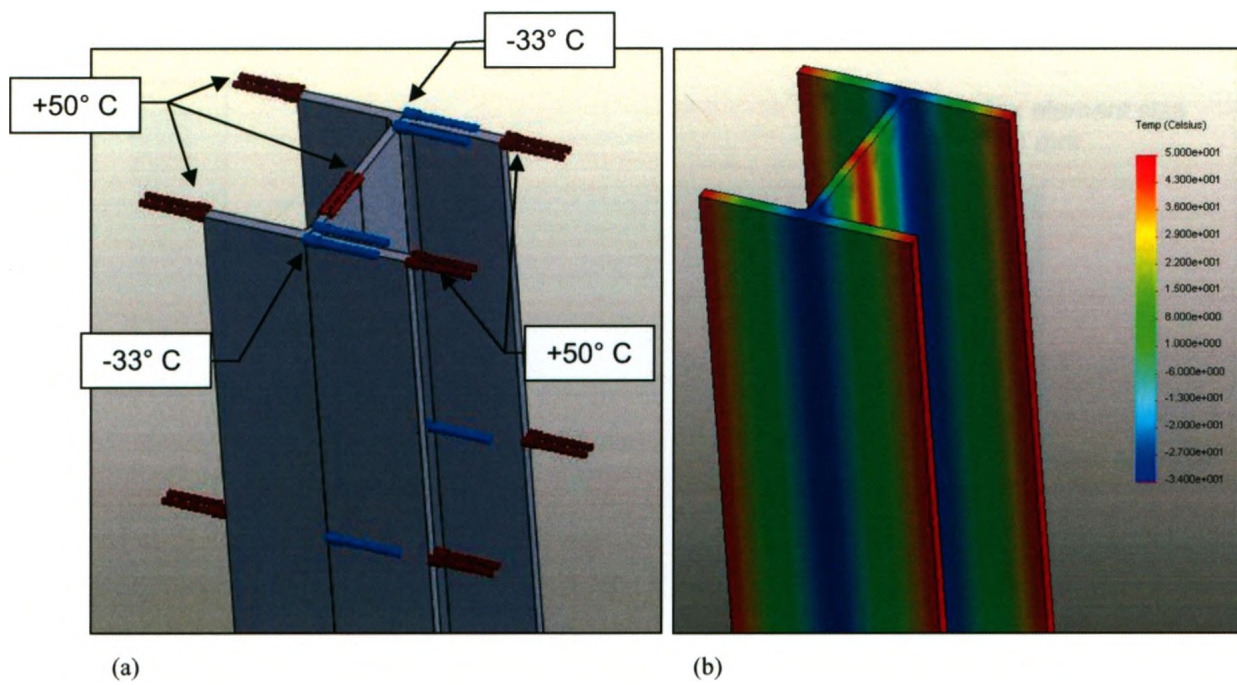


Figure 2-4: Thermal Analysis Used to Develop Residual Stresses  
 (a) Thermal loading  
 (b) Resulting temperature distribution



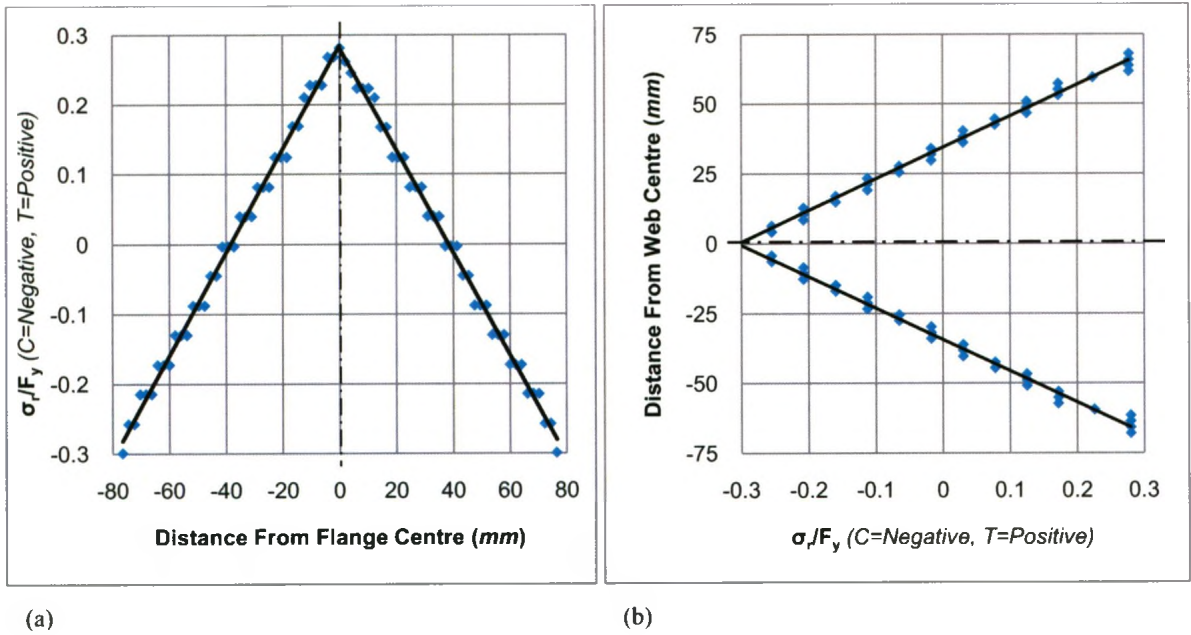


Figure 2-5: Residual Stress Distribution due to Thermal Loading  
(a) Flange  
(b) Web

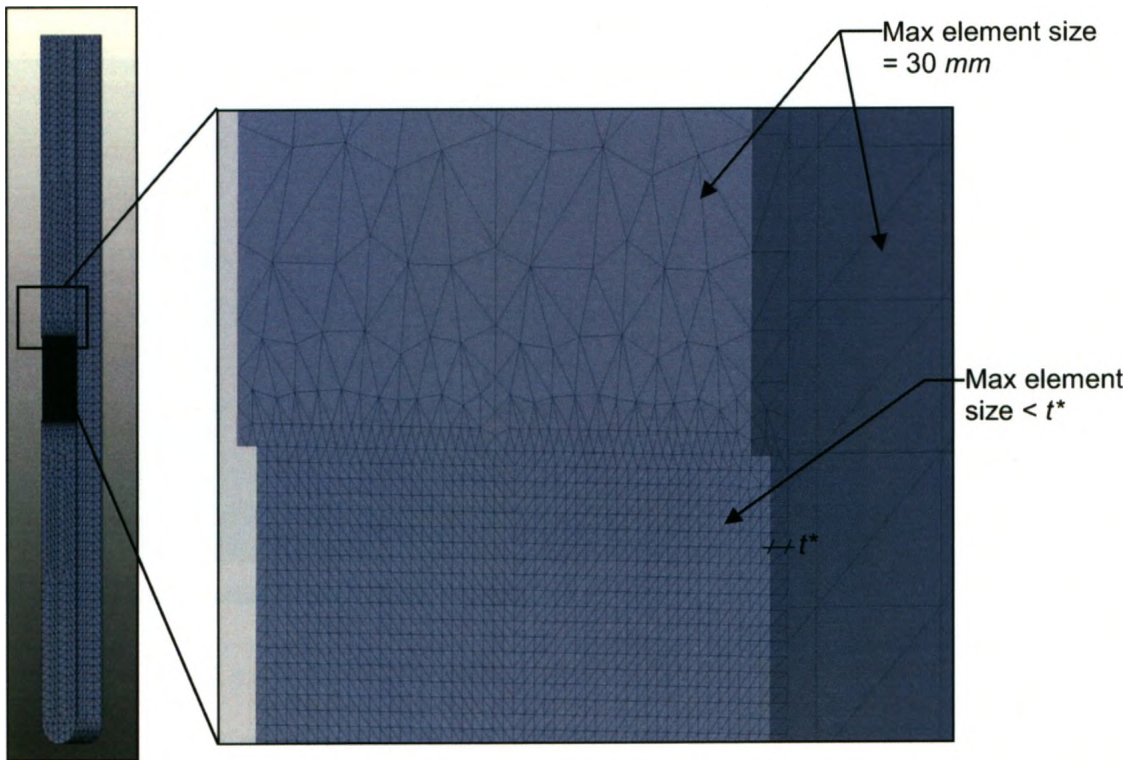


Figure 2-6: Mesh Control in Deteriorated Region

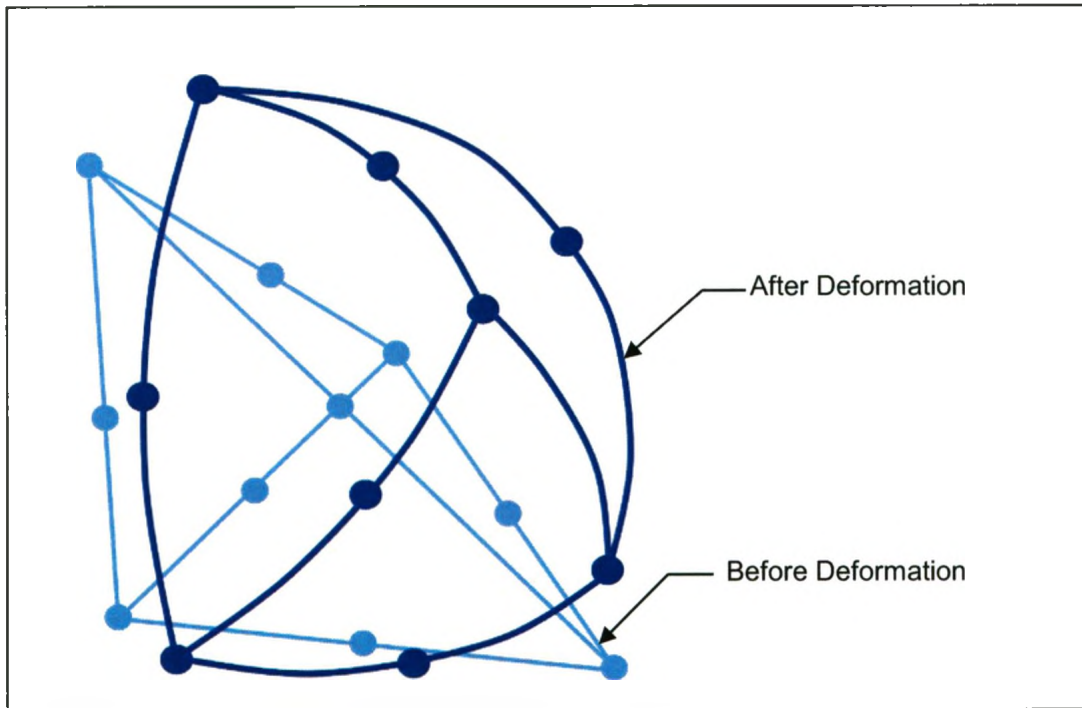


Figure 2-7: Second-Order Tetrahedral Element Used Throughout FEA (after Dassault Systèmes 2010)



Figure 2-8: Local Buckle from a 4-Point Bending Test

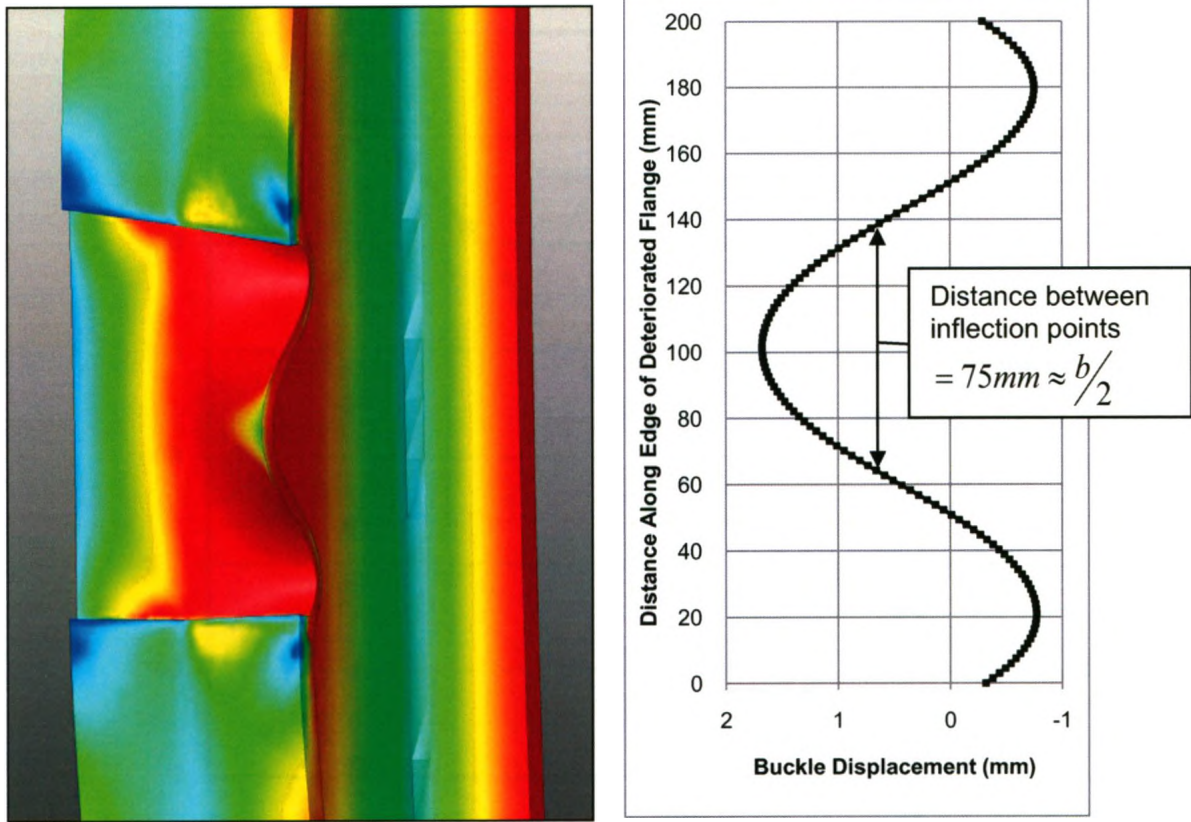


Figure 2-9: Local Buckle from a W150x30 Column with Localized Deterioration at Mid-Height

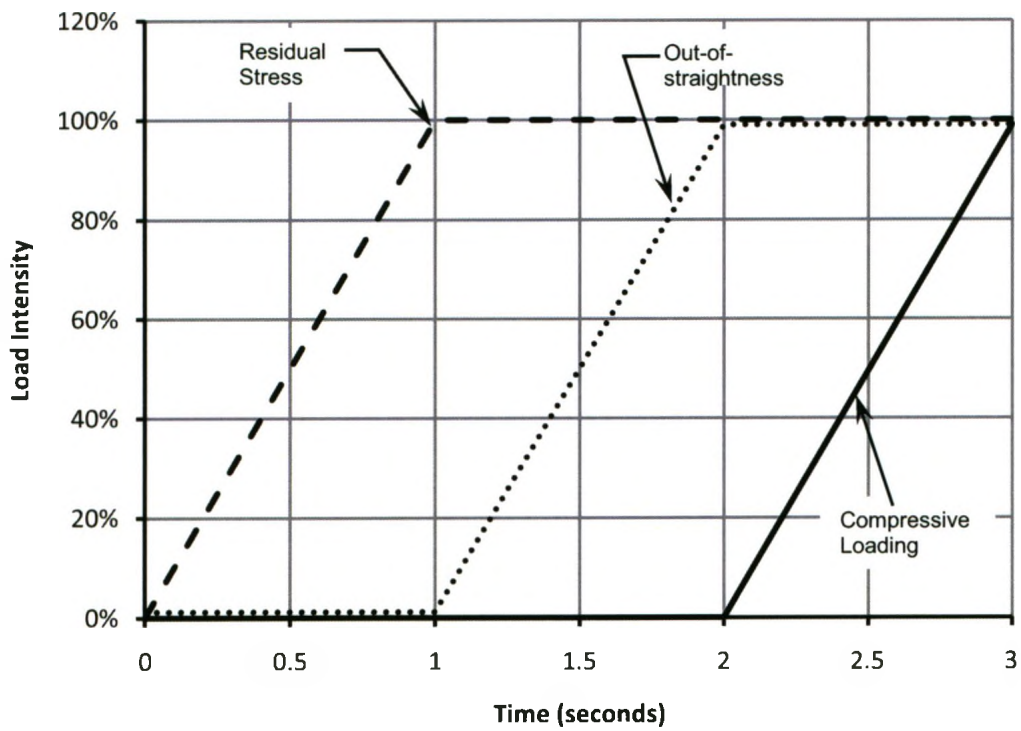


Figure 2-10: Time-Depending Loading Scheme



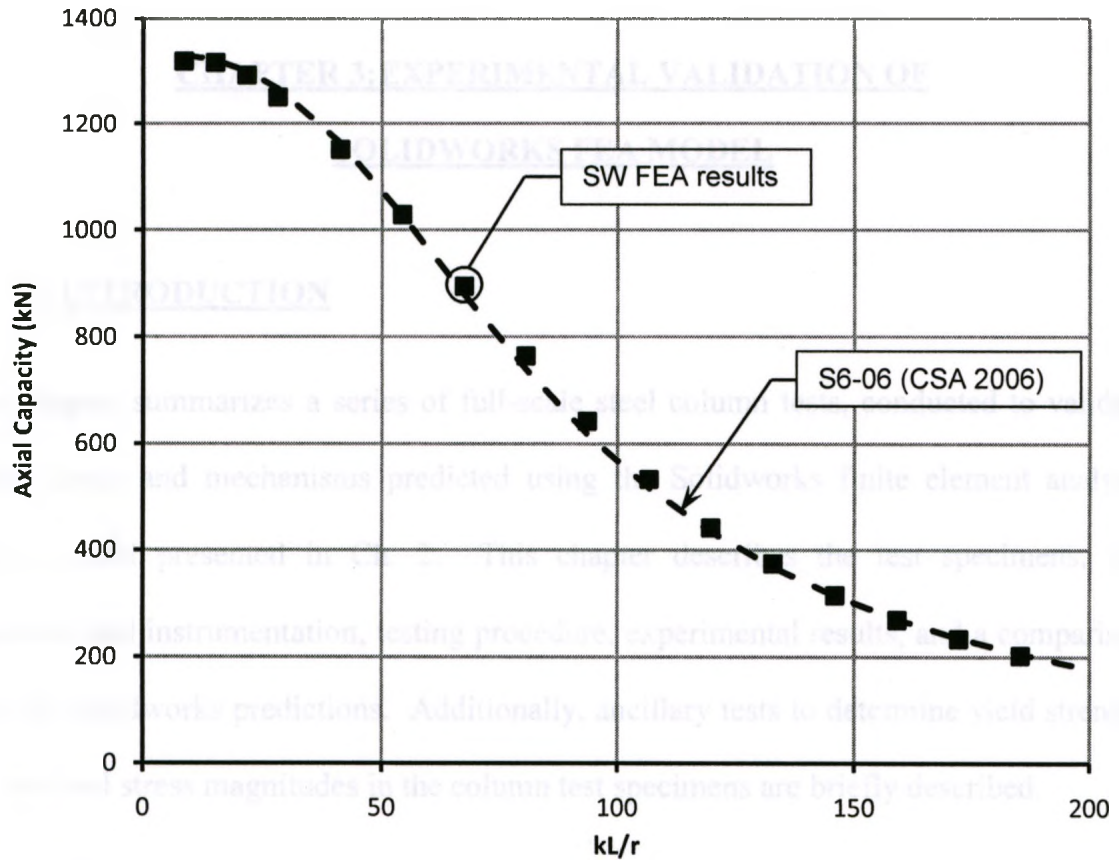


Figure 2-11: Solidworks FEA Results Compared with CSA S6-06 (CSA 2006) for a W150x30 Column

## **CHAPTER 3: EXPERIMENTAL VALIDATION OF**

### **SOLIDWORKS FEA MODEL**

#### **3.1 INTRODUCTION**

This chapter summarizes a series of full-scale steel column tests, conducted to validate failure loads and mechanisms predicted using the Solidworks finite element analysis (FEA) model presented in Ch. 2. This chapter describes the test specimens, test apparatus and instrumentation, testing procedure, experimental results, and a comparison with the Solidworks predictions. Additionally, ancillary tests to determine yield strength and residual stress magnitudes in the column test specimens are briefly described.

#### **3.2 SPECIMEN DESCRIPTIONS**

The five W150x30 column specimens with varying deterioration patterns, each selected to validate key findings in the preliminary sensitivity analysis, are shown in Table 3-1. Although lighter than most bridge compression members, a W150x30 shape was chosen to accommodate the maximum capacity of the MTS 243.70 actuator in the UWO Structures Lab, 1500 *kN*. Additionally, the 2.3 *m* columns had a mass of 69 *kg* (weight of 150 *lbs*) and so could be easily handled by one or two people without the need for the overhead crane. The slenderness ratio,  $kL/r$ , for weak-axis instability was typically 60 and so representative of intermediate columns that fail by inelastic buckling.

Localized flange corrosion was simulated as uniform section loss in rectangular regions, to facilitate direct comparison with the FEA predictions. It was also convenient and

efficient to reduce the flange cross section by machining predetermined patterns. The rationale for selecting each particular specimen is as follows:

1. Control Specimen (No Deterioration): A control specimen with full flange cross sections was tested first. It also served as a pilot test to ensure the test apparatus behaved appropriately, with no significant end fixities or eccentricities. The failure load of the control specimen was the greatest of all specimens tested so adequate performance of the load frame and actuator during this test would ensure that the remaining tests should proceed smoothly.

2. Symmetric Flange Deterioration (Case A): The second test column had symmetric flange deterioration at midheight as shown in Table 3-1. The length of deterioration was 300 *mm* and the thickness of the remaining flange was 3.5 *mm*. The width-to-thickness ratio in the deteriorated region was 21.0, or approximately  $410/\sqrt{F_y}$ , which markedly exceeds the Class 3 limit (CSA 2006) of  $200/\sqrt{F_y}$ . These details were selected to validate the failure load, weak-axis buckling deflections and the geometry of the local buckle predicted using FEA.

3. Non-symmetric Flange Deterioration: The third test column had only one flange with deterioration at midheight as shown in Table 3-1. The length of deterioration was 300 *mm* and the thickness of the deteriorated flange was 3.5 *mm*. This specimen was selected to examine the extent and effect of torsional rotations anticipated at failure and determine the validity of FEA predictions for cases with non-symmetric deterioration.



4. Symmetric Flange Deterioration (Case B): The fourth test column had symmetric flange deterioration at midheight as shown in Table 3-1. The length of deterioration was 100 *mm* and the thickness of the deteriorated flange was 3.5 *mm*. This deterioration geometry was selected to further validate the failure load, weak-axis buckling deflections, and the local buckle geometry as predicted by the FEA. As shown in Figure 3-1, the FEA predicted that the local buckle of test Column 2 would exhibit 2.5 sinusoidal waves while that of Columns 4 would exhibit only 0.5 sinusoidal waves. Additionally, the effect of the length of deterioration on the axial capacity could also be validated.

5. Contingency Column: The fifth test column was reserved as a contingency specimen in the event of an unsatisfactory test or data acquisition malfunction. This turned out to be prudent because Column 4 was accidentally subjected to its failure load before the data acquisition logger was functioning. The local deterioration pattern for Column 4 was recreated on Column 5, i.e., symmetric 100 *mm* lengths at midheight with the thickness of the deteriorated flange of 3.5 *mm*.

### **3.2.1 Initial Geometric Imperfections**

The cross-section dimensions were measured at the top, bottom and midheight of each test column to verify the gross area of steel and indicate any skew of the cross section. Out-of-straightness was measured with a theodolite, assuming that the maximum camber or sweep occurs at the column mid-point. The column was placed with its axis oriented towards the theodolite, as shown in Figure 3-2, the offsets to the column midpoint (b) and far corner (c) were measured with respect to the nearest corner (a). Camber and sweep were computed using:

$$[3.1] \quad \delta_c, \delta_s = x_m - \frac{x_e}{2}$$

where:  $\delta_c$  = camber [mm]

$\delta_s$  = sweep [mm]

$x_m$  = Horizontal offset from Line a-d to Point b, as shown in Fig 3-2

$x_e$  = Horizontal offset from Line a-d to Point c, as shown in Fig 3-2

Given the accuracy inherent in this procedure, it is estimated that the measured cambers and sweeps, shown in Table 3-2, are accurate to  $\pm 0.5$  mm. In general, the columns were very straight, making it difficult to accurately predict the direction of weak-axis buckling before each test.

### 3.2.2 Material Properties and Residual Stresses

Table 3-3 summarizes material yield strengths and maximum residual stresses obtained from tensile coupon tests and stub column tests, respectively. Columns 1 and 4 were obtained from a single member, and Columns 2 and 3 were obtained from a different single member.

Tensile coupon tests were conducted in accordance with ASTM A370 (ASTM 2010a) to determine the yield strengths. The coupons were loaded to failure at a constant load rate of approximately 175 MPa/minute or a strain rate of approximately 15  $\mu\text{e}/\text{sec}$ . Samples were taken from the web and flange, but the flange yield strength was used for analysis because when W-shapes buckle about their weak axis, the flanges yield first and thus govern the axial capacity.

Stub-column tests are conducted on stocky members to determine the magnitude of the maximum residual stress in the cross section (Galambos 1998). The load at which the response deviates from its initial linearity indicates the magnitude of the maximum residual stress present. Three stub-column tests were conducted at McMaster University in accordance with the procedure recommended by Tall (1961). The main objective of the stub column tests was to determine the magnitude of the maximum residual stress, but a second objective was to validate the tensile coupon tests by obtaining the average static yield strength of the full cross section. Further details of these tests are presented Appendix A1.

In general, the average yield strength calculated from the coupon tests were very consistent with those calculated from the stub column tests. The maximum residual stress magnitude ( $\sigma_r$ ), however, was less than the conventionally assumed value of  $0.3F_y$ : only 10.8%, 8.9%, and 6.6% of the average yield strength for the three columns examined. As residual stresses are a function of rates of cooling as defined by the cross section geometry (Galambos 1998), it would appear that the W150x30 shape, with flanges and web of similar widths and thicknesses, cools relatively uniformly.

### **3.3 TEST APPARATUS**

Custom column end supports were necessary to hold the specimens securely at high axial loads yet permit free rotation about the weak axis. To minimize eccentricity, the centroid of the cross-section had to be aligned with the centre of the actuator head throughout the test. The column end supports also required sufficient thickness to distribute the applied compressive force uniformly across the cross-section without significant deformation.

Figure 3-3 shows the knife-edge rocker assembly, similar to that used by Gardner and Nethercot (2003), that was designed and fabricated to achieve this boundary condition reliably. Initially, steel shims were envisaged to secure the end of the cross section during the test (Fig. 3-3a), but, during fabrication, a detail with set-screws (Fig. 3-3b) was adopted to ensure the shims did not become dislodged. The recesses to accept the column ends in each pin plate assembly were oversized by 2 mm in both plan dimensions to allow for deviation from the nominal dimensions of the W150x30 section. Figure 3-3c shows the finished bottom plate, which was attached to the strong floor of the Structures Lab using anchor rods through the long slotted holes, and the top plate which threaded on to the actuator head. A full drawing set of the column end support assembly is presented in Appendix A2.

### **3.3.1 Numerical Analysis of Column End Supports**

To ensure that no significant deformations or internal stress concentrations would be encountered during testing, a finite element analysis (FEA) of the proposed column end supports was conducted prior to fabrication. Figure 3-4 shows the response predicted by FEA at an applied load of 880 kN, which corresponds to the failure load of a 2500 mm long undeteriorated W150x30 column made from Grade 350 steel. The maximum observed stresses in the pin plate (Fig. 3-3c) and base plate (Fig. 3-3d) assemblies were 237 MPa and 73 MPa, respectively. The regions of high stress were highly localized as shown. To reduce these peak stresses, a 2 mm radius fillet at the knife-tips and top and bottom pin plates was adopted for the final design to increase the bearing area. No measurable flexural deflection of any of the plates was predicted by the FEA.

### 3.3.2 Load Frame and Actuator

The expected failure loads of the proposed test columns were in the order of 1000 *kN*. While the MTS 243.70 actuator at the UWO Structures Lab is rated to 1500 *kN*, excessive deflections had been observed in the past when the actuator load exceeded 600-800 *kN* (Logan 2010). Preliminary tests were therefore conducted to examine the frame behaviour at high loads, and so investigate any outstanding issues of safety or serviceability. Figure 3-5 shows the general configuration of the original unbraced load frame and actuator, and Figure 3-6 shows schematically the lateral deformations of the unbraced and braced loading frames that were observed during the preliminary tests. Figure 3-7 illustrates the bracing systems that were progressively implemented into the load frame to minimize these deformations.

Prior to the first preliminary test, a small initial out-of-straightness of the actuator ( $\Delta_i$ ) equal to approximately 5 *mm* at the actuator head was noted (Fig. 3-6a). During this preliminary test, time-lapse video imagery showed 20-30 *mm* ( $\Delta_A$ ) horizontal movement of the top cross-beam caused by rotation of the load frame columns about their bases (Fig. 3-6b) at the maximum applied load of 1200 *kN*. No slip was observed at the crossbeam-column connections of the loading frame, even though the 5% fractile of the slip resistance for the 24 bolts in these connections is only 809 *kN*. However, the out-of-plane sway ( $\Delta_A$ ) would have been unacceptable when testing a pin-ended column to failure, and a system of two inclined HSS braces was designed to secure the columns by preventing rotation (Fig 3-7b) about their bases.



During the first attempt to test Column 1 using the braced loading frame, displacement transducers were placed on the actuator head, Point B on Figure 3-5, to verify that the braces were effectively preventing displacement there. Lateral movement at the actuator head ( $\Delta_B$  in Fig 3-6c) of 24 mm was observed at a load of 375 kN (i.e. only 37.5% of the anticipated failure load), however, and the test was stopped. Analysis of test data and time-lapse video footage indicated that while the diagonal braces had effectively eliminated deflection due to load frame column rotation ( $\Delta_A$ ), the actuator was now pivoting about the centroid of the cross beam (Fig 3-6c). To eliminate this additional displacement and further reinforce the load frame, a horizontal beam was installed between the load frame columns to restrain the actuator head (Fig 3-7c). With these two bracing systems installed, the out-of-plane deflections of the load frame and actuator were essentially eliminated, and the test program could proceed.

### 3.3.3 Instrumentation

To gain a full understanding of column buckling behaviour and facilitate an accurate comparison with the numerical models, it is generally desirable to monitor lateral displacement, twist and overall shortening of the test column (Tall and Tebedge 1970). As shown in Figure 3-8, the test columns were monitored using five displacement transducers deployed to isolate each of these key variables independently. The accuracy of the transducer measurements is approximately  $\pm 0.01$  mm and their readings can be archived continuously. Transducers 1 and 2 were spaced at 120 mm apart on the column flange at mid-height, to capture both lateral displacement due to strong axis bending, if any, and column rotation. Transducer 3 was located at the centre of the web face at mid-height, to capture lateral displacement due to weak axis buckling. Transducer 4, located

on the vertical face of the top plate, monitored lateral movement of the actuator head to verify the effectiveness of the load frame bracing systems and to account for out-of-plane displacement of the load frame, which is necessary to compute the lateral midheight deflection with respect to the ends of the column. Transducer 5, aligned vertically, measured vertical displacement of the top plate with respect to the floor of the Structures Lab, and so essentially measured the vertical contraction of the test specimen.

Columns 2, 3, 4 (and 5) were also instrumented with foil strain gauges. Because the test specimens were generally very straight and the buckling direction could not be accurately predicted, strain gauges were placed on all flange tips with reduced cross sections. Figure 3-9, Figure 3-10 and Figure 3-11 each show the local buckling pattern predicted by the FEA (a) that provided the basis for the number and location of strain gauges (b) fixed to Columns 2, 3, 4 (and 5), respectively.

Each column was also coated with a whitewash consisting of white acrylic paint and water in a 1:2 ratio by volume. This coating was applied to facilitate visual identification of mill scale flaking, indicating local yielding and often the onset of local buckling.

Finally, all tests were recorded using a digital video camera so that failure mechanisms could be confirmed by viewing the column failure in slow motion.

### **3.4 TEST PROCEDURE**

The following general procedure was adopted in accordance with Tall and Tebedge (1970):

1. Top and bottom plates were aligned using a plumb bob and theodolite. No formal error study was conducted, however, both plates were typically aligned to within a horizontal tolerance of  $\pm 2$  mm.
2. Strain gauges were affixed to the column flanges (Tests 2, 3, 4 and 5 only).
3. Pin plates were clamped to test column ends using set-screws (Fig. 3-3b).
4. The column was placed on the lower pin plate and the actuator head was lowered to secure it in place. The weak axis was aligned to be parallel to the free rotational axis of the column-end assembly.
5. A small load ( $\sim 1$  kN) was applied to hold the column in place while the displacement transducers were deployed.
6. A preliminary load, equal to 20% of the anticipated failure load, was applied to minimize unintended displacements due to initial seating. The preliminary seating load was then removed and all instrumentation was zeroed.
7. As shown in Figure 3-12, loading was then applied at two speeds (Tall and Tebedge 1970):
  - a. 28 MPa/minute until 50% of the anticipated failure load is achieved (i.e., while the column response is still fully linear elastic).
  - b. 7 MPa/minute until the maximum load is achieved.
  - c. 0 MPa/minute so that the maximum static load can be determined.
  - d. 7 MPa/minute until the column is fully buckled.

While the above values are given in MPa/minute, the actuator is in stroke-controlled mode at all times to ensure the column does not become dangerously



unstable. The actual loading rates, in  $mm/min$ , were computed assuming the reduced cross section was present over the entire length of the column.

### 3.5 TEST RESULTS

Figure 3-13 shows the load versus midheight weak-axis deflection, measured at the web face, for Columns 1, 2, 3, and 5. Not unexpectedly, each of the deteriorated column curves lie roughly within the failure envelope defined by the undeteriorated pilot test except Column 5, which unexpectedly changed its direction of buckling near failure. Columns 2, 4 and 5 displayed brittle failures because all had symmetric flange deterioration. Very little weak axis lateral deformation occurred prior to the maximum load. Conversely, the failure of Column 3 with unsymmetrical flange deterioration was more ductile because stresses were able to redistribute to the undeteriorated flange after local buckling had occurred in the deteriorated region. This post-buckling strength gain in Column 3 can be seen clearly after approximately 5  $mm$  of web deflection.

As noted in Table 3-2, the columns had very little sweep making it very difficult to predict the direction of buckling before the test. Furthermore, the method of measuring out-of-straightness using a theodolite, discussed in Section 3.2.1, was only accurate to within 0.5  $mm$ . The test results will be discussed qualitatively first and compared with the FEA predictions in Section 3.6.

#### 3.5.1 Column 1: Control

The failure of Column 1 was sudden, but slightly ductile. As shown in Figure 3-14, the load versus lateral deflection response was linear until approximately  $0.95P_u$ . As shown

in Fig 3-15a, flaking of the whitewash coating provided a good indication of yielding, and as expected, yielding was concentrated at midheight on the compression flange ends, opposite to the buckling direction. The presence of Leuder Lines perpendicular to the compressive force after column failure indicates that the specimens may have been cold-straightened.

No significant twist or weak-axis deformation was observed indicating that the load was concentric and uniform throughout the cross section. The column end supports performed very well.

### 3.5.2 Column 2

Despite the extremely slow actuator stroke-controlled loading rate of 0.1 *mm/min*, Column 2 failed very suddenly with little warning. Figure 3-16 shows the plastic hinge that formed in the area of local deterioration as a result of local buckling, which led immediately to the global collapse of the column. Figure 3-17 plots time versus web displacement in the direction of weak-axis buckling throughout the test, and illustrates the extremely brittle nature of the failure.

While the local buckling deformation was not visible until after failure, flaking of the whitewash was evident in the deteriorated region at  $0.93P_u$  indicating the stresses in this region were approaching the yield strength. No significant torsion or strong-axis deformation was observed during or after the test. This feature was typical for all tests with symmetric deterioration.

### 3.5.3 Column 3

While the failure of Column 3 can still be characterized as brittle, it was not as sudden as Column 2 because the non-symmetric flange deterioration allowed for stress redistribution after the deteriorated flange had buckled locally. Figure 3-18 illustrates the progression of Column 3 to failure: yielding begins in the deteriorated flange (as indicated by the arrows in Fig 3-18a and b) followed by local buckling and yielding of the web (Fig 3-18c) and finally, by yielding and buckling of the undeteriorated flange (Fig 3-18d). This sequence also indicates how stresses redistribute after local buckling: first to the web, then to the undeteriorated flange. The redistribution of stresses is accompanied by a 9.9% gain in axial capacity, but also a loss in stiffness.

As expected, Column 3 twisted in torsion about its centroid due to the plastic hinge that was formed by the local buckle in the deteriorated flange. Figure 3-19 shows the midheight twist observed in Column 3, calculated from the measurements obtained from the displacement transducers mounted on the flanges, Instruments 1 and 2 on Fig. 3-8. Twisting of the column becomes detectable at approximately  $0.75P_u$ , and provides some advanced warning of the incipient local buckling. After the deteriorated region had buckled locally and could no longer carry load, at approximately  $0.9P_u$ , the twist increases until the column capacity is reached at approximately  $0.035 \text{ rads}$ . The increased twisting after local buckling occurs is further evidence of stresses redistributing to the undeteriorated flange.

### 3.5.4 Column 4

Unfortunately the failure of Column 4 occurred before of the data logger was started, and the only test parameter recorded was the maximum applied load. The load rate was very rapid and not controlled. The local deterioration pattern therefore was replicated on Column 5, which had a slightly shorter overall length.

### 3.5.5 Column 5

Figure 3-20 shows the load-midheight deflection relationship observed for Column 5. Small positive deflections are noted initially, but as the load exceeded approximately 400 kN, the deflections became negative. At a load of approximately 700 kN, the trend again reversed and the eventual buckling failure corresponded to a large positive midheight deflection. There is no explanation for this behaviour. Similar to Column 2, the failure of Column 5 was brittle with little warning of failure. The failure mode was local buckling followed by plastification at midheight leading to global collapse of the column.

Some minor flaking of the whitewash was evident in the deteriorated region just prior to failure indicating the stresses in this region were approaching the yield strength. The progression of the flaking was not sufficient, however, to provide warning of failure. No significant torsion or strong-axis deformation was observed during or after the test, indicating that the two deteriorated flanges buckled simultaneously.



### 3.5.6 Strain Gauge Readings

Figure 3-21 shows the locations of the strain gauges in the deteriorated region of Column 2 at midheight, relative to the failed shape shown as dashed lines. Figure 3-22 and Figure 3-23 show the strain gauge data obtained from the left flange and right flange, respectively. The interaction between global buckling of the column and local buckling in the deteriorated region is reflected by the strain readings. Local buckling can be clearly identified by the abrupt change in direction of the light grey lines, located on the tension side of the local buckle (SG18 and SG11). As the local buckle forms, the compressive strains recorded by those gauges quickly decrease. Similarly, the strain gauges located on the compression side of the local buckle (SG14 and SG3) show increasing compressive strains. Global column buckling is indicated by the abrupt reversal of strain increments at the strain gauges on the flange tips located on the tension side of the global buckling direction (SG19, SG22, SG8 and SG4).

The decrease in the compressive strains in Gauges SG19, SG22, SG4 and SG8 indicate the onset of global buckling at an applied load of approximately 600 *kN*. The reversed strain increments in Gauges 18 and 11 indicate the onset of local buckling at a slightly higher load. Both local buckling and global buckling propagate simultaneously at approximately 650 *kN*. These observations are consistent with the weak-axis deformations at midheight, shown in Figure 3-24.

In general, the strain gauge data were typical for the different test columns. In all cases, the measured strains at a cross section were uniform, indicating concentric loading. In

some cases, however, several gauges became detached prior to failure and so stopped registering with the data logger.

### 3.6 COMPARISON TO FEA

In general, the Solidworks models accurately predicted the observed failure loads and weak-axis midheight deflections. Table 3-2 summarizes the measured camber and sweep, yield strength, and the predicted and actual failure loads for each specimen. The flange deterioration investigated ( $1-t^*/t_o = 0.62$ ) caused the capacity to be reduced to between 60% and 69% of that of the undeteriorated column, depending on the length and symmetry of the deteriorated regions. The professional factor,  $P$ , is the ratio of, the actual failure load,  $P_t$ , to the FEA predicted failure load,  $P_{FEA}$ :

$$[3.2] \quad P = \frac{P_t}{P_{FEA}}$$

The average professional factor for all five test columns is 1.010 and the coefficient of variation (CoV) is 3.8%. These values are similar to the professional factor statistics for regular W-shape columns which were reported by Kennedy and Gad Aly (1980) to have a mean value of 1.030 and a CoV of 5.0%. Thus the accuracy of the FEA to predict the strength of columns with deteriorated flanges is similar to that of Eq. [2.2] to predict the strength of W-shape columns.

Table 3-4 compares the predicted shapes of the local buckles with those observed in the test columns. In general, the length and amplitude of the individual local buckles were consistent with FEA predictions, but symmetry and the presence of plate buckling was not, despite accurate machining of the deteriorated regions. These inconsistencies can

perhaps be attributed to minor imperfections in the cross-sectional geometry and residual stress distributions locally that are different from those idealized. Despite the slight differences in the geometry of the local buckle, the overall axial capacity and global column deformations are still accurately predicted by the FEA. Furthermore, yielding in the web and flanges, indicated by flaking of the whitewash during testing, was consistent with predicted yielding stresses in the FEA, shown by red in Table 3-4. The adequacy of the FEA model will now be explored for each test specimen individually.

### **3.6.1 Column 1: Control**

The purpose of the initial pilot test was to validate that the test frame and end supports performed adequately. The anticipated failure load predicted by FEA was 1151 *kN*, and the column failed at a maximum static load of 1087 *kN*. In general, the failure can be described as brittle, with slight ductility.

Figure 3-14 compares the lateral web displacement at midheight obtained from the FEA to test data. The FEA accurately predicts the global response until the maximum axial load, but does not accurately predict the post-buckling behaviour after the maximum axial load is achieved.

As expected, yielding was concentrated on the flange tips opposite of the buckling direction, and there was good correlation between flaking of the whitewash (Fig. 3-15a) coating and yielded regions predicted by the FEA (red regions in Fig 3-15b).

In Ch. 2 it was shown that the FEA predicted strengths of a W150x30 column closely approximated capacities determined using CAN/CSA S6-06 for a range of slenderness

ratios. The control test, when compared to the FEA prediction given the measured out-of-straightness and residual stress magnitude, therefore indicates any bias associated with the test apparatus. The control column failed at a load that was 5.3% less than the predicted value, indicating that the test apparatus simulated the loading and idealized boundary conditions adequately. No modifications to the FEA model are necessary.

### 3.6.2 Column 2

The anticipated failure load predicted by FEA was 652.3 *kN* and the test column failed at 653 *kN*, a difference of 0.1%. Figure 3-24 compares the web deflection at midheight in the direction of weak-axis buckling observed during the test with that predicted in the FEA. As in the control specimen, the FEA predicts overall column response well until the maximum load, but indicates an even more brittle response than that observed during the test. This may be due to the lack of perfect symmetry in the test specimen, which may increase the axial capacity slightly because both deteriorated regions do not buckle simultaneously as they do in the FEA.

While the failure load and weak-axis deflection of the test specimen was in good agreement with those predicted by the FEA, the geometry of the local buckle was different. As shown in Table 3-4, the observed local buckle was not symmetric as predicted by the FEA. Minor variance in flange thickness distributions may have caused the right flange to buckle first before the plate buckling pattern could fully develop in the left flange. Yielding in the web and the inside faces of local buckles predicted by the FEA, indicated as red, was in good agreement with flaking of the whitewash during the test.



### 3.6.3 Column 3

The anticipated failure load predicted by FEA was 692 *kN* and the test column failed at 710 *kN*, a difference of 2.5%. Figure 3-25 compares the weak-axis deflection of the web at midheight observed during the test with that predicted by FEA. There is good agreement in the elastic range, however, the FEA does not accurately predict deflections after of the deteriorated flange buckles locally at a load of approximately 620 *kN*.

Figure 3-19 compares the torsional rotation predicted by FEA to that observed for Column 3. While the general trend between the two is consistent, there was more rotation during the test than was predicted by the FEA, especially after local buckling had occurred. In the test column, there was a loss in stiffness followed by significant rotation after the local buckle formed, at approximately  $0.90P_u$ . The rotation was followed by strain hardening and a slight increase in stiffness, indicated by the marked reduction in slope at approximately  $0.92P_u$ . This behaviour was not accurately predicted because the stress-strain curve adopted for the FEA was bilinear (elastic-perfectly plastic).

As Column 2 was cut from the same stock and so has the same material properties as Column 3, it is appropriate to compare them. In Figure 3-25, the dashed horizontal line represents the axial capacity of Column 2 with symmetric flange loss. Both columns exhibit an initial failure by local buckling at approximately 640 *kN*, but Column 2 does not exhibit post-local-buckling strength gain exhibited by Column 3. It is conservative, therefore, to assume symmetric deterioration when analyzing columns with non-symmetric deterioration.

As shown in Table 3-4, the FEA predicted plate buckling in the deteriorated region, where multiple adjacent local buckles develop simultaneously, however, only one local buckle developed in the test column. In general, the yielded regions in the FEA, shown in red, are in good agreement with flaking of the whitewash. The FEA did not predict full yielding of the undeteriorated flange, however, because it did not predict the post-local-buckling strength gain.

#### **3.6.4 Column 4**

Despite the lack of data and the rapid application of axial load, the FEA prediction closely approximated the maximum failure load: the predicted failure load was 664 *kN* and the observed failure load was 641 *kN*, a difference of 3.4%. The geometry of the local buckle observed in the test corresponded well with that predicted by FEA as shown in Table 3-4. Yielding in the web predicted by the FEA, indicated in red, was also in good agreement with whitewash flaking observed during the test.

#### **3.6.5 Column 5**

The predicted failure load was 719 *kN* and the test column failed at 749 *kN*, a difference of 4.0%. Figure 3-20 compares the weak-axis deflection of the web at midheight observed during the test with that predicted by FEA. The observed brittle failure corresponded well with FEA predictions. The differences between observed and predicted web deflections can be attributed to the unexpected change in buckling direction.

As shown in Table 3-4, the observed geometry of the local buckle was close to that predicted using FEA. In both cases, one half-sine wave develops at the at the centre of

the deteriorated region, however, the buckles predicted by FEA are symmetric about the column centreline whereas those observed are not. Additionally, web yielding predicted by the FEA, indicated in red, is in good agreement with whitewash flaking observed during the test.

### 3.7 SUMMARY

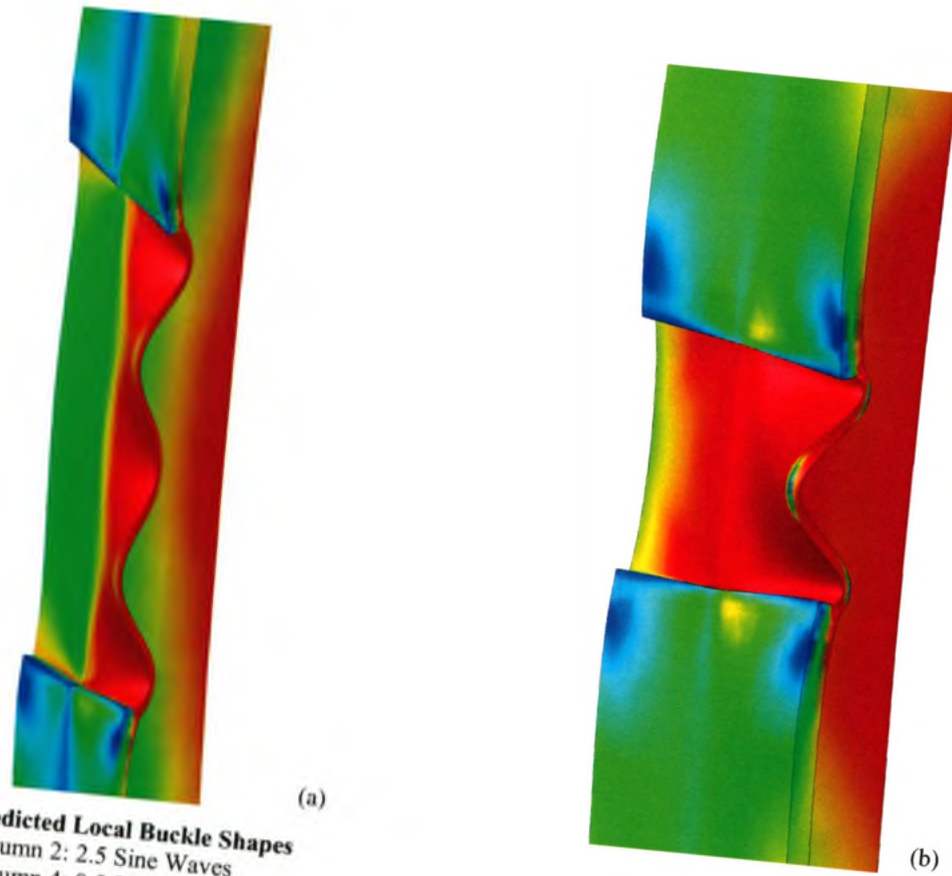
This chapter has presented experimental validation that was undertaken to validate the column failure loads and behaviour predicted by the finite element model. The five test specimens were discussed in detail, the test apparatus and test procedure were described, and results from all full-scale column tests were presented. Finally, comparisons were made between the test results and the FEA predictions.

It can be concluded that FEA modeling using Solidworks, as described in Ch. 2, can accurately predict the failure load of columns with local deterioration subject to axial loading, provided that both residual stress and initial out-of-straightness are accounted for. The professional factor,  $P$ , of the test failure load,  $P_t$ , to the predicted failure load,  $P_{FEA}$ , had a mean of 1.01 and a coefficient of variation of 3.8%. These values are consistent with those reported by Kennedy and Gad Aly (1980) who reported a professional factor of 1.03 with a CoV equal to 5.0% for numerous full-scale column tests.

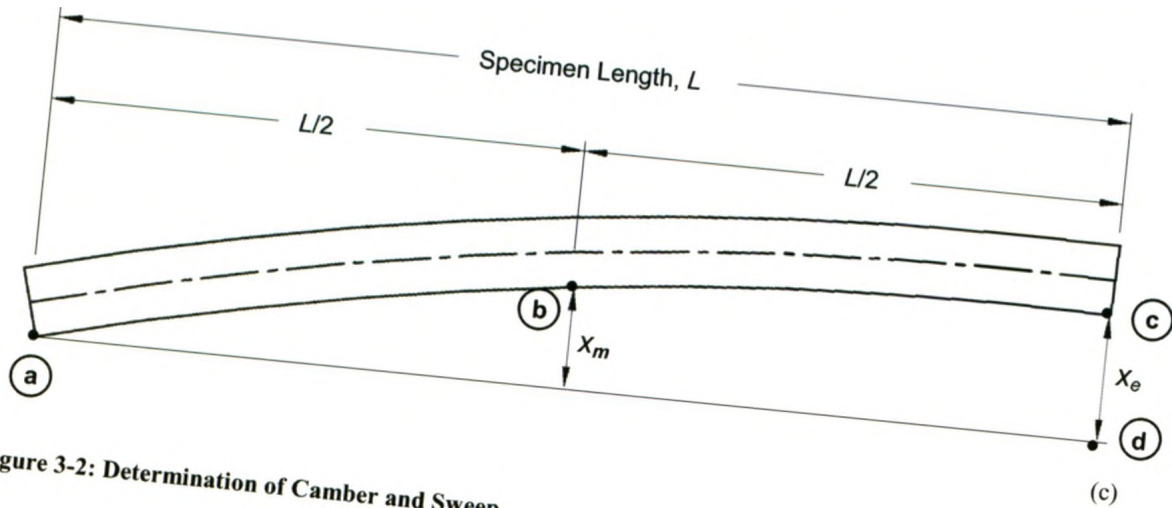
The FEA predicts the lateral midheight column deformation accurately in the linear-elastic range, but not necessarily in the plastic range just prior to failure. Furthermore, the analysis generally indicates a less ductile failure mode than observed, possibly because the bilinear stress-strain relationship for steel used in the analysis does not

account for strain hardening that can occur in the test columns. While the length and amplitude of individual local buckles are consistent with FEA predictions, symmetry and the presence of multiple adjacent local buckles was not. Despite these inconsistencies, however, the maximum axial capacity and global response can still be accurately predicted using the Solidworks FEA model.

Columns with non-symmetric flange loss display more ductile failures than columns with symmetric flange loss because stresses are able to redistribute to the undeteriorated flange after local buckling occurs, resulting in some post-local-buckling strength gains. The FEA does not accurately predict the response after local buckling initiates. It is proposed that, in practice, symmetric deterioration be assumed for all cases, effectively creating a lower-bound solution that is more reliable to calculate using FEA.

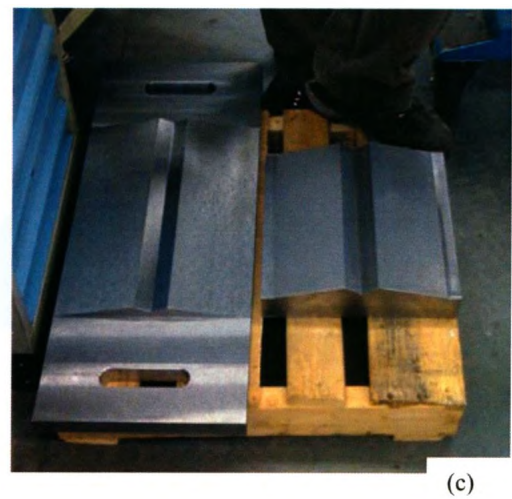
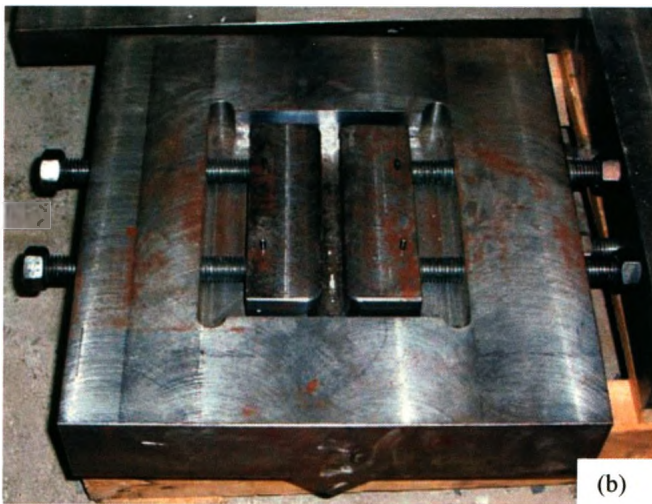
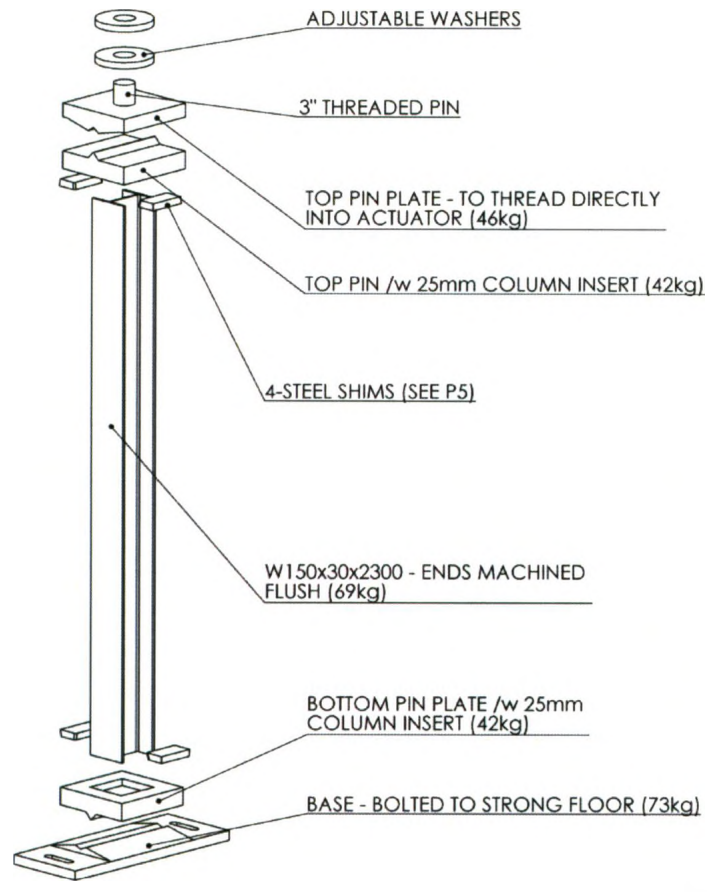


**Figure 3-1: FEA Predicted Local Buckle Shapes**  
 (a) Test Column 2: 2.5 Sine Waves  
 (b) Test Column 4: 0.5 Sine Waves



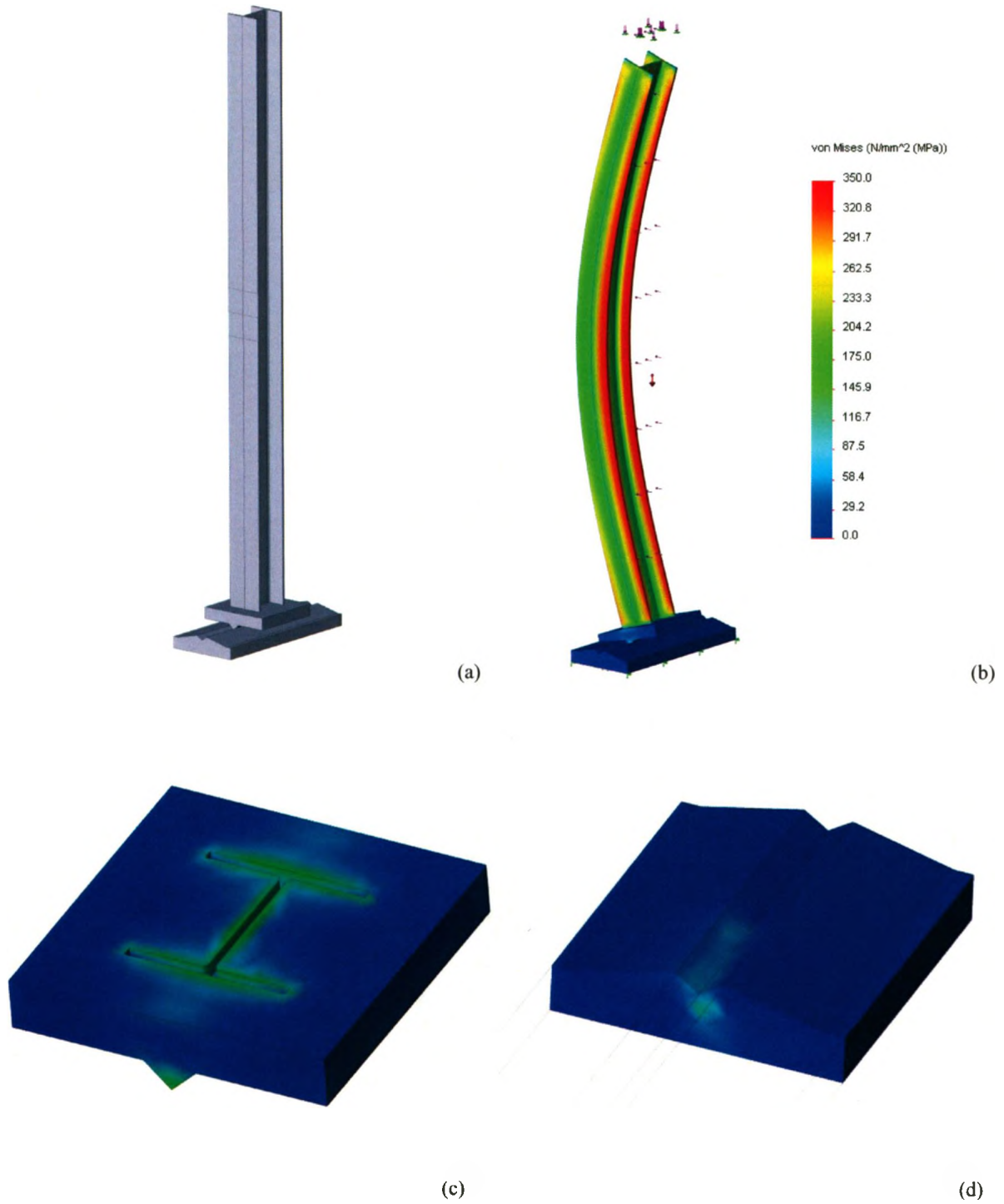
**Figure 3-2: Determination of Camber and Sweep**





**Figure 3-3: Column End Support Assembly**

- (a) Design Overview
- (b) Screw Jacks in Finished Knife-Edge Component
- (c) Finished Bottom (left) and Top (right) Plates



**Figure 3-4: FEA of Column End Supports Prior to Fabrication**

(a) Model Prior to Analysis

(b) Model After Column Failure (Deformation Scale = 40x)

(c) Stresses in Bottom Pin Plate

(d) Stresses in Bottom Plate

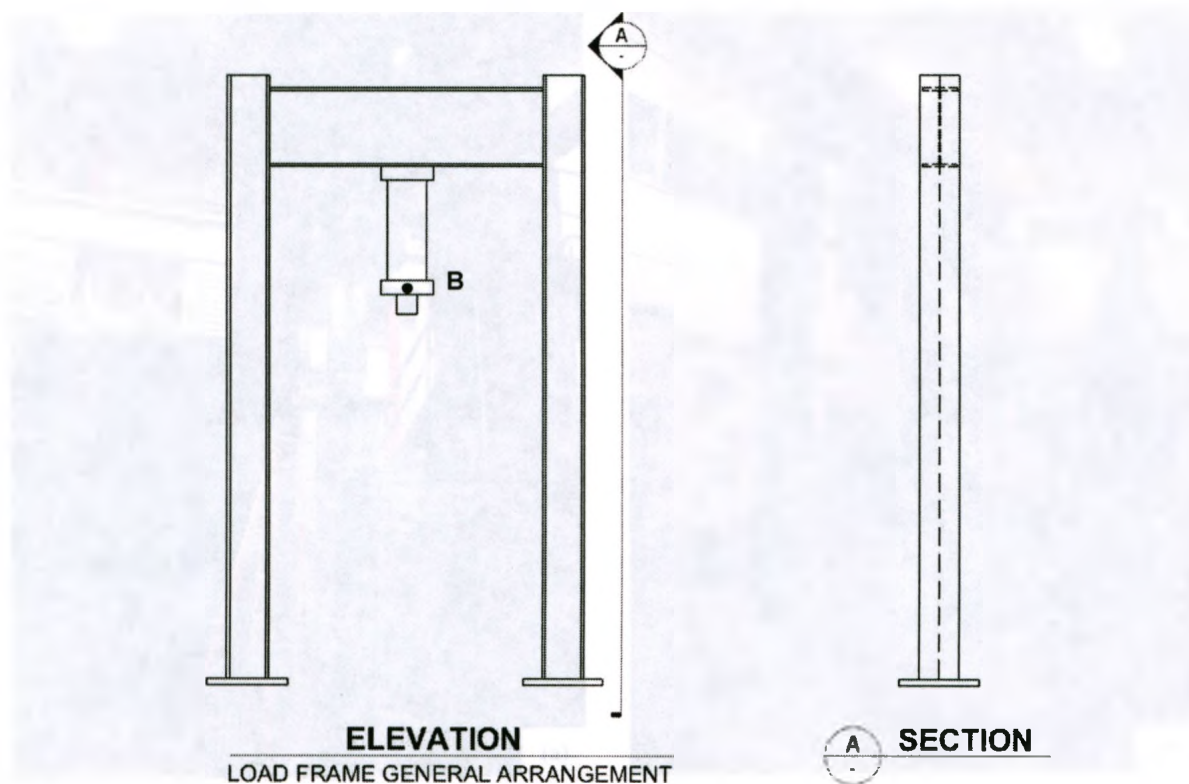


Figure 3-5: Load Frame General Arrangement

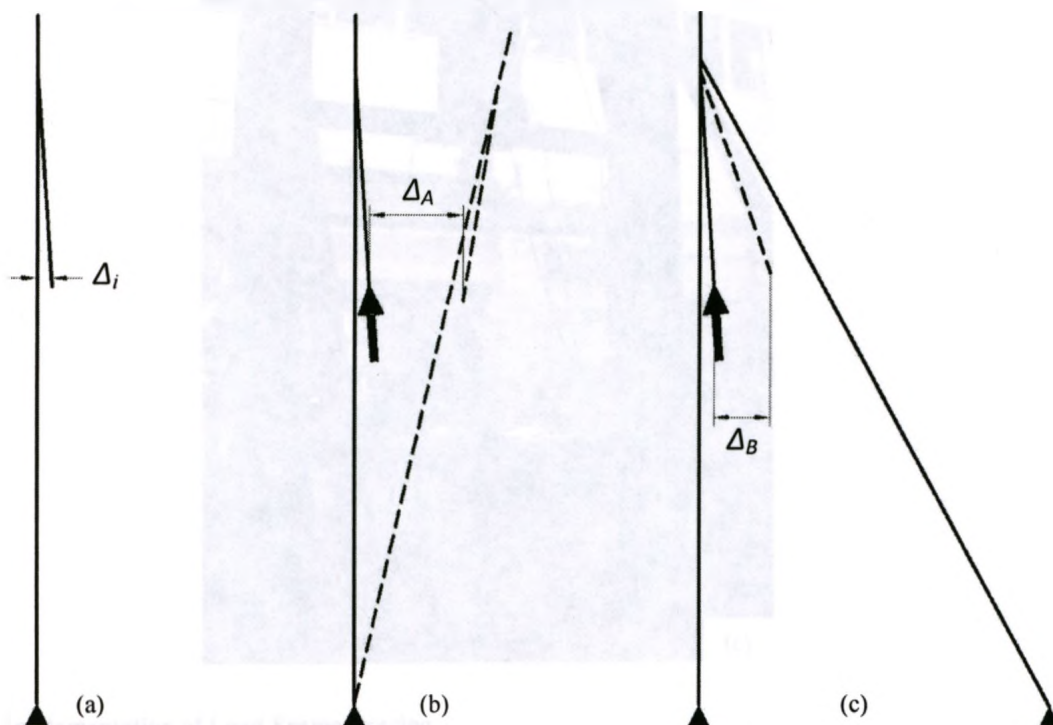


Figure 3-6: Lateral Deformations Observed in Load Frame

- (a) Undeformed Shape of Unbraced Frame ( $\Delta_i$  = initial actuator out-of-straightness)
- (b) Observed Deformation of Unbraced Frame
- (c) Observed Deformation of Braced Frame





**Figure 3-7: Implementation of Load Frame Bracing**

(a) Original Unbraced Frame (during initial capacity test)

(b) Frame With Diagonal Braces

(c) Frame With Actuator Head Brace Installed

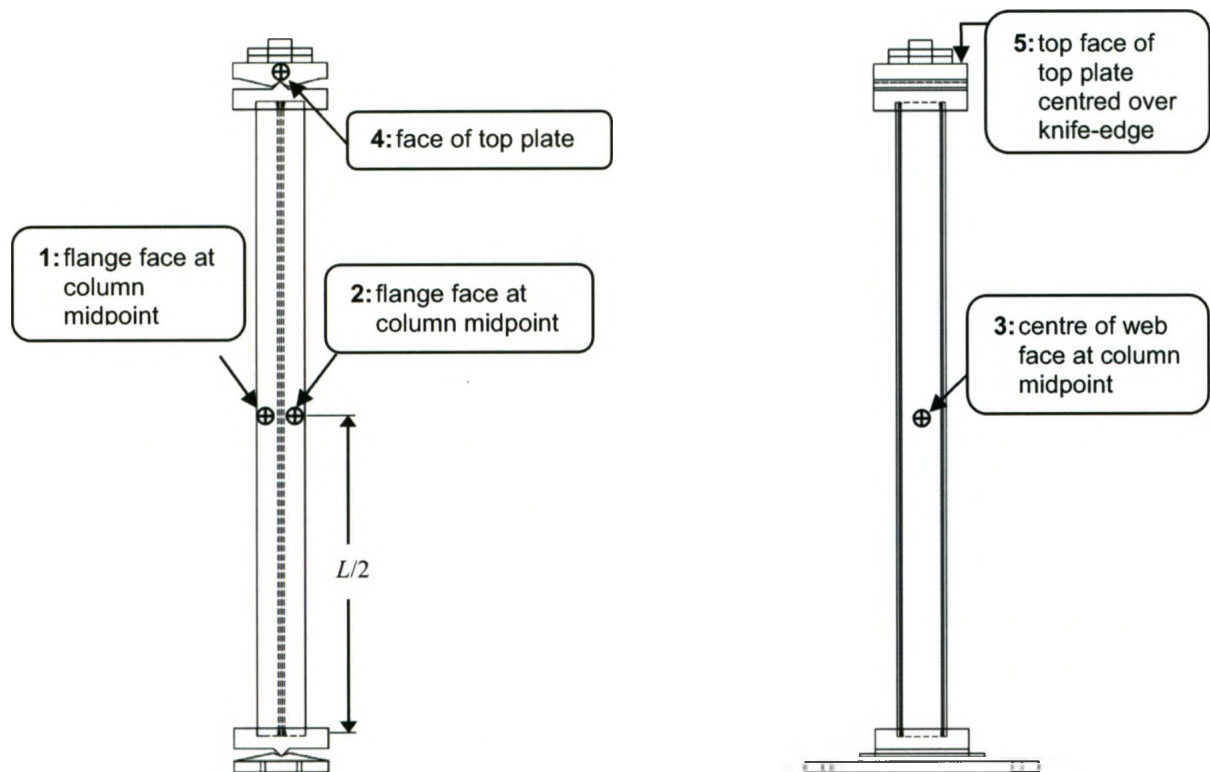


Figure 3-8: Displacement Transducer Locations

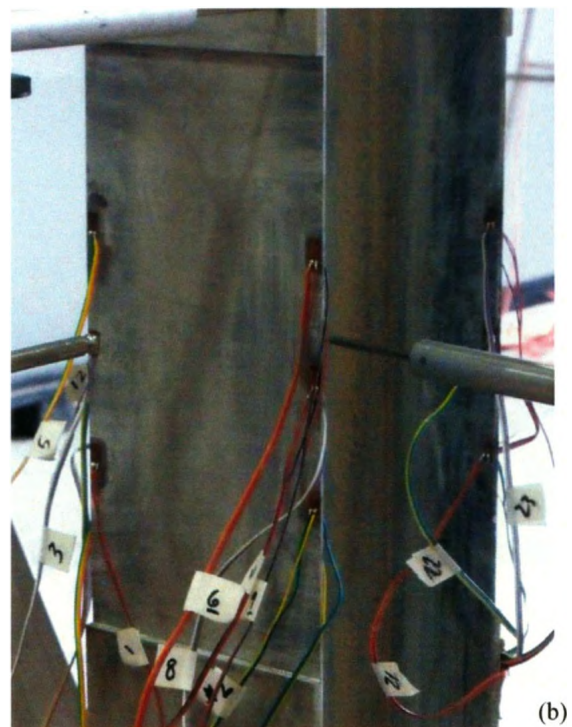
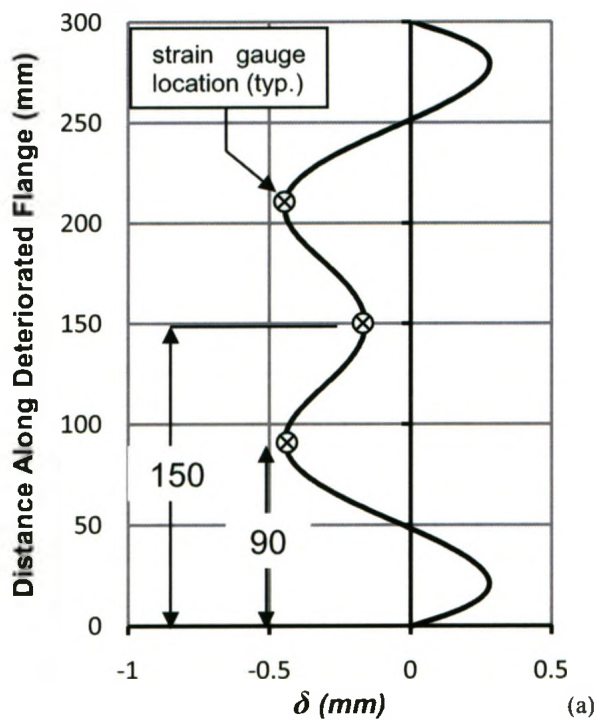
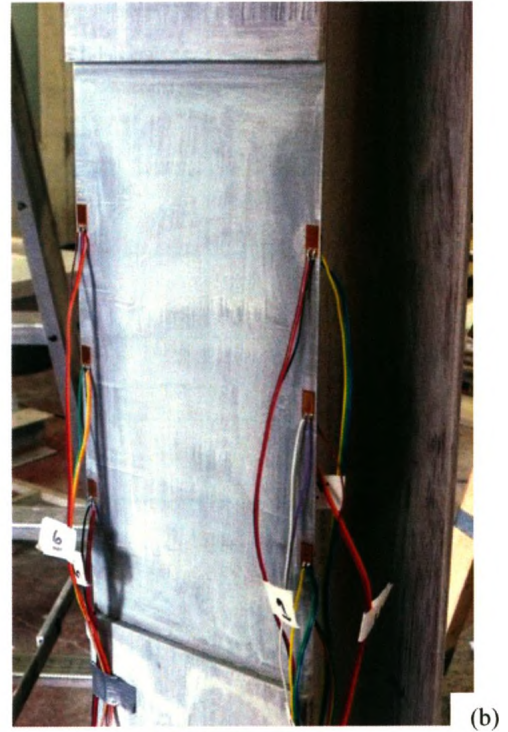
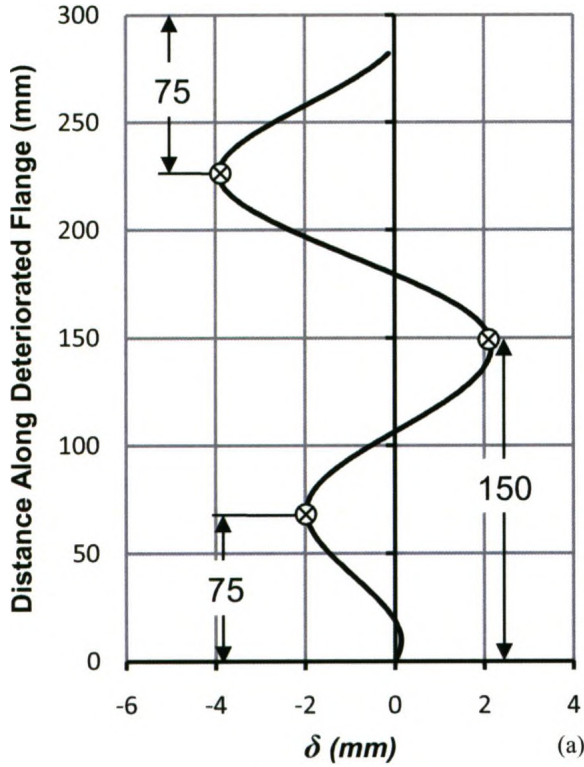


Figure 3-9: Strain Gauge Locations for Column 2

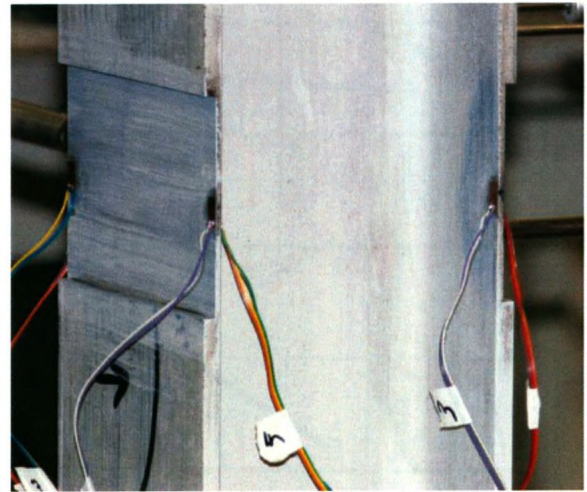
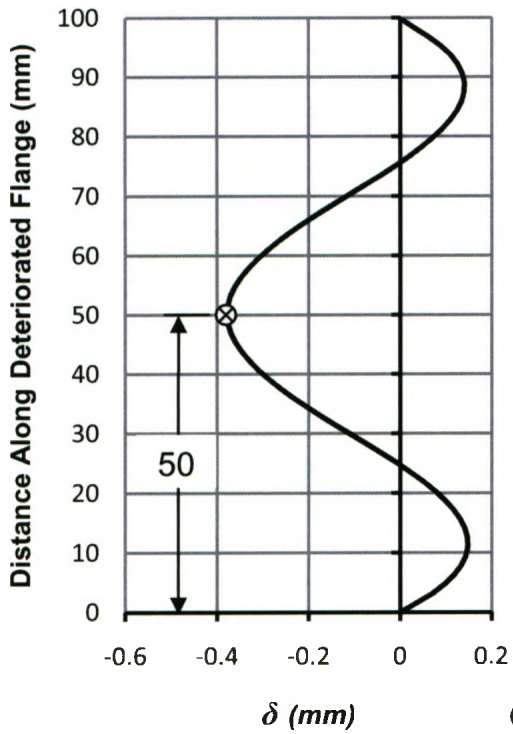
(a) Predicted Local Buckle

(b) Strain Gauge Locations in Deteriorated Region

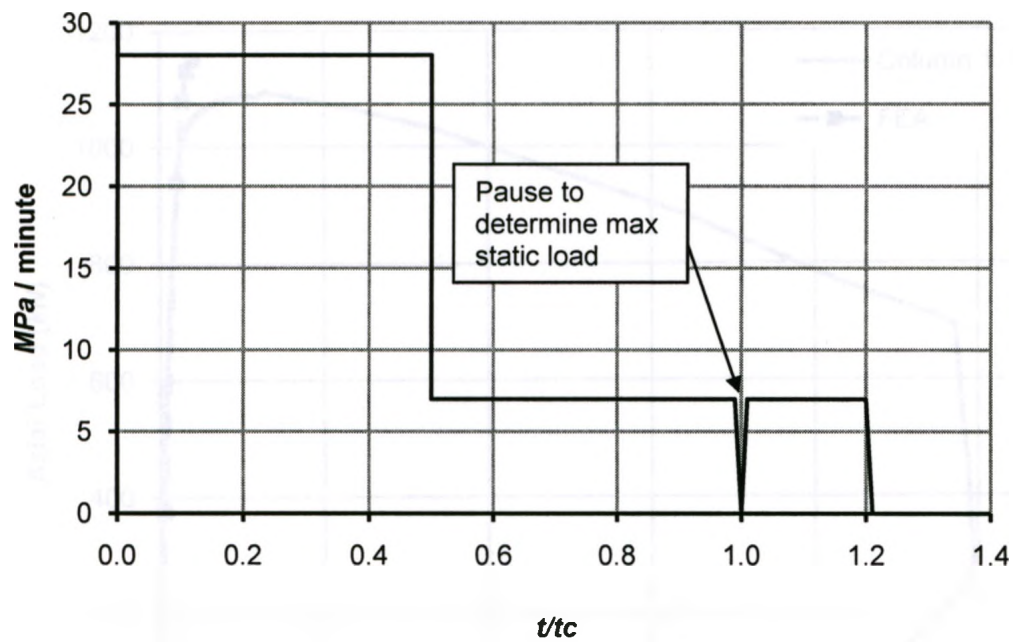




**Figure 3-10: Strain Gauge Locations for Column 3**  
 (a) Predicted Local Buckle  
 (b) Strain Gauge Locations in Deteriorated Region



**Figure 3-11: Strain Gauge Locations for Columns 4 and 5**  
 (a) Predicted Local Buckle  
 (b) Strain Gauge Locations in Deteriorated Region



Where:  $t_c$  is the time required to achieve the maximum compressive load

Figure 3-12: Actuator Loading Rate Used during Column Tests

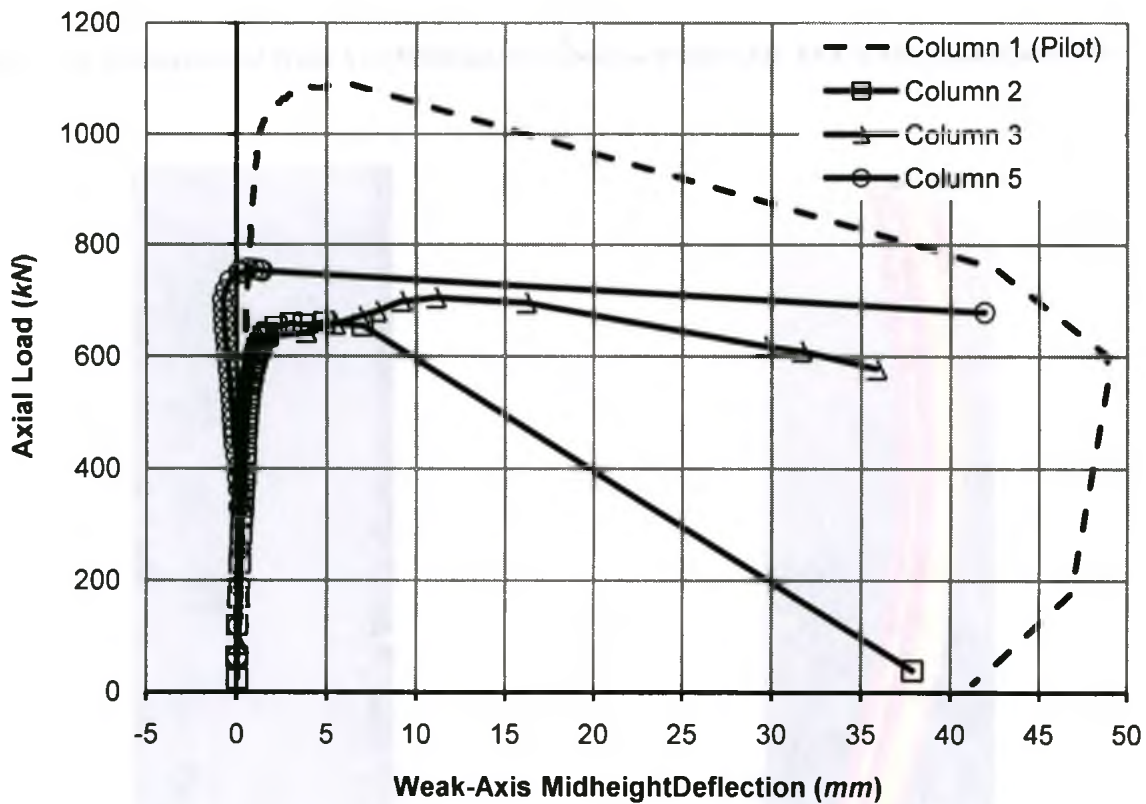


Figure 3-13: Comparison of Overall Column Buckling Deformation for Column Tests 1, 2, 3 and 5

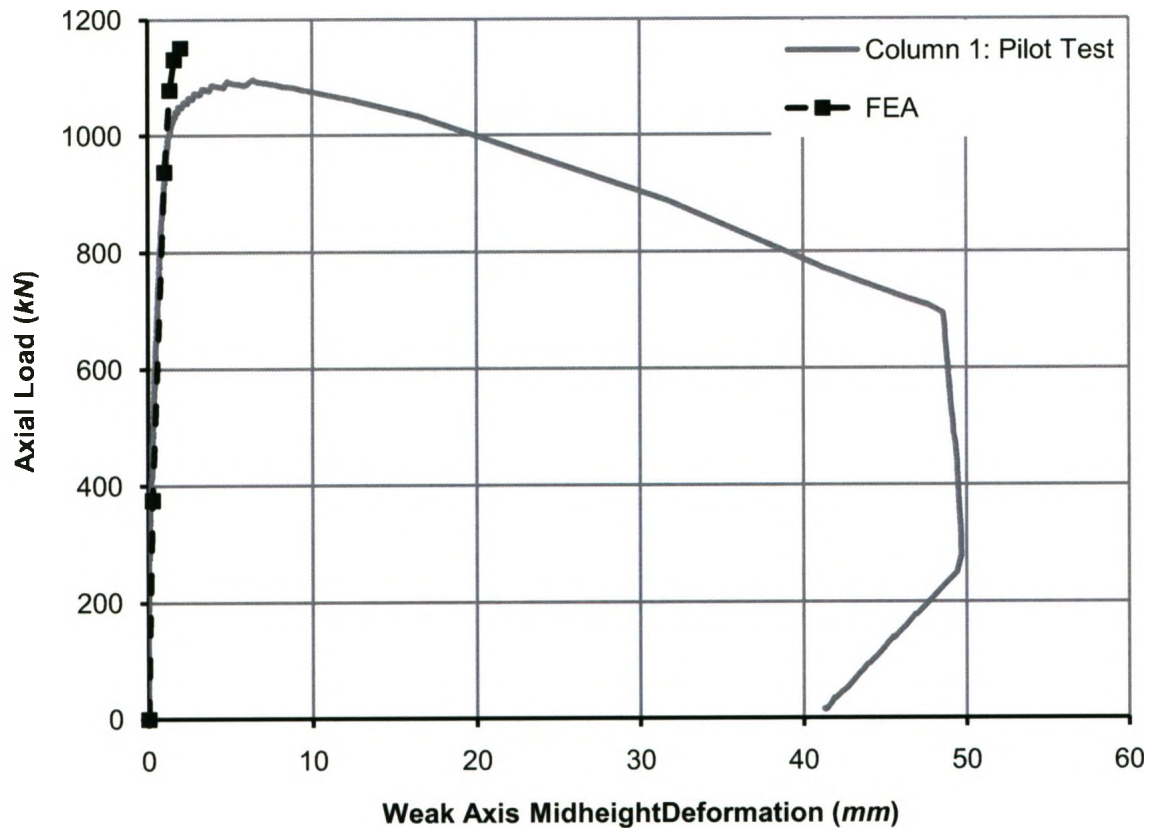


Figure 3-14: Comparison of Weak Axis Midheight Deformation Predicted by FEA to Test Data (Column 1)

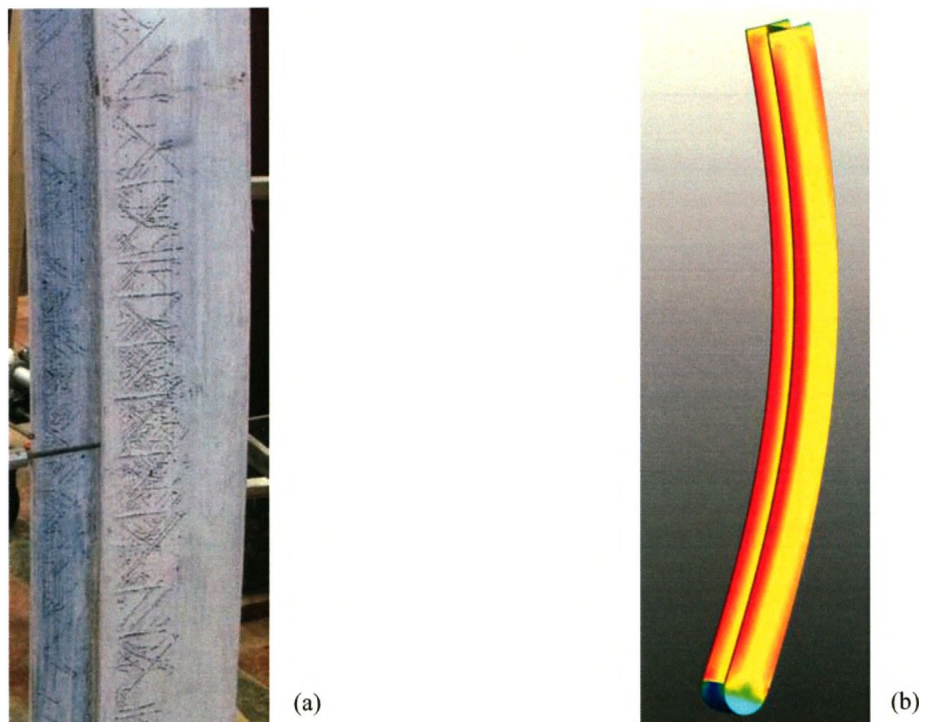


Figure 3-15: Yielding in Flange of Column 1

(a) Leuder Lines Observed

(b) Extent of Yielding Predicted by FEA (shown in red)





Figure 3-16: Plastic Hinge at Midheight (Column 2)

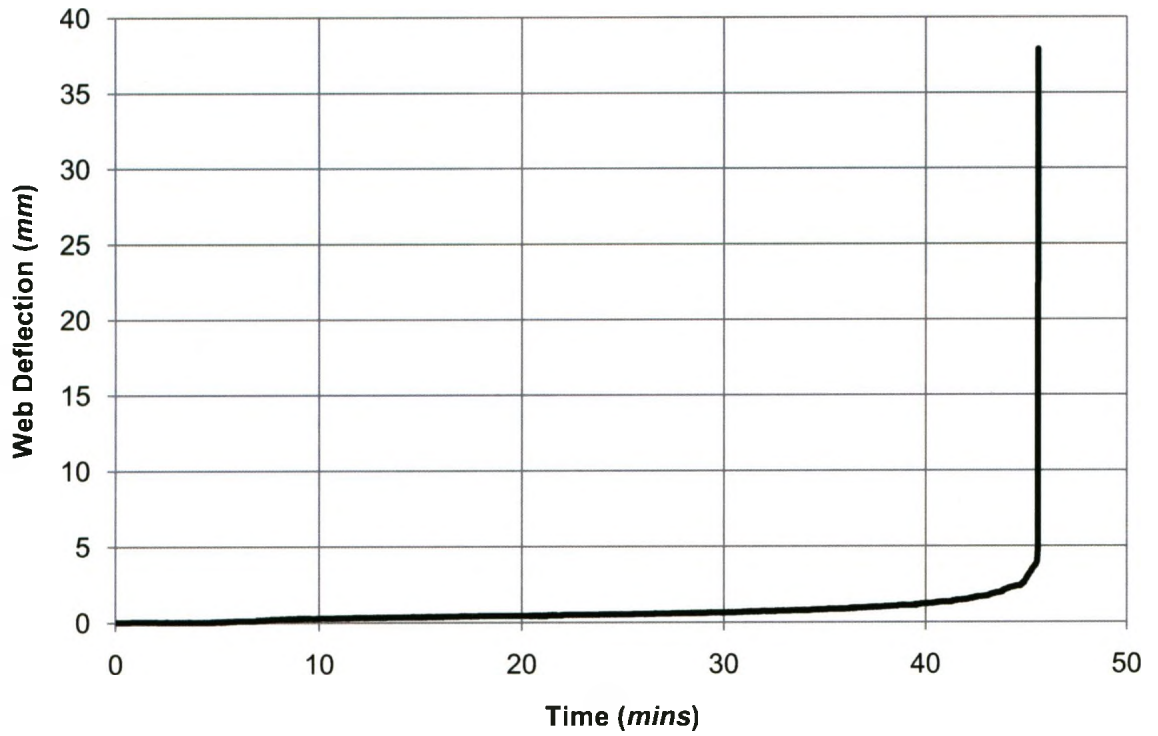
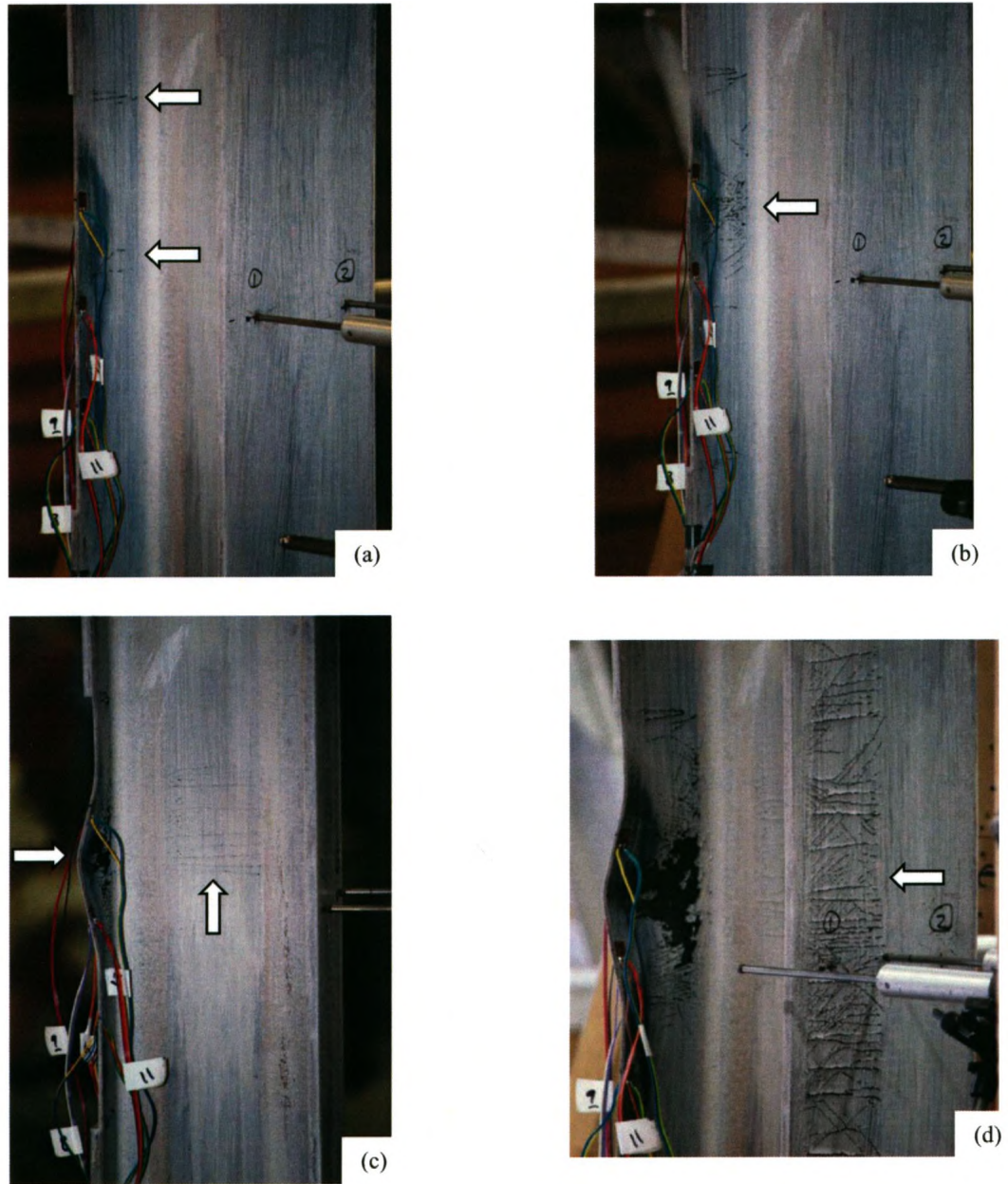


Figure 3-17: Web Displacement in Direction of Weak Axis Buckling Over Time of Test Column 2



**Figure 3-18: Failure Progression in Column 3**

- (a) Yielding begins in the deteriorated flange.
- (b) Yielding progresses in the deteriorated flange.
- (c) Local buckling in deteriorated flange, yielding extends to web.
- (d) Undeteriorated flange yields and buckles.

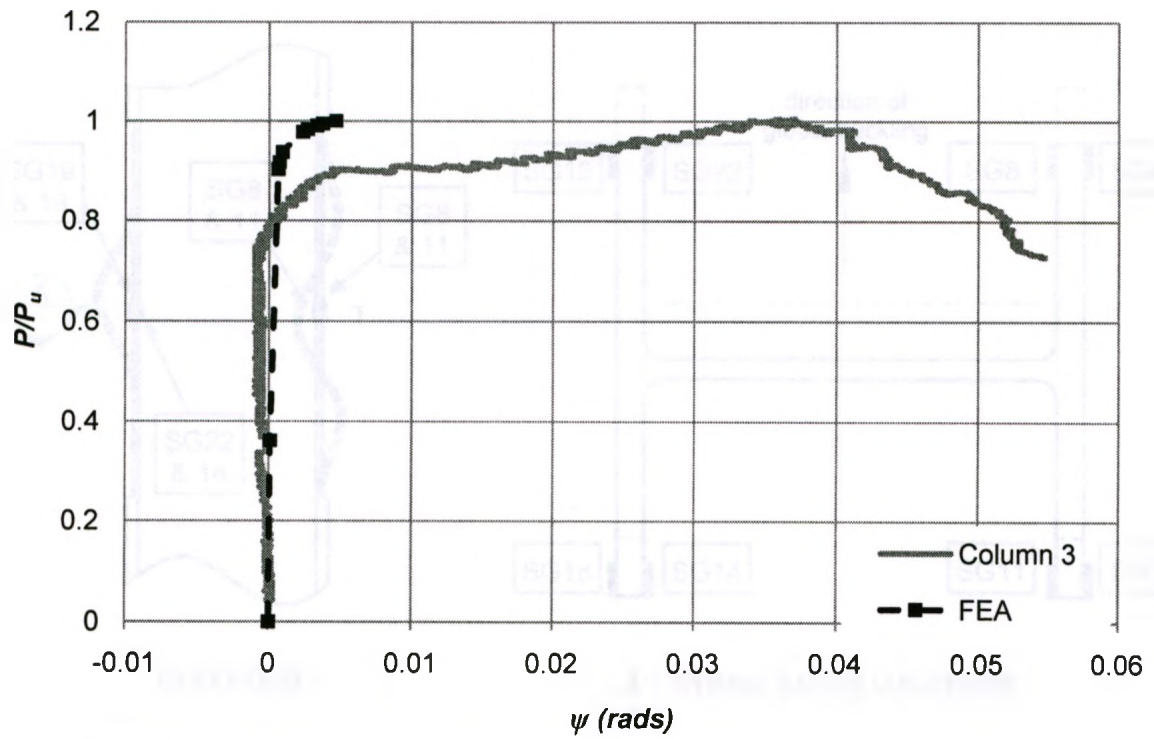


Figure 3-19: Comparison of Curvature Predicted by FEA to Test Data (Column 3)

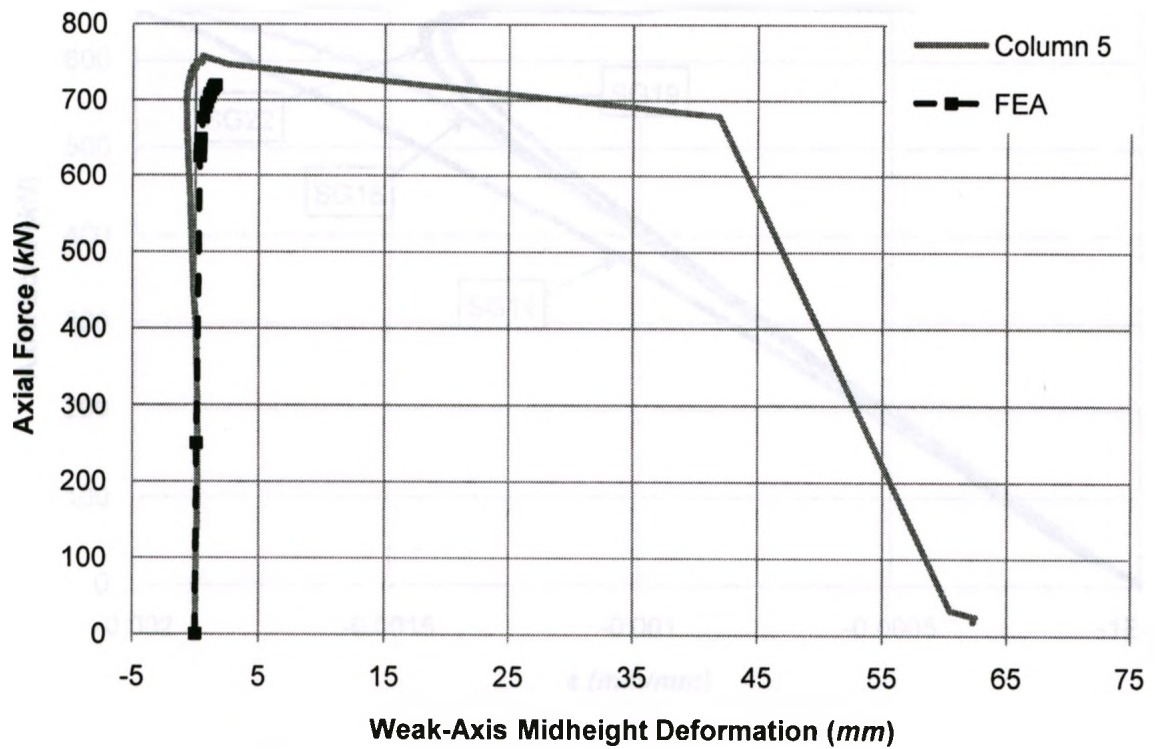


Figure 3-20: Comparison of Weak Axis Midheight Deformation Predicted by FEA to Test Data (Column 5)



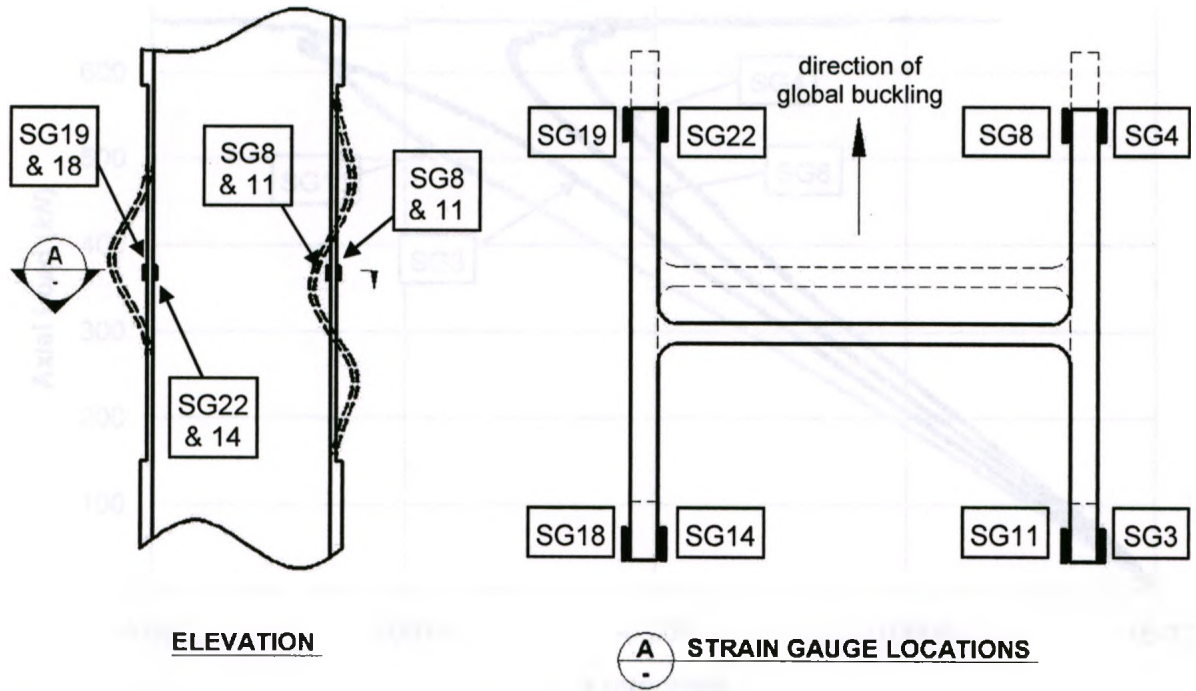


Figure 3-21: Strain Gauge Locations on Column 2 Relative to Failed Shape

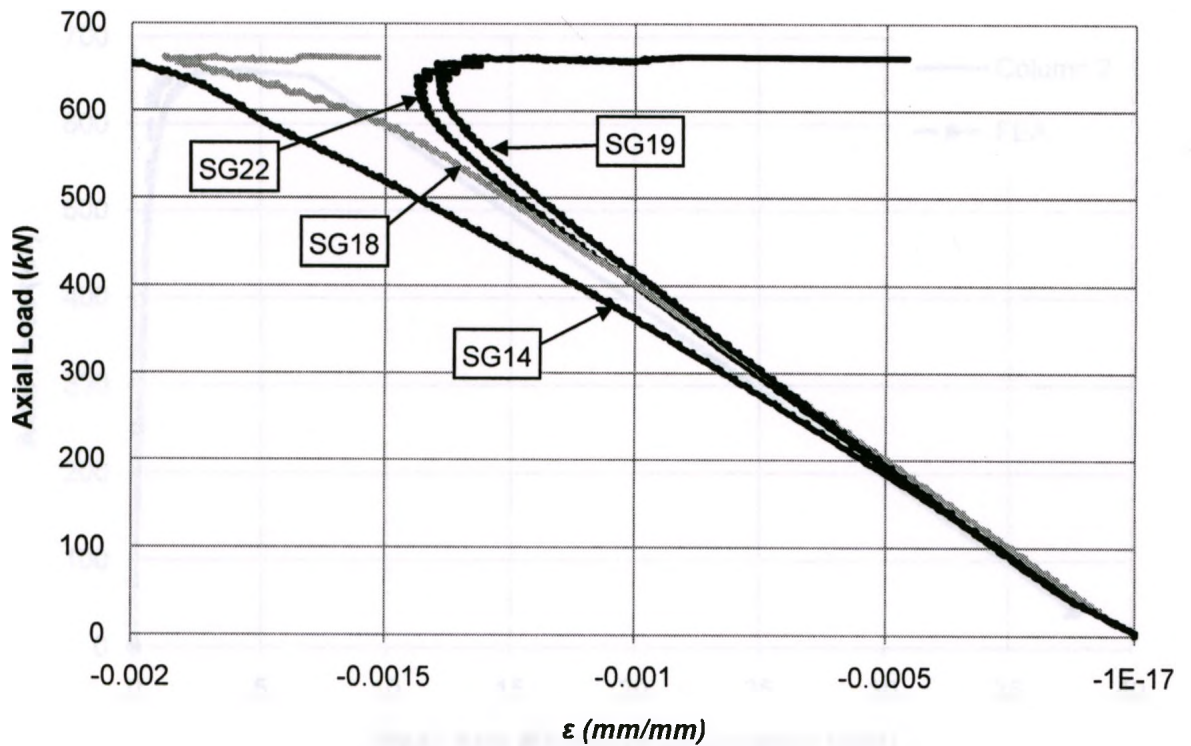


Figure 3-22: Strain Gauge Data for Column 2 (Left Flange)

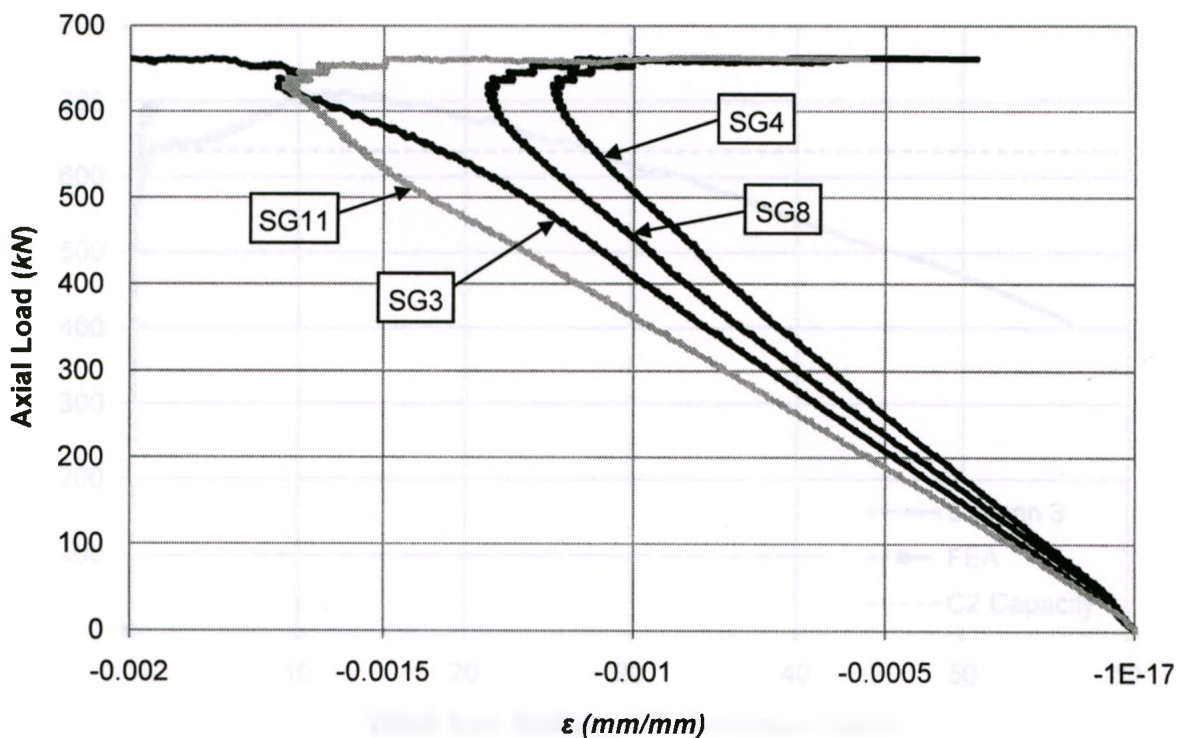


Figure 3-23: Strain Gauge Data for Column 2 (Right Flange)

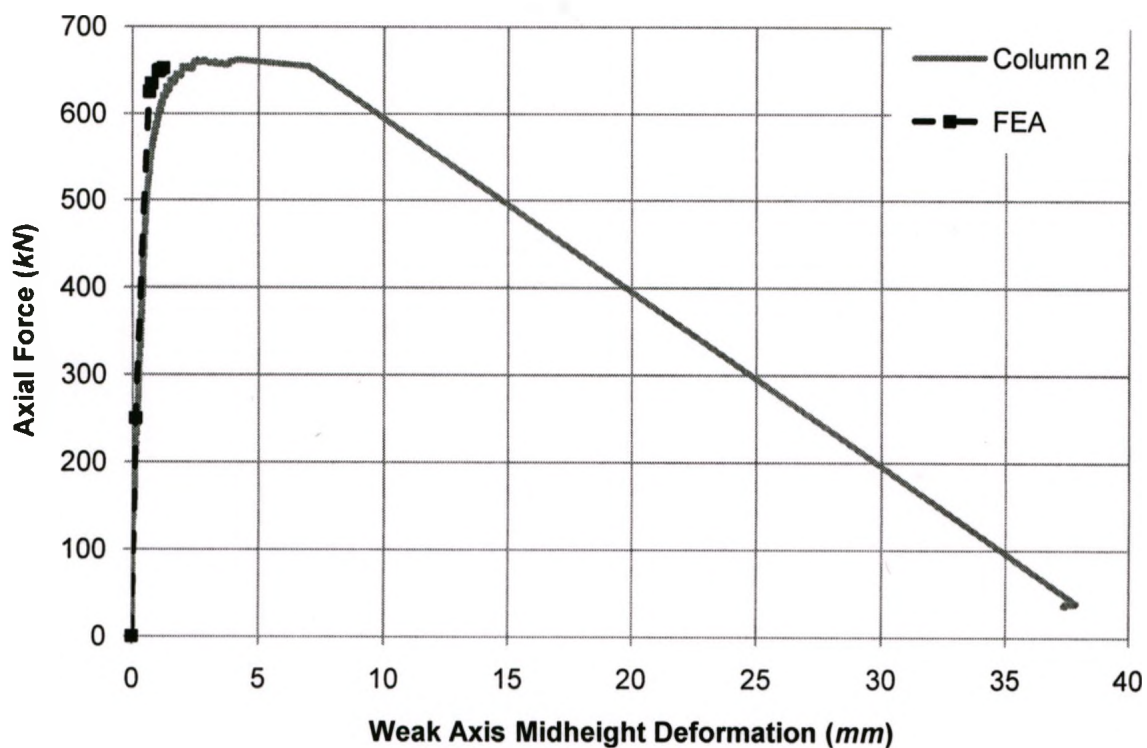


Figure 3-24: Comparison of Weak Axis Midheight Deformation Predicted by FEA to Test Data (Column 2)

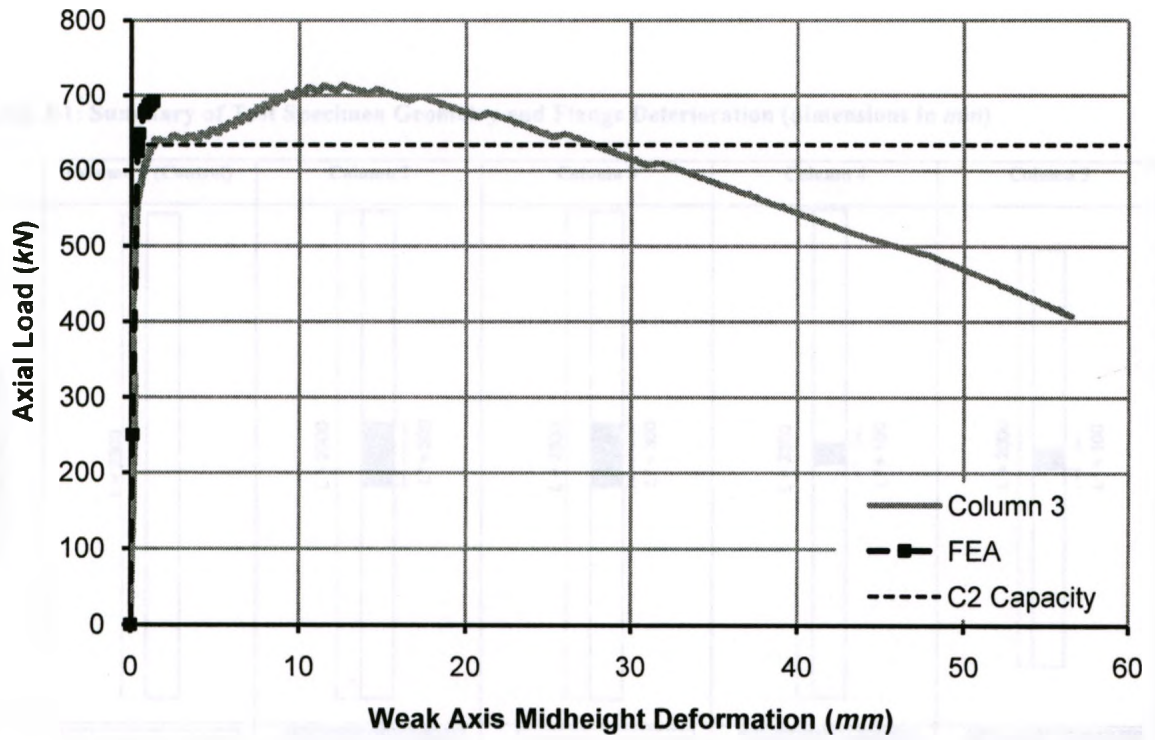


Figure 3-25: Comparison of Weak Axis Midheight Deformation Predicted by FEA to Test Data (Column 3)

Table 3-1: Summary of Test Specimen Geometry and Flange Deterioration (dimensions in mm)

	Column 1 (Control)	Column 2	Column 3	Column 4	Column 5
COLUMN OVERVIEW	<p><math>L = 2300</math></p>	<p><math>L = 2300</math> <math>L^* = 300</math></p>	<p><math>L = 2300</math> <math>L^* = 300</math> <math>50^\circ</math></p>	<p><math>L = 2300</math> <math>L^* = 100</math></p>	<p><math>L = 2000</math> <math>L^* = 100</math></p>
CROSS-SECTION AT MIDPOINT		<p><math>t^* = 3.5</math></p>	<p><math>t^* = 3.5</math></p>	<p><math>t^* = 3.5</math></p>	<p><math>t^* = 3.5</math></p>




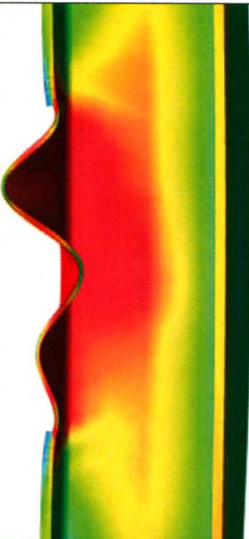
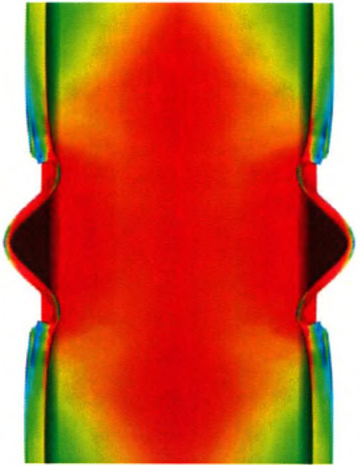
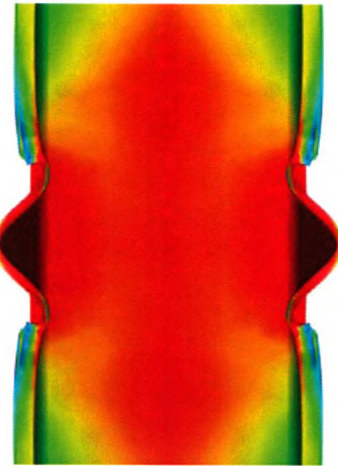
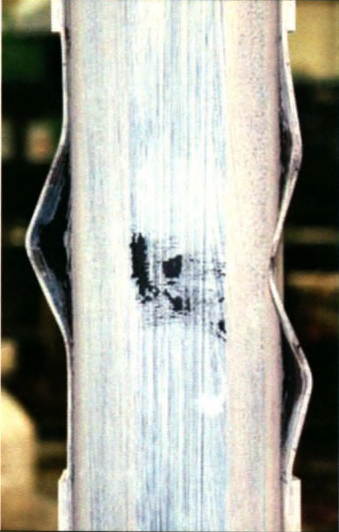
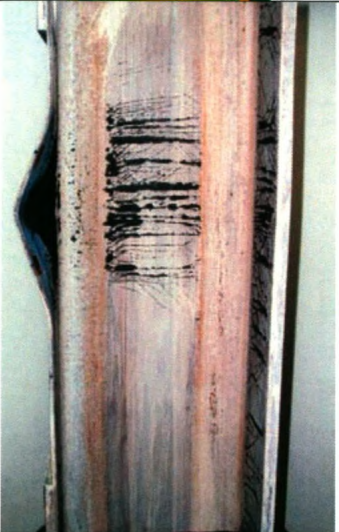
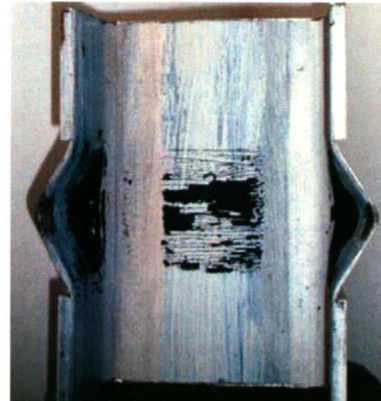
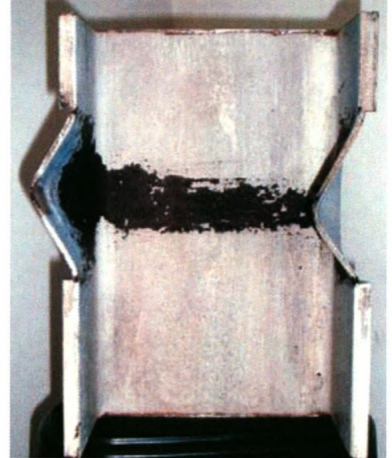
Table 3-2: Summary of Test Data

Specimen	Camber (mm)	Sweep (mm)	$F_y$ -Flange (MPa)	$P_{FEA}$ (kN)	$P_t$ (kN)	$P$
Column 1 (Pilot)	0.5	1.1	365	1150	1090	0.948
Column 2	0.1	0.5	368	652	653	1.002
Column 3	0.8	1.1	368	692	710	1.026
Column 4	0.5	1.0	365	641	664	1.036
Column 5	1.0	0.6	380	719	749	1.042
Mean =						1.010
Std. Dev. =						0.038
CoV =						3.8%

Table 3-3: Material Data from Tensile Coupon and Stub Column Tests

Specimen	Tensile Coupons		Stub Columns		
	Flange $F_y$ (MPa)	Web $F_y$ (MPa)	Average $F_y$ (MPa)	Max $\sigma_r$ (MPa)	$\frac{\sigma_r}{F_y}$
Column 1 (Control)	365	364	370	40	10.8%
Column 2	368	371	372	33	8.9%
Column 3	368	371	372	33	8.9%
Column 4	365	364	370	40	10.8%
Column 5	380	394	378	25	6.6%

**Table 3-4: Comparison of Local Buckle Geometry Observed in Failed Test Specimens and Predicted by FEA**

	Test Column 2	Test Column 3	Test Column 4	Test Column 5
FEA				
TEST				

## CHAPTER 4: SENSITIVITY ANALYSIS

### 4.1 INTRODUCTION

The objective of the research reported in this chapter is to determine the sensitivity of the compressive strength of a simply supported steel W-shape column to several geometric parameters that quantify flange section loss caused by corrosion. In this case, compressive strength is defined as the maximum load that the column can withstand, after which either excessive deflections cause column instability or section yielding prevents the member from resisting further compressive loading. As shown in Figure 4-1, the dimensional variables that will be examined in the sensitivity study are: extent of flange loss  $(1-t^*/t_o)$ , where  $t^*$  is the thickness of the deteriorated flange and  $t_o$  is thickness of the original flange; length of deterioration ( $L^*$ ); distance of the corroded region from the column midpoint ( $y^*$ ); and, initial out-of-straightness in the weak axis direction ( $\delta$ ). Table 4-1 summarizes the ranges of each parameter, selected to clarify how the critical local buckling load and primary failure mechanism (yielding, local buckling, intermediate column buckling, or Euler buckling) are influenced. The cross section aspect ratio ( $d/b$ ), the ratio of the flange area to web area ( $A_f/A_w$ ), and symmetric versus non-symmetric flange losses will also be investigated. As shown in the reference sketches to the left of Table 4-1, symmetric flange loss represents uniform corrosion of both flanges whereas unsymmetric flange loss represents uniform corrosion of a single flange only. The ranges of parameters investigated do not necessarily reflect realistic



conditions that may be encountered in a typical bridge, but are exaggerated to explore the underlying mechanics behind local buckling failures.

## 4.2 SENSITIVITY ANALYSIS RESULTS

Although the sensitivity analysis has been carried out for a W150x30 shape with a yield strength,  $F_y$ , of 350 MPa, the results presented in this section are expressed as much as possible in dimensionless form, to be more broadly applicable. The W150x30 has an overall depth,  $d$ , of 157 mm, a flange that is 153 mm wide by 9.3 mm thick, and a web thickness,  $w$ , of 6.6 mm. Linear variations of residual stresses in the flanges and web, as shown in Figure 2-3, with maximum values of  $0.3F_y$ , are assumed.

### 4.2.1 Extent of Flange Section Loss

Flange section losses of 0% (0 mm), 25% (2.33 mm), 50% (4.65 mm), 62.5% (5.81 mm), and 75% (6.98 mm) were considered. These losses cause flange width-to-thickness ratios,  $b/2t^*$ , to vary from  $154/\sqrt{F_y}$  to  $614/\sqrt{F_y}$  as shown in Table 4-2. The limits given in CAN/CSA S6-06 (CSA 2006) and CAN/CSA S16-09 (CSA 2009) indicate that shapes with  $b/2t^* > 200/\sqrt{F_y}$  should not be expected to achieve the yield capacity of the flange but will fail by local buckling. Local buckling might therefore be expected to govern the capacity of sections with 25% or more flange section loss.

Neglecting the dotted lines, Figure 4-2 illustrates the sensitivity of the axial capacity to flange section loss for a W150x30 column with a 200 mm length of local deterioration on both flanges at mid-height. Clearly, localized changes in flange thickness can have a significant impact on compressive strength, particularly for low slenderness ratios.

Strength loss is relatively less at higher slenderness ratios, and the axial capacity tends to converge to that of the undeteriorated column, except when flange section loss is 75%, the worst case examined. Such extreme cross-sectional losses cause local buckling to occur at loads that are less than the Euler buckling load of the undeteriorated column because the applied stress is markedly amplified in the region of deterioration.

Table 4-3 compares global and local deformed shapes at failure of columns with a constant flange section loss of 50% for various slenderness ratios. The primary failure mechanism tends to transition from local buckling to Euler buckling as the column slenderness ratio increases from 15 to 172. Stocky columns exhibit large local buckling deformations at failure in the deteriorated region but do not appear to have significant global buckling deformations. Slender columns, on the other hand, appear to fail mainly by elastic buckling with very little local deformation. The effect of flange section loss on buckling capacity and failure mode is best described by looking at slender columns, stocky columns and intermediate columns separately.

### Slender Columns

The axial capacity of slender columns with local deterioration tends to converge to that of the undeteriorated column because Euler buckling occurs when the applied stress is much less than the critical local buckling stress. Table 4-4 compares the deformed shapes at failure of slender columns having slenderness ratios  $kL/r = 159$ , where  $kL$  is the effective length and  $r$  is the radius of gyration, with varying flange section losses. The degree of deterioration can affect both the load and slenderness ratio at which Euler-dominated buckling failure occurs. Symmetric flange section loss of 25% causes a

reduction in axial capacity of only 3% compared to that of the undeteriorated column. However, for the worst case of 75% symmetric flange section loss, the compressive resistance is only 59% of that of the undeteriorated column. As confirmed by the local deformation for this member shown in Table 4-4, local buckling contributes to the reduction of axial capacity. As the flange loss increases, the local buckle becomes more defined, particularly for the cases of 62.5% and 75% flange loss shown, and the column fails essentially by local buckling before Euler buckling occurs.

In general, very slender members fail by Euler buckling because critical stresses are too small, even in the reduced cross sections, to cause local buckling unless the flange is very severely deteriorated.

### Stocky Columns

Stocky columns subject to localized deterioration also have reduced axial resistances. In general, stocky columns with localized deterioration fail by yielding or local buckling, depending on the severity of section loss. The deformed shape of stocky columns at failure suggests that this decrease in capacity is largely due to local buckling. This can be seen in Table 4-3: clearly significant local deformations occur at failure in columns with low slenderness ratios (e.g.  $kL/r = 15$  and  $kL/r = 41$ ).

At the left edge of Figure 4-2, the failure load of stocky columns determined by FEA, shown by the solid lines, are compared with the yield capacity of the reduced cross section,  $C_y$ , shown by the dotted lines for  $0 < kL/r < 20$ . The  $C_y$  value is computed as:

$$[4.1] \quad C_y = A_d F_y$$

where:  $A_d$  is the reduced cross-sectional area [ $mm^2$ ]

Clearly, there is little difference between the value computed using Eq. [4.1] and the FEA-predicted failure load until the flange loss is between 50% and 62.5, where the difference jumps from 1.7% to 8%, as noted in the table in the corner of Figure 4-2. This indicates that while local buckling deformations may occur, they do not significantly decrease the axial capacity of stocky columns until the section loss becomes quite severe (i.e. in this case:  $0.50 < t^*/t_o < 0.375$ ).

Figure 4-3 examines several additional points in this region and compares flange section loss to the percent-difference between FEA-predicted failure loads and  $C_y$ . Local buckling does not reduce axial capacity by more than 5% until the flange section loss exceeds approximately 60%. This corresponds to a width-to-thickness limit of  $380/\sqrt{F_y}$  or nearly double the limit for columns that develop the yield capacity of the flange. If the width-to-thickness ratio of the deteriorated flange exceeds this limit, local buckling further reduces the yield capacity of the reduced cross section.

Similarly, Figure 4-4 shows flange section loss variation with the ratio  $\delta_{max}/t^*$ , where  $\delta_{max}$  is the maximum local buckling displacement at failure perpendicular to the flange and  $t^*$  is the thickness of the reduced flange. The method for determining  $\delta_{max}$  is shown in Figure 4-5: it is the maximum amplitude of the buckle measured from the original centreline of the undeformed flange. The limiting ratio that corresponds to 60% flange



loss is  $\delta_{max}/t^* = 0.45$ . This ratio gives a quantitative guideline for identifying when local buckling may be contributing to the reduction of axial capacity. It may not be useful in practice because loading approaching the failure load may cause  $\delta_{max}$  to escalate quickly.

### Intermediate Columns

Table 4-5 shows the failure progression of a W150x30 column with an intermediate slenderness ratio of 80.5 and 75% symmetric flange loss. The initial uniform curvature at  $P/P_{FEA} = 0$  is created by thermal loading as described in Chapter 2 to simulate sweep. At low loads, e.g.  $P/P_{FEA} \lesssim 0.56$ , the global deformed shape exhibits relatively uniform curvature and resembles that of early Euler buckling. However, at higher loads, local buckling at mid-height causes an unstable global plastic mechanism to develop. At failure, the deformed shape of the column consists essentially of two tangents that intersect at the local buckle at mid-height. Thus, intermediate columns can initially fail by local buckling which creates a plastic hinge at mid-height causing global inelastic instability.

### Summary

The axial capacity of columns with flange deterioration is very sensitive to the changes in flange loss for both stocky and intermediate columns but not necessarily for slender columns, unless the extent of deterioration is particularly severe.

Local buckling does not begin to significantly decrease axial capacity until the flange width-to-thickness ratio reaches  $380/\sqrt{F_y}$ , even though local deformations are observed in failed columns with a lower width-to-thickness ratio. Additionally, when analyzing

the FEA results, local buckling can be deemed to reduce the axial capacity when  $\delta_{\max}/t^* \geq 0.45$ .

#### 4.2.2 Symmetry of Flange Section Loss

The effect of symmetric and non-symmetric flange losses was examined concurrently with the extent of flange section loss  $(1-t^*/t_o)$ . Figure 4-6 shows how the axial capacity is affected by uniform flange losses across the width of one (non-symmetric) or both (symmetric) flanges of 25%, 50% and 75% of the flange thickness. As expected, as the extent of flange section loss increases, the capacity is more sensitive to the absence of symmetry. For the case of 75% flange section loss, the axial capacity of the section with symmetric flange loss is as much as 38% less than the capacity of the section with non-symmetric flange loss. For cases with less flange section loss, this difference reduces: for example, the column with 25% symmetric flange loss is only a maximum of 7% weaker than the column with 25% non-symmetric flange loss.

Non-symmetric flange loss increases the axial capacity because the reduction in cross-sectional area is only half that for symmetric flange loss. As shown in Figure 4-7, however, the relationship between strength gain and symmetry is complex because non-symmetric section loss introduces torsion that is magnified as buckling progresses. As demonstrated by test Column 3, in Figure 3-25, the response is even more complex because strain hardening can produce a post-local-buckling strength peak that is not captured by the FEA model.

Due to the complexity of including torsion in an evaluation procedure, and the unlikelihood of extremely severe corrosion progressing unnoticed in steel bridge compression members, only the case of symmetric flange loss will be further investigated. This is conservative because the symmetric loss case provides a lower bound on the capacity of a member with non-symmetric flange losses.

#### **4.2.3 Length of Deterioration**

Figure 4-8 shows how the axial capacity is affected by the length of deterioration ( $L^*$ ). A W150x30 column with flange loss centered at the midpoint was analyzed with lengths of deterioration of: 0 mm, 50 mm, 100 mm, 200 mm, 400 mm and full column length. The axial capacity is not particularly sensitive to the length of deterioration for very stocky and very slender columns, however, capacity loss becomes more evident for intermediate slendernesses, in this case when  $40 \lesssim kL/r \lesssim 100$ .

The worst case examined,  $L^*=L$ , is meant to simulate uniform corrosion over the full length of the member. When  $kL/r < 30$ , the axial capacity converges to the crushing capacity of the deteriorated cross section given by Eq. [4.1]. As expected, when  $kL/r > 30$ , the axial capacity is further reduced because uniform flange corrosion reduces the second moment of area of the entire column, and thus, decreases the critical Euler buckling load.

Because typical steel bridge compression members generally have slenderness ratios that fall in the intermediate range,  $L^*$  should be taken into consideration when evaluating localized deterioration. Long sections of deterioration should be treated as uniform corrosion over the full length of the column.



#### **4.2.4 Distance from Corroded Region to Column Midpoint**

Figure 4-9 shows how the distance from the centroid of the deteriorated region to the column midpoint ( $y^*$ ) affects axial capacity. W150x30 columns with relative distances of  $y^*$  equal to  $0L$ ,  $L/8$ , and  $L/4$  were considered. For stocky columns, where failure is largely governed by the yield capacity of the reduced cross section, the location of deterioration along the length of the column has no effect on compressive strength. As expected, for slender and intermediate columns the worst case is when the deterioration is centered at the column mid-point. While there is a minor increase in axial capacity for slender and intermediate columns as localized deterioration moves away from the column midpoint, the column curves align very closely indicating that the axial capacity of the deteriorated member is not very sensitive to  $y^*$ . For the purposes of evaluation it can be assumed, slightly conservatively, that deterioration occurs at the column midpoint,  $y^*=0$ , for all cases.

#### **4.2.5 Initial Out-of-Straightness**

Figure 4-10 shows how axial capacity is affected by initial out-of-straightness in the direction of weak-axis buckling ( $\delta$ ). A W150x30 column with flange deterioration centered at the midpoint was analyzed. Two cases of out-of-straightness were examined: sweeps of  $L/1000$  and  $L/500$ . Because it is permissible for steel mills to supply rolled shapes with a camber or sweep of up to  $L/1000$  (ASTM 2010), it is unsafe to assume the out-of-straightness to be less than  $L/1000$ .

Doubling the initial out-of-straightness can decrease axial capacity as much as 9.3% in intermediate columns. The effect of small changes in initial column out-of-straightness

on axial capacity, however, is minimal which is consistent with current literature (e.g. Galambos 1998).

Vehicle collision, pack rust, or other factors could potentially cause such larger initial out-of-straightness deflections to occur during the service life of a steel bridge compression member. Including out-of-straightness that occurs during the service life of a bridge in an evaluation method, however, is beyond the scope of this research study because other factors, such as local yielding and non-uniform deformation, complicate the analysis. If such distress is observed during an evaluation, a more detailed analysis is necessary.

#### 4.2.6 Cross-Section Aspect Ratio

The W150x30 section used throughout the sensitivity analysis has an aspect ratio roughly equal to 1.0. While most W-shapes used as columns are roughly square, the  $d/b$  ratio may vary and the effect on local buckling should be investigated. Figure 4-11 shows the custom cross section used in the analysis, which was created by modifying a W150x30 such that the modified cross section had the same cross-sectional area but  $d/b = 1.5$ , which is the upper limit for column shapes listed in the CISC "Handbook of Steel Construction" (CISC 2010). The cross-sectional width,  $b$ , remains constant, as does the geometry of the localized deterioration. The width-to-thickness ratio of the modified web is:  $h/w = 917/\sqrt{F_y}$ , and while this is greater than the Class 3 limit given in CAN/CSA S6-06 (CSA 2006) of  $h/w \leq 670/\sqrt{F_y}$ , no local deformation in the web was observed throughout the FEA of the modified cross section. The reasoning for this is twofold:

1. The local buckling limits specified in S6-06 are conservative with respect to the FEA predictions. As stated in Section 4.2.1, while the Class 3 limit for flanges is  $b/2t \leq 200/\sqrt{F_y}$ , local buckling did not decrease axial capacity determined by FEA until  $b/2t = 380/\sqrt{F_y}$ .
2. The increased flange slenderness in the region with localized deterioration causes the flange to be 47% more slender than the Class 3 limit, while the modified web is only 27% more slender than the Class 3 limit. Therefore, it can be assumed that the flange would attract a local buckle before the web.

Figure 4-12 shows how axial capacity is affected by the aspect ratio ( $d/b$ ) of the cross section. Clearly it can be seen that changing the aspect ratio of a cross section does not affect axial capacity. Therefore, the simplified general conclusions of the sensitivity analysis are applicable to typical W-shape columns, irrespective of their  $d/b$  ratio.

#### **4.2.7 Ratio of Flange Area to Web Area**

The ratio of the flange area to web area ( $A_f/A_w$ ) for the W150x30 section used throughout the sensitivity analysis is 3.1. To ensure that the conclusions obtained in the sensitivity analysis are valid for a variety of W-shapes, the effect of  $A_f/A_w$  of the undeteriorated cross section on the axial capacity was investigated for both slender and stocky columns independently. Figure 4-13 shows the distribution of  $A_f/A_w$  for W-shape columns that may be prone to local buckling given 25% section loss. In general, as the gross cross-sectional area increases, so too does  $A_f/A_w$ . The mean ratio of flange to web area is 3.4 with a coefficient of variation of 12.2%, with a maximum of 3.8 and a

minimum of 2.5. The study presented in this section will examine  $2.5 \leq A_f/A_w \leq 4.0$ , however, 13 out of the 15 columns shown have a flange to web area approximately equal to or greater than that of a W150x30.

Figure 4-14 shows the effect of  $A_f/A_w$  on the axial capacity of stocky columns ( $kL/r = 15$ ). To isolate the effect of local buckling, the axial capacity predicted by FEA,  $C_{FEA}$ , is normalized by the yielding capacity of the net cross section,  $C_y$ , and plotted against the ratio  $t^*/t_o$ . For flange section losses where  $t^*/t_o = 0.38$ , the effect of local buckling is less pronounced for W-shapes with larger flange-to-web area ratios. As the flange section loss progresses ( $t^*/t_o < 0.38$ ),  $C_{FEA}/C_y$  converges for all ratios of flange to web area. This is consistent with Section 4.2.1 where it was shown that local buckling does not significantly reduce  $C_y$  until the width-to-thickness ratio of the deteriorated flange exceeds  $380/\sqrt{F_y}$ . Therefore, the data obtained from a W150x30 column would be slightly conservative for stocky columns with  $A_f/A_w \geq 3.1$ .

Figure 4-15 shows the effect of  $A_f/A_w$  for slender columns ( $kL/r = 159$ ). To isolate the effect of local buckling,  $C_{FEA}$  is normalized by the axial capacity of the undeteriorated column  $C_o$ . Clearly, the flange to web area has no significant impact on the axial capacity reduction caused by localized deterioration unless the flange section loss is particularly extreme, i.e.  $t^*/t_o \leq 0.25$ .



### 4.3 SUMMARY

Table 4-6 summarizes variables that will be included in the simplified evaluation technique presented in Chapter 5. They are based on conclusions made during the sensitivity analysis, which are summarized below.

The axial capacity of columns with local deterioration is very sensitive to the extent of flange loss for stocky and intermediate columns. Slender columns tend to be dominated by Euler buckling at failure except when the severity of flange loss becomes especially severe, as seen for the cases of 62.5% and 75% flange loss on a W150x30. While the axial capacity of stocky columns decreases for all cases of flange loss examined, the difference between the theoretical crushing capacity of the deteriorated cross section and the failure load determined by FEA does not deviate significantly until the flange loss on a W150x30 exceeds 60%. This infers that local buckling does not adversely affect axial capacity of stocky columns until the width-to-thickness ratio exceeds  $380 / \sqrt{F_y}$ .

Columns with localized deterioration may exhibit some local buckling deformation without a reduction in axial capacity. For a W150x30 column made from Grade 350 steel, this is true for flange losses less than 60%. This relationship can be further identified in the FEA when the ratio of the maximum deflection of the local buckle to the remaining thickness of the deteriorated flange is less than 0.45. If such conditions are present, the axial capacity is not significantly reduced by local buckling.

Columns with non-symmetric deterioration have increased strength compared to those with symmetric deterioration because less steel is removed from the cross section. Such

columns exhibit torsional deformations as they buckle and due to the complexity of including torsion in a simplified analysis, symmetric deterioration can conservatively be assumed.

The axial capacity of columns with local deterioration is sensitive to the length of deterioration  $L^*$ , so this variable should be included as a parameter in the proposed evaluation procedure. If  $L^*$  is especially long uniform loss along the entire length of the member should be assumed.

The axial capacity is not sensitive to the distance from the mid-height of the column to the deteriorated region,  $y^*$ . For the purposes of the proposed evaluation, it should be assumed that the deterioration is centered about column midpoint.

Although very large initial column out-of-straightness can affect axial capacity, it is not likely to occur in a bridge compression member except under extenuating circumstances which are beyond the scope of this research. Therefore, the proposed simplified assessment method will assume the worst case permitted by ASTM A6/A6M-10,  $L/1000$ . If an inspection reveals a greater out-of-straightness, a more detailed assessment will be required.

The axial capacity is not sensitive to the aspect ratio of the cross-section. Furthermore, the reduction in axial capacity caused by deterioration is not sensitive to the ratio of the flange to web area of the cross section for stocky or slender members unless the flange section loss is very extreme ( $t^*/t_o > 0.63$ ). Therefore, the proposed simplified



assessment method will be applicable to all W-shape columns regardless of  $d/b$  and for  $2.5 \leq A_f/A_w \leq 4.0$ .



Figure 1. Comparison with 2000 Edition

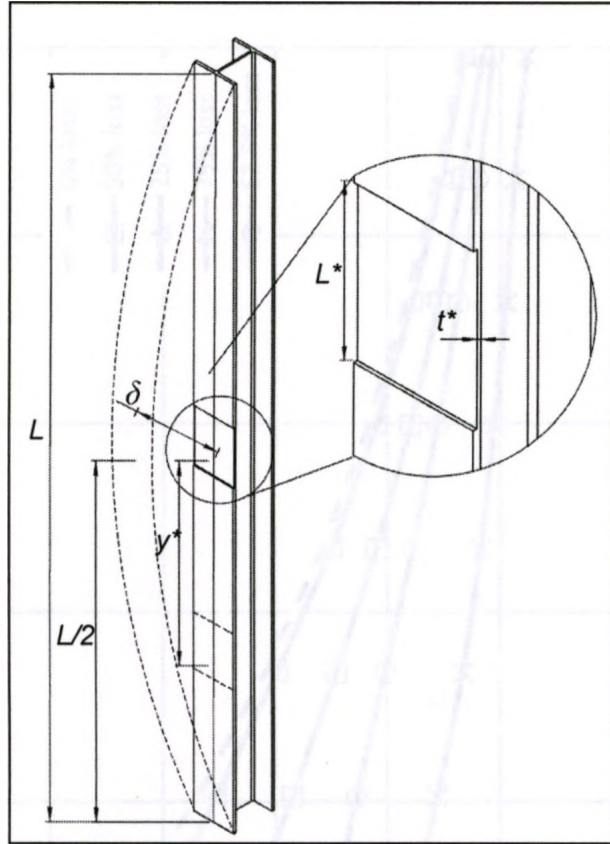


Figure 4-1: Variables in Sensitivity Analysis

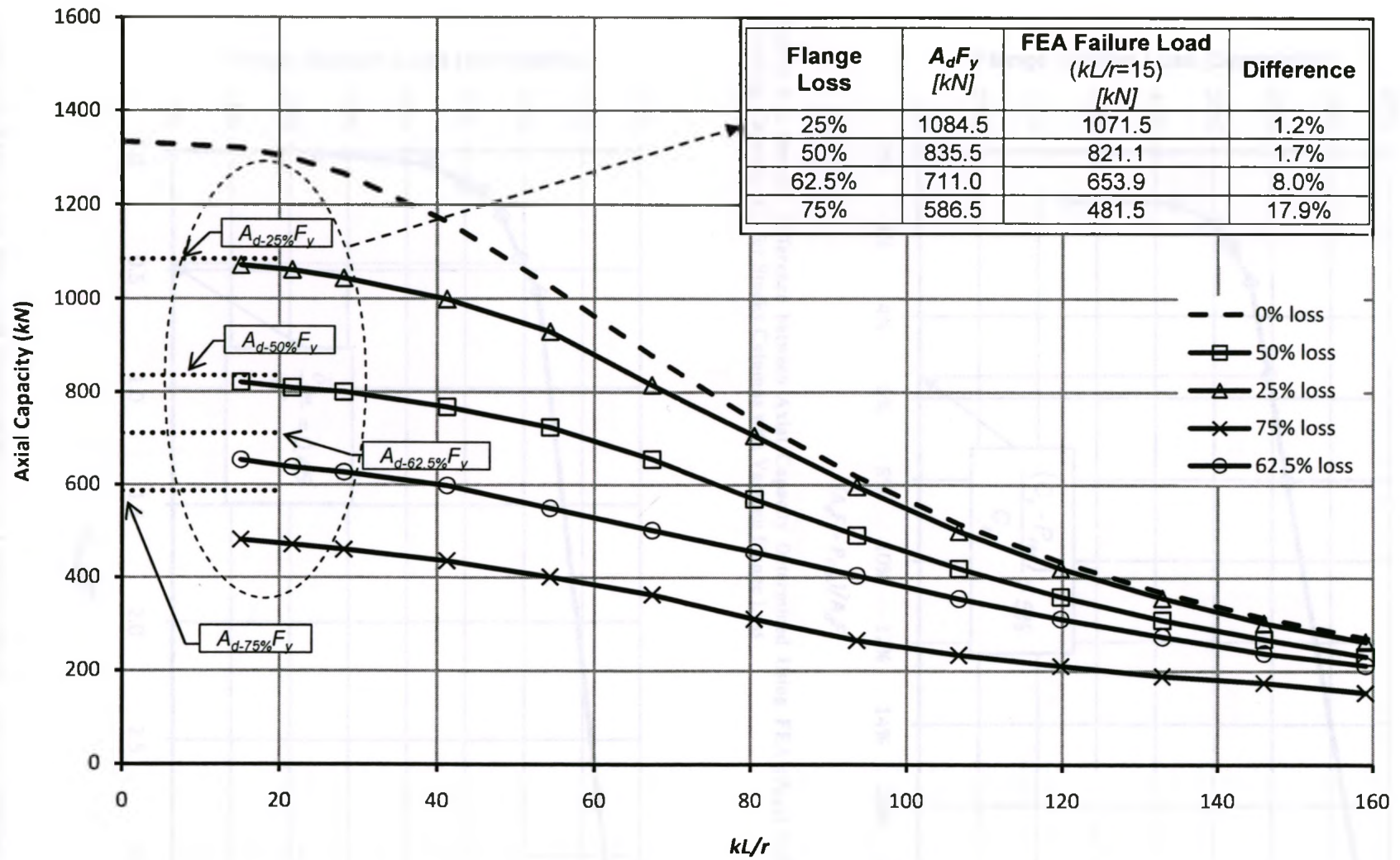


Figure 4-2: Sensitivity of Axial Capacity to Flange Loss (W150x30, Symmetric Deterioration,  $L^* = 200 \text{ mm}$ ,  $y^* = 0 \text{ mm}$ ,  $\delta = L/1000$ )  
 (Dotted lines compare FEA and Theoretical Crushing Capacity for Stocky Columns with Varying  $t^*/t_o$ )

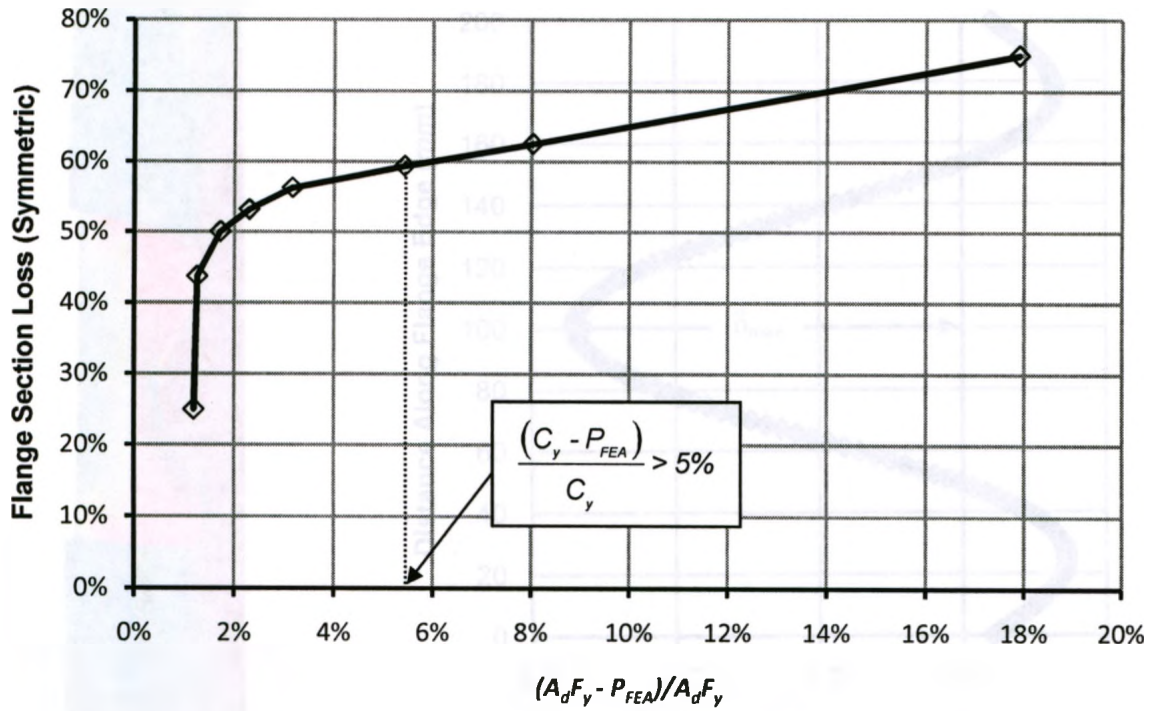


Figure 4-3: Percent Difference between Axial Capacity Determined Using FEA ( $P_{FEA}$ ) and the Theoretical Crushing Capacity ( $C_y$ ) for Stocky Columns with Varying Flange Loss

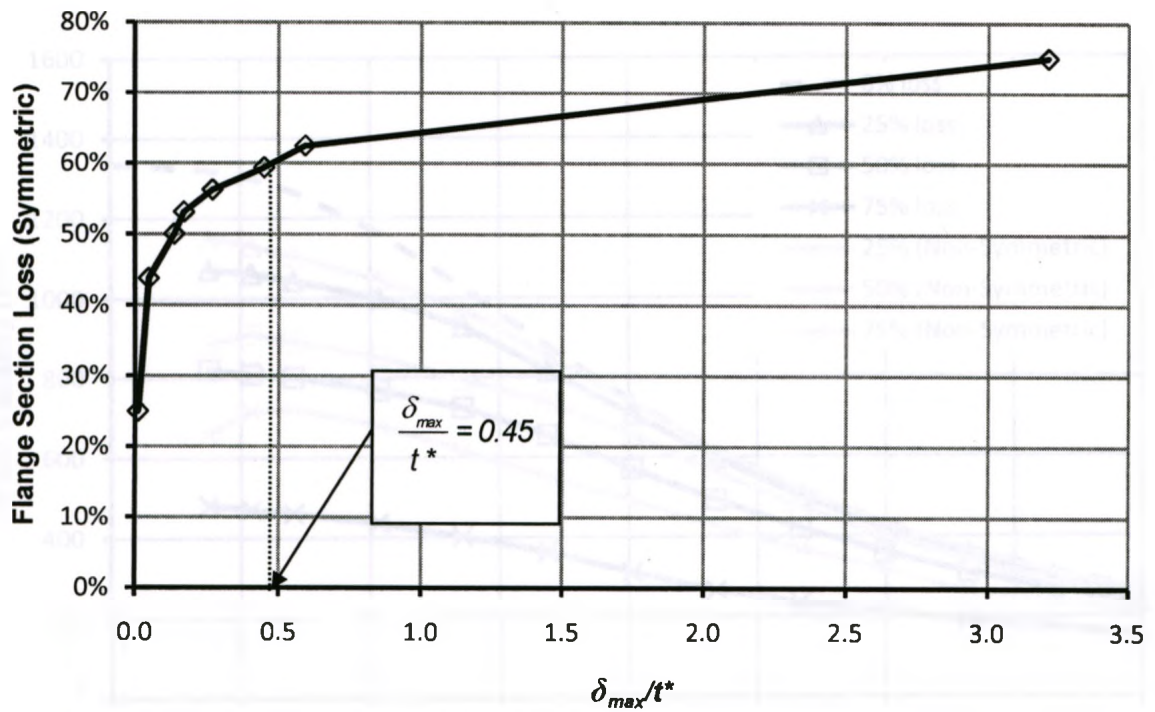


Figure 4-4: Ratio of the Maximum Displacement of the Local Buckle ( $\delta_{max}$ ) to the Thickness of the Reduced Flange ( $t^*$ ) for Varying Flange Loss



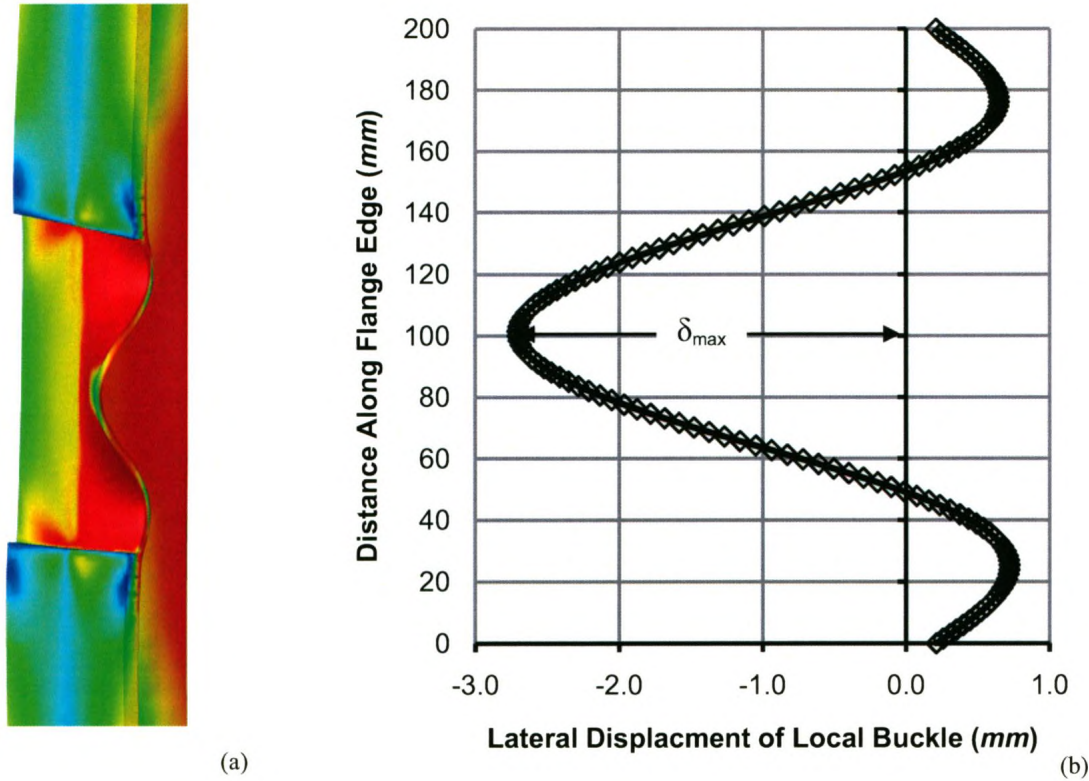


Figure 4-5: Method for Determining  $\delta_{max}$   
 (a) Deformed Shape after Failure  
 (b) Measurement of  $\delta_{max}$

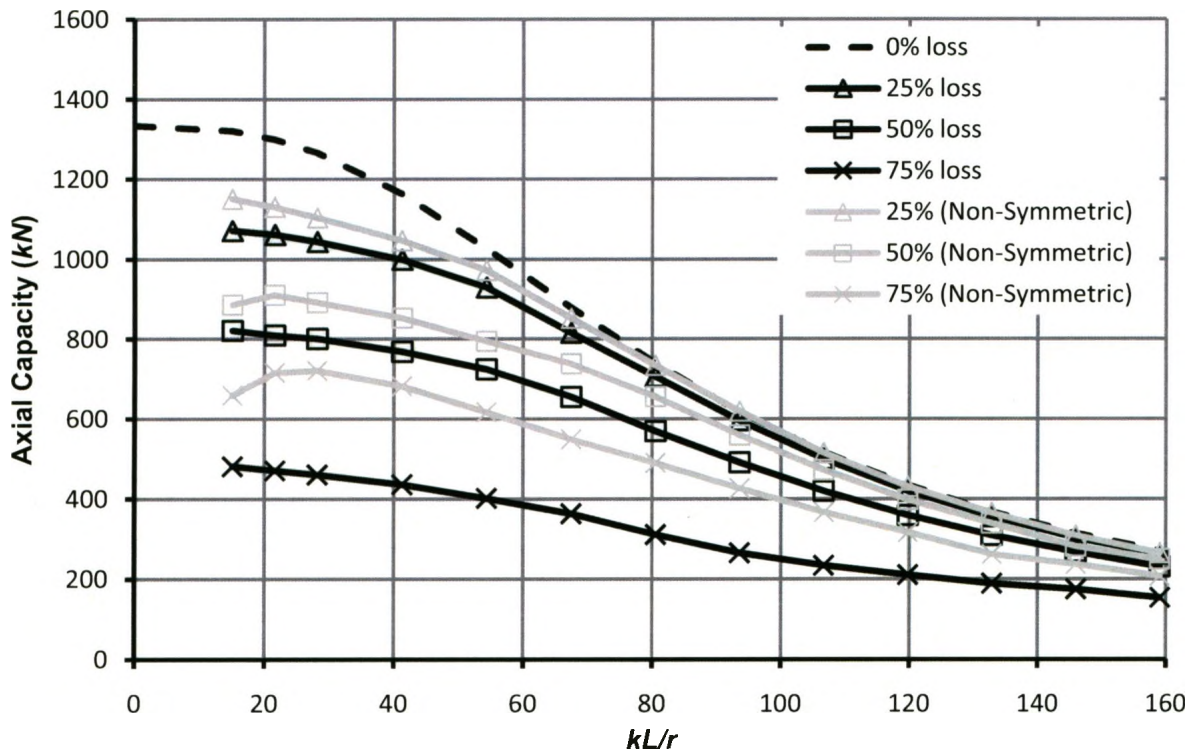


Figure 4-6: Sensitivity of Axial Capacity to Symmetric and Non-Symmetric Flange Deterioration (W150x30,  $t^*/t_o=0.5$ ,  $L^*=200\text{ mm}$ ,  $y^*=0$ ,  $\delta=L/1000$ )



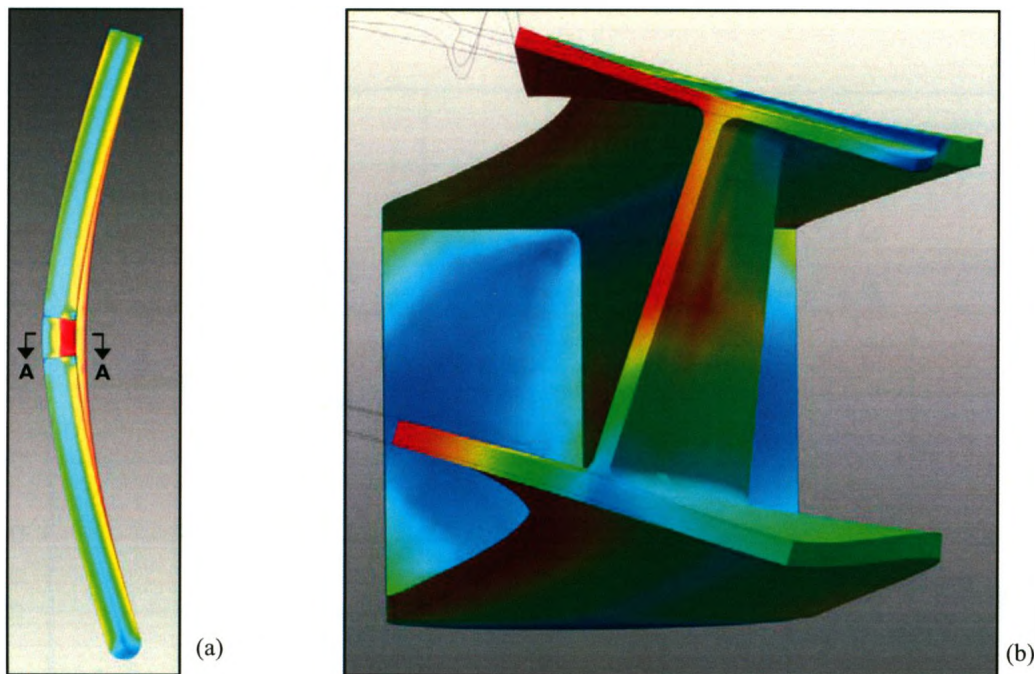


Figure 4-7: Torsional Rotation Caused by Non-Symmetric Corrosion  
 (a) Elevation  
 (b) Section A-A

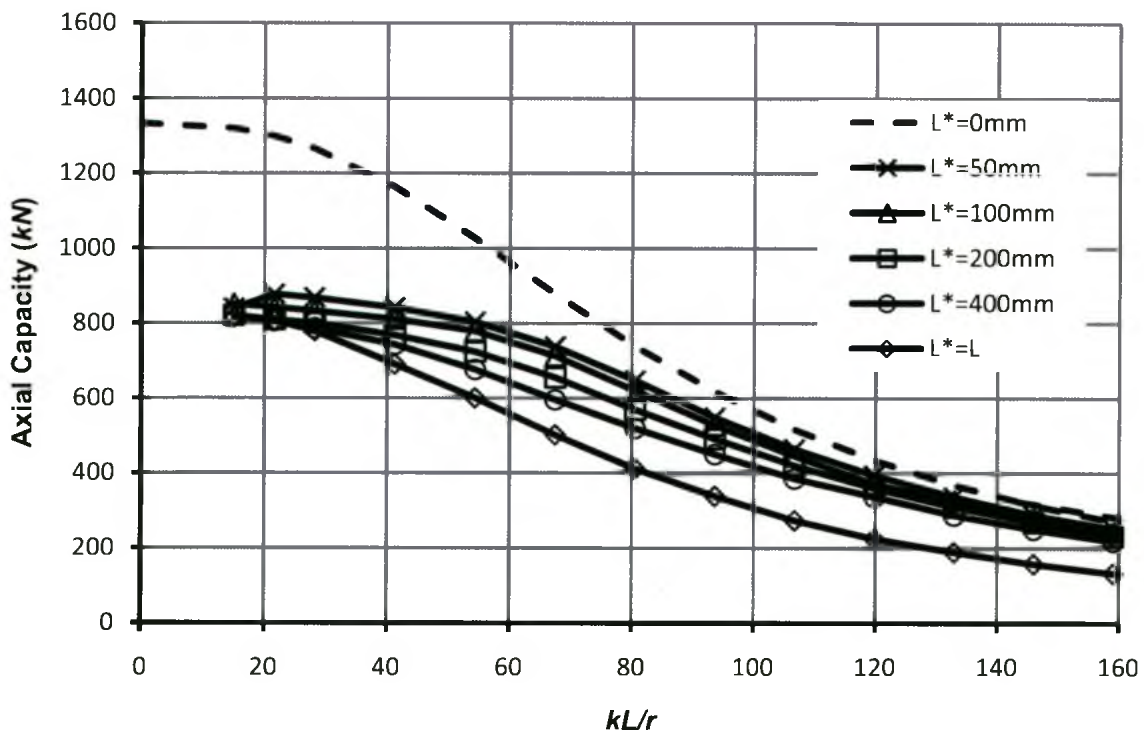


Figure 4-8: Sensitivity of Axial Capacity to  $L^*$  (W150x30, Symmetric Deterioration,  $t^*/t_o=0.5$ ,  $y^*=0L$ ,  $\delta=L/1000$ )

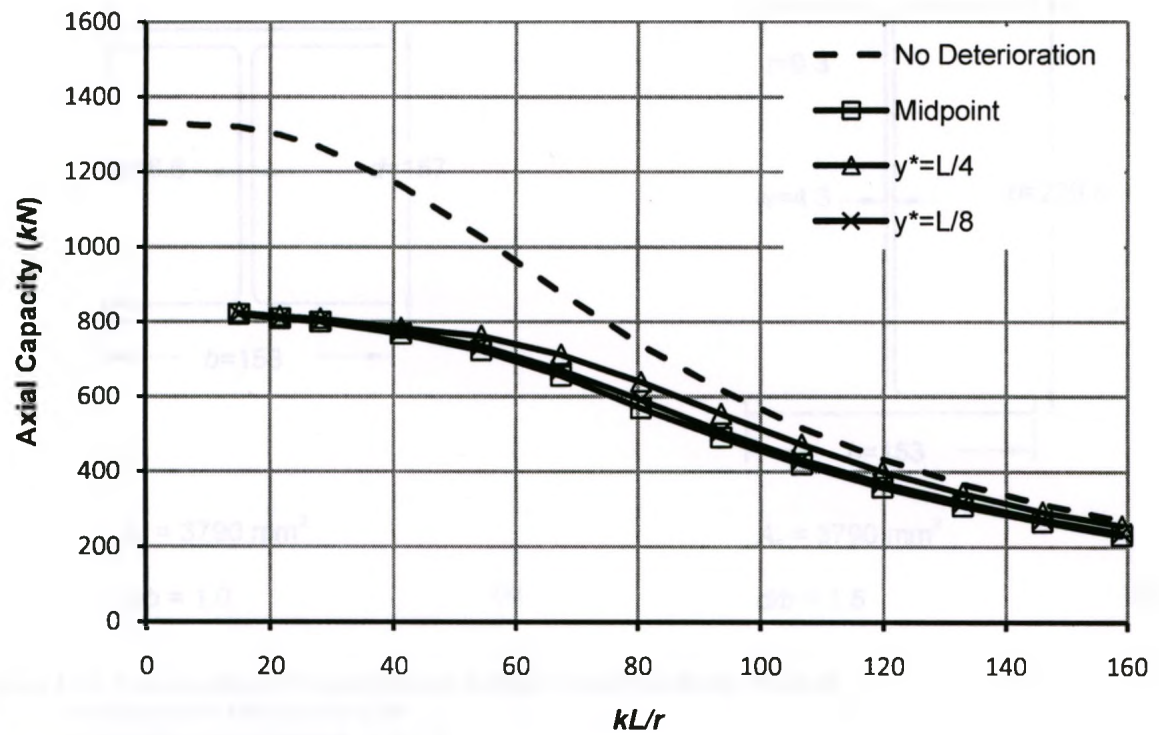


Figure 4-9: Sensitivity of Axial Capacity to  $y^*$  (W150x30, Symmetric Deterioration,  $t^*/t_o=0.5$ ,  $L^*=200$  mm,  $\delta=L/1000$ )

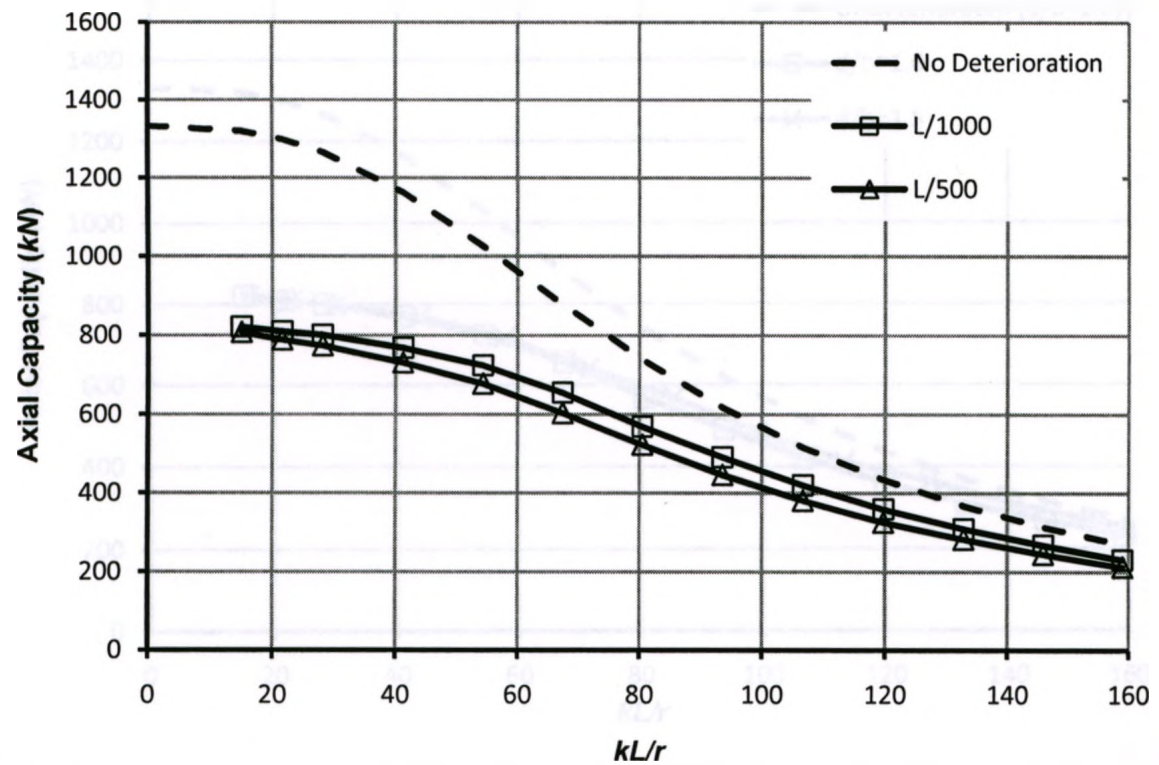
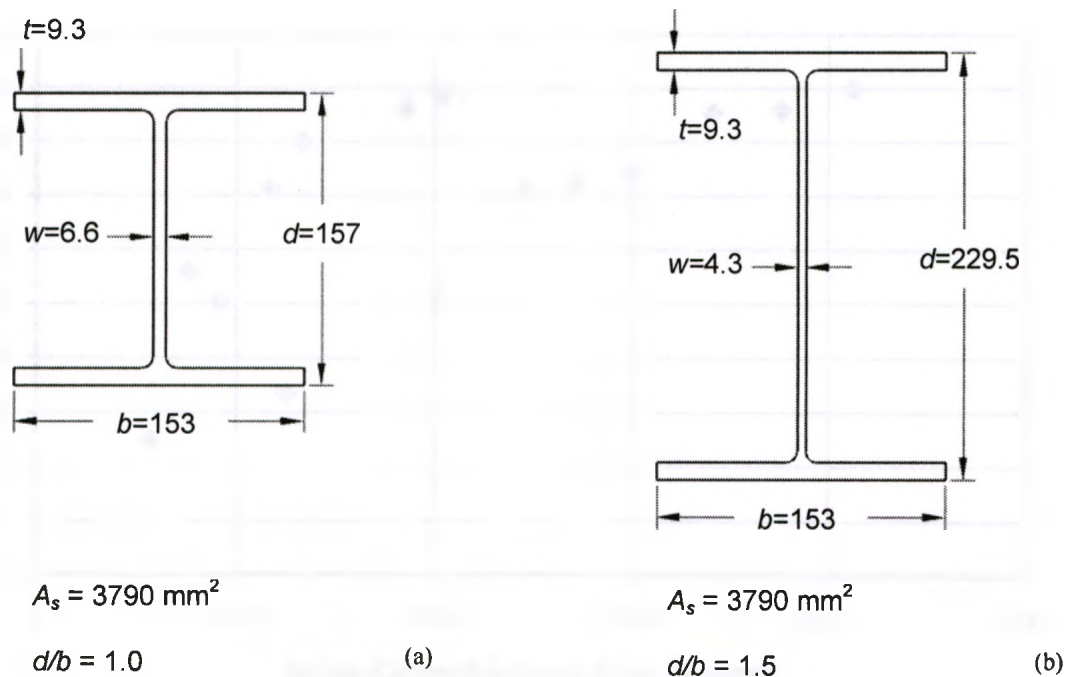
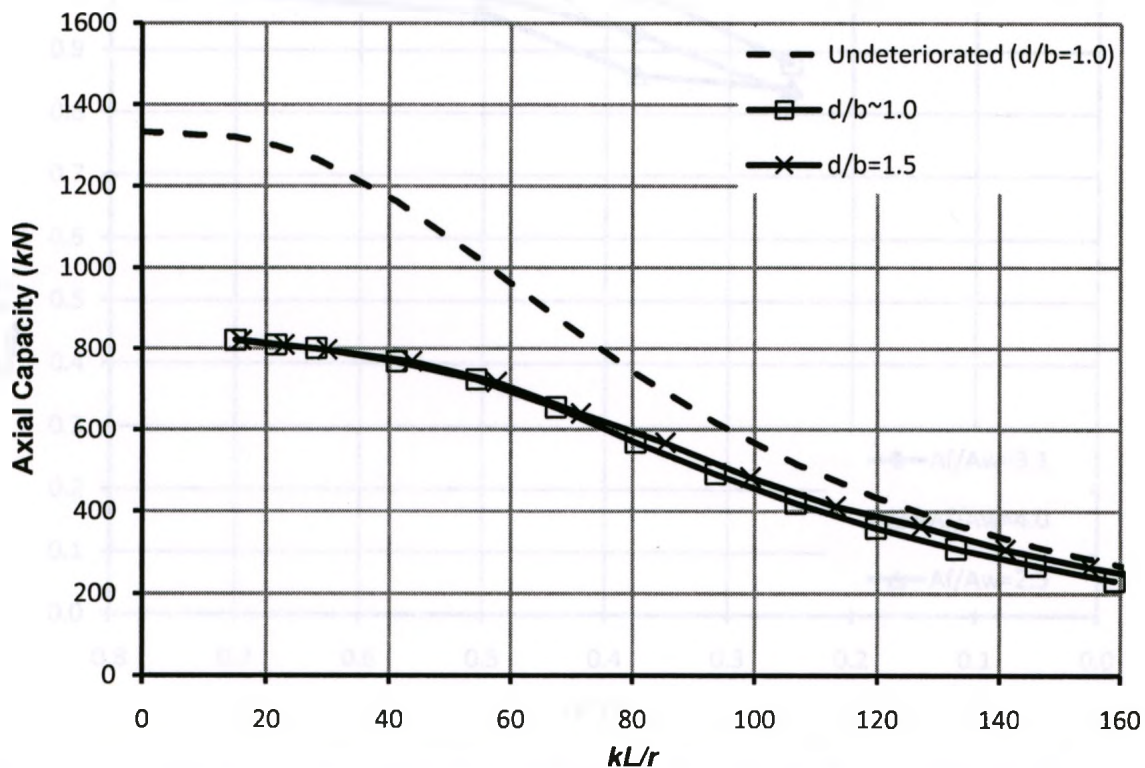


Figure 4-10: Sensitivity of Axial Capacity to  $\delta$  (W150x30, Symmetric Deterioration,  $t^*/t_o=0.5$ ,  $L^*=200$  mm,  $y^*=0L$ )



**Figure 4-11: Cross-sectional Properties Used in Aspect Ratio Sensitivity Analysis**

- (a) Original W150x30 ( $d/b \sim 1.0$ )  
 (b) Modified Cross Section ( $d/b = 1.5$ )



**Figure 4-12: Sensitivity of Axial Capacity to Aspect Ratio of the Column Cross Section (Symmetric Deterioration,  $t^*/t_o=0.5$ ,  $L^*=200 \text{ mm}$ ,  $y^*=0L$ ,  $\delta=L/1000$ )**



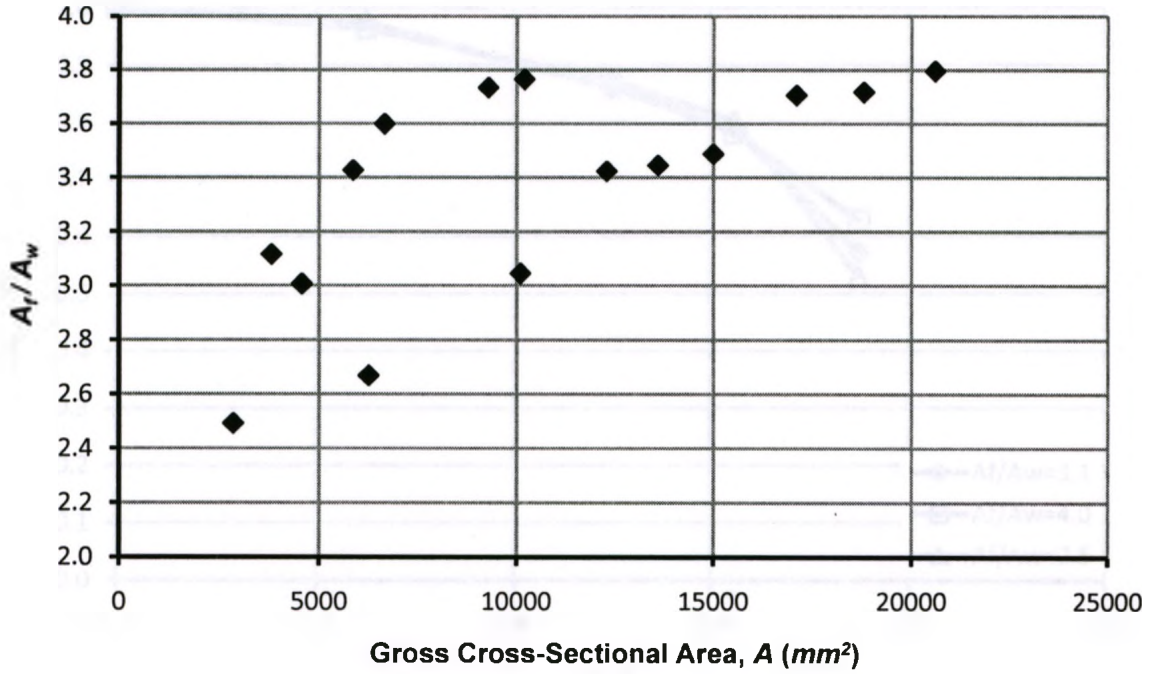


Figure 4-13: Ratio of Flange to Web Area for W-Shape Columns Prone to Local Buckling

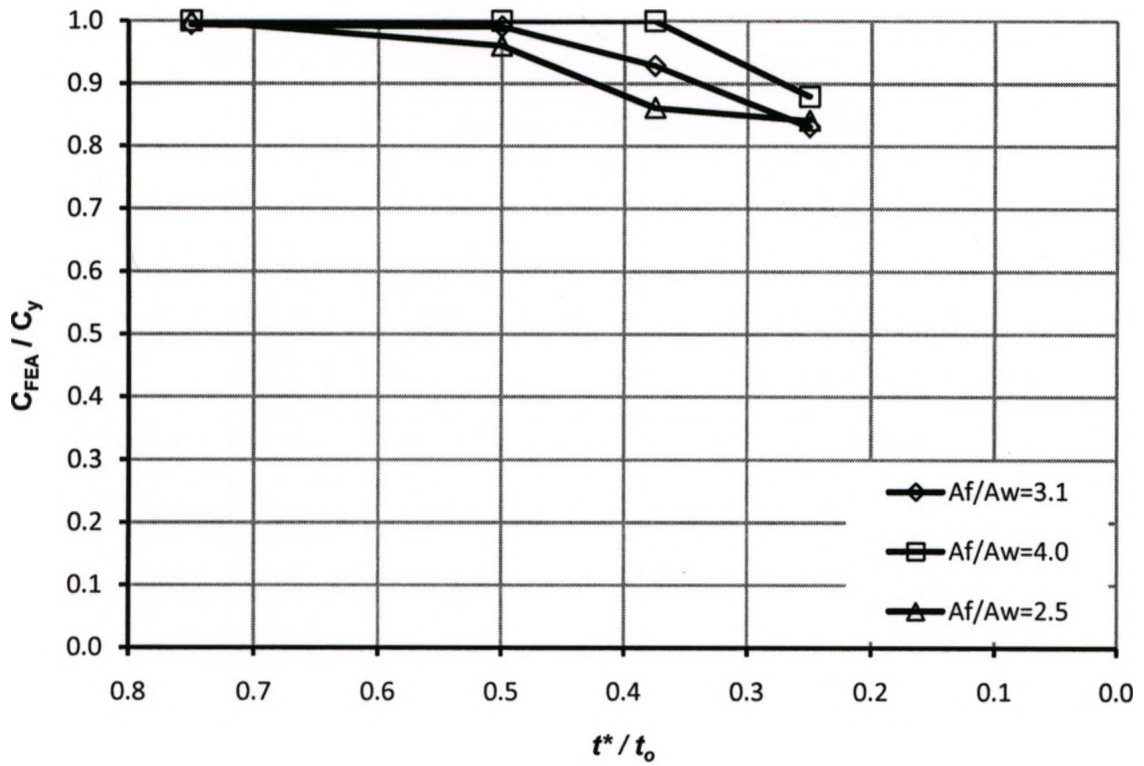


Figure 4-14: Sensitivity of the Axial Capacity of Stocky Columns to  $A_f/A_w$  (W150x30, Symmetric Deterioration,  $L^*=200$  mm,  $y^*=0L$ ,  $kL/r=15$ )

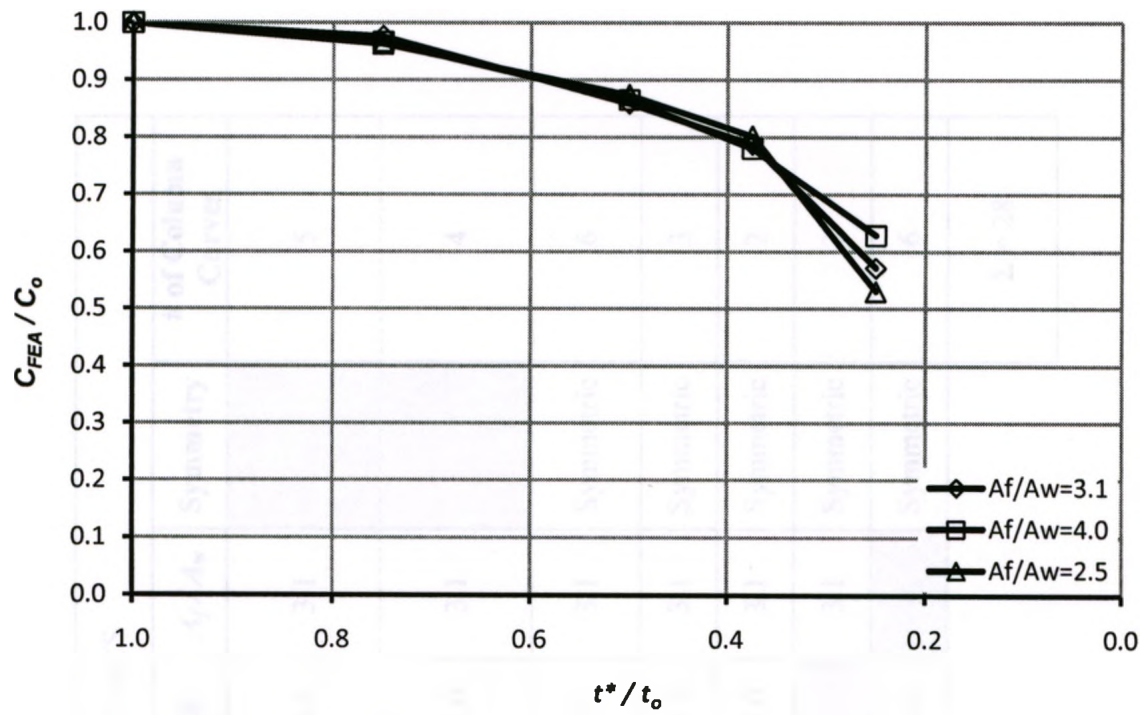



Figure 4-15: Sensitivity of the Axial Capacity of Slender Columns to  $A_f/A_w$  (W150x30, Symmetric Deterioration,  $L^*=200$  mm,  $y^*=0L$ ,  $kL/r=159$ )



Table 4-1: Parameter Matrix



VARIABLES	CONSTANTS							
	$1-t^*/t_o$	$L^*$ (mm)	$y^*$ (mm)	$\delta$ (mm)	$d/b$	$A_f/A_w$	Symmetry	# of Column Curves
$1-t^*/t_o$ (%): Symmetric {0, 25, 50, 62.5, 75}		200	0L	L/1000	~1.0	3.1		5
$1-t^*/t_o$ (%): Non-Symmetric {0, 25, 50, 75}		200	0L	L/1000	~1.0	3.1		4
$L^*$ (mm) {0, 50, 100, 200, 400, L}	50%		0L	L/1000	~1.0	3.1	Symmetric	6
$y^*$ (mm) {0L, L/8, L/4}	50%	200		L/1000	~1.0	3.1	Symmetric	3
$\delta$ (mm) {L/1000, L/500}	50%	200	0L		~1.0	3.1	Symmetric	2
$d/b$ {~1.0, 1.5}	50%	200	0L	L/1000		3.1	Symmetric	2
$A_f/A_w$ {2.5, 3.1, 4.0}	{25%, 50%, 62.5%, 75%}	200	0L	L/1000	~1.0		Symmetric	6
								$\Sigma = 28$

Table 4-2: Flange Section Loss as a Function of Yield Strength

Flange Section Loss	Remaining Flange	Flange Width-to-Thickness
0%	9.3 mm	$\frac{b}{2t} = \frac{153.9}{\sqrt{F_y}}$
25%	6.98 mm	$\frac{b}{2t} = \frac{205.0}{\sqrt{F_y}}$
50%	4.65 mm	$\frac{b}{2t} = \frac{307.8}{\sqrt{F_y}}$
62.5%	3.49 mm	$\frac{b}{2t} = \frac{410.1}{\sqrt{F_y}}$
75%	2.33 mm	$\frac{b}{2t} = \frac{614.2}{\sqrt{F_y}}$

**Table 4-3: Variation of Failure Mode with Slenderness Ratio**

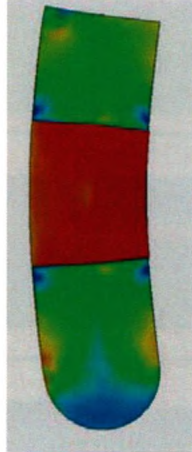


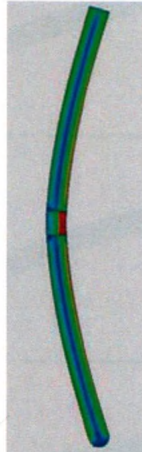




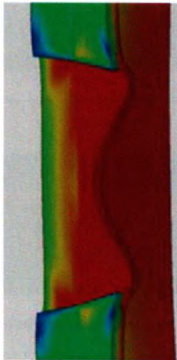






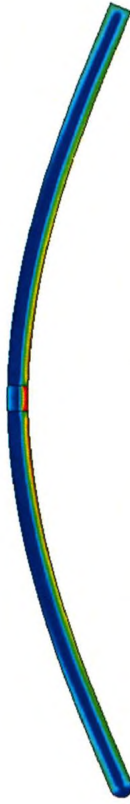
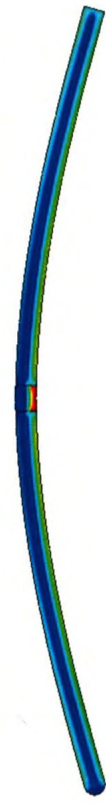
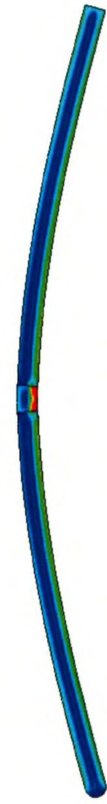





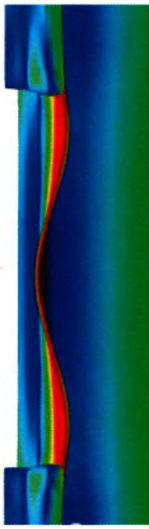
		$kL/r$						
		15	41	67	94	120	146	172
<b>GLOBAL DEFORMATION</b> (25x deformation scale)								
								

Table 4-4: Deformed Shapes of Slender Columns ( $kL/r=159$ ) with Varying  $t^*/t_o$  after Failure

		Flange Loss (Symmetric)				
		0	25%	50%	62.5%	75%
GLOBAL DEFORMATION (15x deformation scale)						
	LOCAL DEFORMATION (15x deformation scale)					
$P_{FEA}$	270.7 kN	262.9 kN	231.2 kN	212.1 kN	159.3 kN	



**Table 4-5: Development of Failure Mode for Intermediate Columns ( $kL/r=80.5$ ,  $t^*/t_o=0.25$ )**



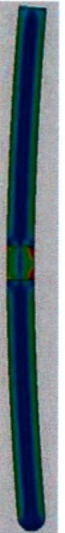
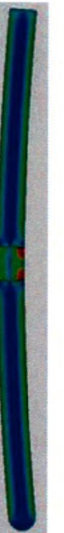


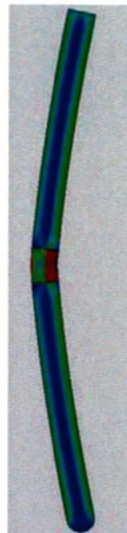



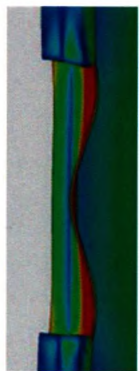

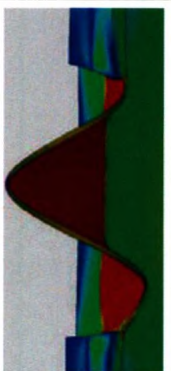
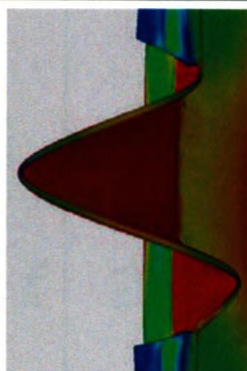
		$P/P_{FEA}$						
		0	0.20	0.56	0.80	0.87	0.93	1.0
<b>GLOBAL DEFORMATION</b> (15x deformation scale)								
								



Table 4-6: Summary of Sensitivity Variables to Include in Analysis

Variable	Significant Effect on Axial Capacity?	Include in Simplified Evaluation Procedure?
Flange Loss ( $1-t^*/t_o$ )	Yes	Yes
Symmetry	Yes	<b>No:</b> Difficult to accurately account for torsion. Assume symmetric.
Length of Deterioration ( $L^*$ )	Yes	Yes
Distance of Deterioration from Column Mid-point ( $y^*$ )	No	<b>No:</b> Assume centered at column mid-point.
Initial Out-of-Straightness ( $\delta$ )	No	<b>No:</b> Assume $L/1000$ unless damage observed.
Aspect Ratio ( $d/b$ )	No	No
Ratio of Flange Area to Web Area	No	No

## **CHAPTER 5: SIMPLIFIED ASSESSMENT OF CORRODED STEEL**

### **COMPRESSION MEMBERS**

#### **5.1 INTRODUCTION**

Though CAN/CSA S6-06 (CSA 2006) requires evaluators to account for deterioration caused by corrosion, it fails to provide guidance for calculating the axial capacity of compression members with deteriorated flanges that do not satisfy the Class 3 local buckling limit. The numerical techniques presented in Chapter 2 have been shown in Chapter 3 to be accurate but are too time consuming for design-office use. Therefore, the primary objective of the research reported in this chapter is to formulate a simplified assessment procedure for steel bridge compression members with corroded flanges that may be susceptible to local buckling, based on the research findings presented in Chapters 3 and 4. As a secondary objective, the accuracy of the CAN/CSA S16-09 (CSA 2009) provisions for assessing the capacity of W-shapes with Class 4 flanges will also be investigated.

In this chapter: necessary parameters for the simplified assessment method are identified; the method is introduced and illustrated using several examples; the analysis of Class 4 members using CAN/CSA S16-09 is investigated; and realistic maximum limits of deterioration are discussed. Finally, the capacities of W-shapes with deteriorated flanges as determined using Finite Element Analysis (FEA), CAN/CSA S16-09, and the proposed simplified assessment method are compared. The FEA methodology presented in Chapter 2 has been thoroughly validated in Chapter 3, so the FEA results will serve as

the gold standard when evaluating the accuracy of capacities determined using the simplified assessment method and CAN/CSA S16-09.

## **5.2 SIMPLIFIED ASSESSMENT METHOD**

### **5.2.1 Identification of Key Parameters**

As previously shown in Table 4-6, the most critical factor affecting the axial capacity of columns with local flange deterioration is flange section loss,  $(1 - t^*/t_o)$ , where  $t^*$  is the remaining thickness of the deteriorated flange and  $t_o$  is the undeteriorated flange thickness. Additionally, the length of deterioration,  $L^*$ , also affects axial capacity, especially when it approaches the full column length, as shown previously in Figure 4-8, as is typical for the case of uniform corrosion.

The data points in Figure 5-1, derived directly from the sensitivity analysis data presented in Chapter 4, show the variation of the reduced axial capacity,  $C_d$ , shown as a fraction of the original axial capacity,  $C_{S6}$ , with the column weak-axis slenderness ratio,  $kL/r$ , for flanges with varying width-to-thickness ratios. The dashed lines on the figure show 4th-order polynomials fit to these data. Irrespective of the slenderness ratio, increasing the width-to-thickness ratio dramatically reduces axial strength, and thus the degree of flange section loss is a critical variable that controls the reduced axial capacity. The strength loss is particularly significant for relatively stocky columns with  $kL/r \lesssim 60$ .

The data points in Figure 5-2, also derived from the sensitivity analysis data, show the variation of the normalized reduced axial capacity with  $kL/r$  for columns with varying  $L^*/b$ . The dashed lines on the figure show 4th-order polynomials fit to the data for

$L^*/b=1.3$  and 2.6, and  $L^*=L$ . It is appropriate to normalize the length of deterioration,  $L^*$ , using the flange width,  $b$ , because as noted in Section 2.6, the length of the typical local buckle is proportional to the half flange width. The ratio of the reduced axial capacity to the benchmark axial capacity exceeds 1.0 if the normalized deteriorated length  $L^*/b$  is less than 1.3 because the W150x30 column used as the benchmark case in the sensitivity analysis had  $L^*=200\text{mm}$ ,  $b=153\text{mm}$  so  $L^*/b=1.3$ . For slender columns with  $kL/r \geq 80$ , long lengths of deterioration can significantly reduce the axial capacity while changes in the width-to-thickness ratio have less impact. Clearly, the axial capacity of columns with deteriorated flanges prone to local buckling can only be accurately captured if both the flange width-to-thickness ratio and the normalized length of deterioration are considered. As a simplification, deteriorated lengths of  $L^*/b=1.3$ ,  $L^*/b=2.6$  and  $L^*=L$  will be used as bounds for actual deteriorated lengths when deriving the simplified assessment procedure.

The proposed assessment method will therefore provide two reduction factors that account for flange section loss and the length of deterioration independently.

### 5.2.2 Proposed Method

The simplified equation to allow engineers to quickly assess the reduced capacity of deteriorated compression members is:

$$[5.1] \quad C_d = \Psi \times \Omega \times C_{S6}$$

but



$$[5.2] \quad C_d \leq A_d F_y$$

where:  $C_d$  = nominal axial capacity of the deteriorated column

$\Psi$  = Factor accounting for the increased width-to-thickness ratio  $b/2t^*$

$\Omega$  = Factor accounting for the length of deterioration  $L^*$

$A_d$  = Reduced cross-sectional area in the deteriorated region

and the nominal capacity of the undeteriorated column,  $C_{S6}$ , is:

$$[2.2] \quad C_{S6} = A F_y (1 + \lambda^{2n})^{1/n}$$

The inequality shown in Eq. [5.2] requires that the nominal capacity of the deteriorated column cannot be taken larger than the yield capacity of the deteriorated cross section.

Both  $\Psi$  and  $\Omega$  are functions of the column slenderness ratio and are determined empirically using the design charts presented in the next section.

### 5.2.3 Design Charts

This section presents design charts that may be used to determine  $\Psi$  and  $\Omega$ , for use in Eq. [5.1]. For cases of very localized deterioration,  $\Omega = 1.0$  and the axial capacity is reduced only by  $\Psi$ . For cases of deterioration along a greater length of the column,  $\Omega < 1.0$ , and so further reduces the axial capacity.

Figure 5-3 shows the reduction factor  $\Psi$  for width-to-thickness ratios,  $b/2t^*$ , ranging from  $205/\sqrt{F_y}$  to  $410/\sqrt{F_y}$ , as derived from the sensitivity analysis data shown in



Figure 5-1. The equations of the 4th order polynomials shown are given in Appendix A3. Knowing  $(b/2t^*)\sqrt{F_y}$  of the deteriorated flange and the column slenderness ratio,  $kL/r$ ,  $\Psi$  is obtained directly.

Figure 5-4 is the design chart for the reduction factor,  $\Omega$ , that accounts for the length of deterioration,  $L^*$ , as derived from the sensitivity data shown in Figure 5-2. The equations for the curves shown are given in Appendix A3. The factor has been quantified for cases of localized deterioration where  $L^*/b \leq 1.3$  and  $\Omega = 1.0$ , and deterioration along a greater length of the column,  $L^*/b > 1.3$  and  $\Omega < 1.0$ . The assumption that  $L^*/b > 2.6$  is equivalent to uniform deterioration over the entire length of the column is conservative, but represents the lower bound on  $\Omega$ .

While the majority of the data obtained in the sensitivity analysis were for a W150x30 cross section, geometric changes to the ratio of the flange area to the web area,  $A_f/A_w$  and the aspect ratio,  $d/b$ , did not significantly affect axial strength. To further facilitate the assumption that this data can be applied to a broad selection of W-shapes, however, a number of deteriorated columns with varying cross sections will be compared with new FEA results in Section 5.4.2.

#### **5.2.4 Assessment Procedure**

The following procedure is envisaged for evaluators using the simplified assessment method:

1. Determine the remaining thickness of the deteriorated flange,  $t^*$ .

2. Quantify the length of deterioration,  $L^*$ , as that which would contain the entire corroded region.
3. Verify the flange width and length of the column.
4. Determine the nominal yield strength of the steel, perhaps using the provisions of Clause 14 of CAN/CSA S6-06 (CSA 2006).
5. Compute the column slenderness ratio,  $kL/r$ , assuming no deterioration is present.
6. Compute  $(b/2t^*)\sqrt{F_y}$  and obtain  $\Psi$  from Figure 5-3.
7. Compute  $L^*/b$  and obtain  $\Omega$  from Figure 5-4.
8. Compute the nominal strength of the undeteriorated column using Eq. [2.2].
9. Compute the reduced nominal strength of the deteriorated column using Eqs. [5.1] and [5.2].

### 5.2.5 Example Calculations

#### Example 1: W310x90 With Localized Flange Deterioration

Figure 5-5a shows a W310x79 column rolled from Grade 350W steel with localized deterioration over a 200 mm length of one flange as shown. Using the simplified assessment method, the nominal reduced capacity of the deteriorated column is computed as follows:

1. The corroded region is thoroughly wire-brushed and cleaned and the minimum undeteriorated flange thickness,  $t^*$ , is measured as 11 mm.

2. The corroded region can be fully enclosed in the rectangle shown by the dashed lines that has a vertical dimension,  $L^*$ , of 200 mm.
3. The flange width,  $b$ , is measured as 254 mm and the column length,  $L$ , is measured as 3150 mm.
4. The nominal yield strength,  $F_y$ , is determined to be 350 MPa.
5. The column slenderness ratio is computed for weak-axis buckling of the undeteriorated cross section, with  $r_y = 63$  mm.  $kL/r = 1.0 \times 3150 \text{ mm} / 63 \text{ mm} = 50$ .

6. The width-to-thickness constant is computed as

$$(b/2t^*)\sqrt{F_y} = 254 \text{ mm} / (2 \times 11 \text{ mm}) \sqrt{350 \text{ MPa}} = 216$$

For this value,  $\Psi$  is obtained by interpolation on Fig. 5.3 as 0.87.

7. The  $L^*/b$  is computed as  $200 \text{ mm} / 254 \text{ mm} = 0.8$ . For this value, from Fig 5.4,  $\Omega = 1.0$ .

8. The nominal strength of the undeteriorated column is computed. First, the slenderness parameter  $\lambda$  is determined:

$$[2.3] \quad \lambda = \frac{kL}{r} \sqrt{\frac{F_y}{\pi^2 E}}$$

$$[2.3a] \quad = 50 \sqrt{\frac{350 \text{ MPa}}{\pi^2 (200000 \text{ MPa})}} = 0.666$$

For this value, from Eq. [2.2], for  $A = 10100 \text{ mm}^2$  and  $n = 1.34$ :

$$[2.2a] \quad C_{S6} = 10100 \text{ mm}^2 \times 350 \text{ MPa} \left[ 1 + 0.666^{(2 \times 1.34)} \right]^{-1}$$

$$= 2850 \times 10^3 \text{ N} = 2850 \text{ kN}$$

9. The reduced nominal strength of the deteriorated column,  $C_d$ , is calculated, using Eq. [5.1] as:  $\Psi \times \Omega \times C_{S6} = 2850 \text{ kN} \times 0.87 \times 1.0 = 2480 \text{ kN}$ . Next, the yield capacity of the deteriorated cross section, assuming symmetric deterioration, is computed using Eq. [5.2]. For a flange section loss of  $(14.6 \text{ mm} - 11.0 \text{ mm}) = 3.6 \text{ mm}$ , the area at the deteriorated section is  $A_d = (10100 \text{ mm}^2 - 2 \times 254 \text{ mm} \times 3.6 \text{ mm}) = 8271 \text{ mm}^2$ .

Thus,

$$A_d F_y = (8271 \text{ mm}^2 \times 350 \times 10^{-3} \text{ kN/mm}^2) = 2895 \text{ kN} \text{ and, because this exceeds the value calculated using the two factors from Steps 6 and 7, } C_d = 2480 \text{ kN}.$$

### **Example 2: W310x79 With Uniform Flange Deterioration**

Figure 5-5b shows the same W310x79 column considered in Example 1 except that the length of the deterioration,  $L^*$ , is now 2300 mm. Using the simplified assessment method, the nominal reduced capacity of the deteriorated column is computed as it was in Example 1 except:

2. The corroded region can be fully enclosed in the rectangle shown by the dashed lines that has a vertical dimension,  $L^*$ , of 2300 mm.
7. The  $L^*/b$  is computed as  $2300 \text{ mm}/254 \text{ mm} = 9.1$ . For this value, from Fig 5.4,  $\Omega = 0.85$ .

9. The reduced nominal strength of the deteriorated column,  $C_d$ , is calculated as:
- $$\Psi \times \Omega \times C_{S6} = 2850 \text{ kN} \times 0.87 \times 0.85 = 2110 \text{ kN}.$$
- As in Example 1, the yield capacity of the deteriorated cross section is computed as  $A_d F_y = 2895 \text{ kN}$  and, because this exceeds the value calculated using the two factors from Steps 6 and 7,
- $$C_d = 2110 \text{ kN}$$

### 5.3 CAN/CSA S16-09 PROCEDURE FOR EVALUATING COLUMNS WITH CLASS 4 FLANGES

CAN/CSA S16-09 (CSA 2009) provides two methods for evaluating columns with Class 4 flanges. Based on the Class 3 width-to-thickness limit of  $200/\sqrt{F_y}$ , the evaluator may compute a reduced equivalent yield strength,  $(F_y)_{eq}$ :

$$[1.3] \quad (F_y)_{eq} = \left( \frac{400}{b^*/t^*} \right)^2$$

Where  $b^*$  is the net flange width and  $t^*$  is the net flange thickness. Alternatively, the evaluator may compute a reduced equivalent flange width,  $b_{eq}$ :

$$[1.4] \quad b_{eq} = \frac{400t^*}{\sqrt{F_y}}$$

and recomputed geometric properties based on this reduced width. As described in Chapter 1, the resistance obtained using  $(F_y)_{eq}$  will likely exceed that obtained using  $b_{eq}$  for slender columns, and vice-versa, so the evaluator can use the larger of these two resistances. This section explores in detail the difference between the resistances



computed using these two methods. Significantly, it is assumed using either method that the deterioration extends the full length of the column.

Figure 5-6 shows the variation of the nominal capacity of the deteriorated shape,  $C_{S16}$ , expressed as a fraction of the nominal capacity of the original undeteriorated column,  $C_o$ , for a Grade 350W W150x30 with 50% symmetric flange section loss, as predicted using the two methods. The maximum length shown corresponds to a slenderness ratio of approximately 160. In general, reducing  $b$  causes the column to be more susceptible to global buckling at high slenderness ratios while reducing  $F_y$  causes premature yielding at low slenderness ratios. There exists a critical length,  $L_c$ , where the capacity computed using the reduced flange width method exactly equals that computed using the reduced yield strength method. As an alternative to computing the capacities based on both methods and selecting the larger value, an evaluator could compute  $L_c$  and compare it to the actual column length  $L$ : for  $L > L_c$  the larger capacity will be obtained using the reduced flange width method, Eq. [1.4], and for  $L < L_c$  the larger capacity will be obtained using the reduced yield strength method, Eq. [1.3].

The critical length values for the strong and weak-axis capacities for W-shape columns, first derived by Bartlett (2011), are shown in Appendix A4. For weak-axis buckling:

$$[5.3] \quad \frac{L_c}{t^*} = 2\pi \sqrt{\frac{E}{3F_y}} \left[ \frac{\left( \frac{\alpha^2}{4\alpha + \beta} \right)^n - \left( \frac{\gamma^2}{4\gamma + \beta} \right)^n}{\left( \frac{1}{\gamma} \right)^n - \left( \frac{\gamma^2}{\alpha^3} \right)^n} \right]^{\frac{1}{2n}}$$

where  $E$  is Young's modulus (200 000 MPa for structural steel),  $n = 1.34$  for rolled W-shapes, and:

$$[5.4] \quad \alpha = b/2t^*$$

$$[5.5] \quad \beta = \frac{(d-t^*)w}{t^{*2}}$$

$$[5.6] \quad \gamma = \frac{200}{\sqrt{F_y}}$$

For strong-axis buckling:

$$[5.7] \quad \frac{L_c}{(d-t^*)} = \frac{\pi}{\gamma} \sqrt{\frac{E}{F_y}} \left[ \frac{\left( \frac{\alpha^2}{4\alpha + \beta} \right)^n - \left( \frac{\gamma^2}{4\gamma + \beta} \right)^n}{\left( \frac{1}{\gamma + \beta/12} \right)^n - \left( \frac{1}{\alpha + \beta/12} \right)^n} \right]^{\frac{1}{2n}}$$

In practice it may be computationally more difficult to use Eqs. [5.3] and [5.7] than to simply compute the capacities based on Eqs. [1.3] and [1.4] and select the larger value.

#### 5.4 COMPARISON WITH FINITE ELEMENT ANALYSIS RESULTS

This section examines the accuracy and conservatism of the simplified assessment method by comparing it to FEA results and the CSA S16-09 methods. Before doing an in-depth comparison, however, realistic flange section loss needs to be considered so the

analysis procedure can be adequately validated with cases that are typical of those that would likely be experienced in practice.

#### **5.4.1 Realistic Maximum Flange Section Loss in Bridge Compression Members**

The very wide range of flange thickness losses examined in Chapter 4 included extreme cases of 50% to 75% section loss. In practice, it seems likely that the discovery of flange section loss in excess of 25% during a routine inspection would trigger some form of intervention, either strengthening the compression member or posting the bridge with a maximum truck weight restriction. It is unlikely that an assessment method would be used to determine the capacity if more severe deterioration was noted, although it would be beneficial if the assessment consistently underestimated the capacity for such extreme cases, given the uncertainty present. It is therefore worthwhile to identify the W-shape cross sections commonly used as columns that would be susceptible to local flange buckling if a flange thickness loss of up to 25% occurred. These shapes represent the domain of realistic shapes that should be considered in the comparison of the assessment methods with the FEA results.

Table 5-1 lists Grade 350W W-shapes specifically referred to as columns in the *Handbook of Steel Construction* (CISC 2010) that would have a width-to-thickness ratio,  $(b/2t^*)$ , in excess of  $200/\sqrt{F_y}$  given 25% flange section loss. This list is not exhaustive as compression members in older bridges may consist of custom built-up sections or obsolete W-shapes. The most slender flange has  $b/2t^* = 287/\sqrt{F_y}$ , and 11 of 16 have  $b/2t^* \leq 230/\sqrt{F_y}$ .

#### 5.4.2 Comparison of Columns Sensitive to Corrosion

This section examines the accuracy of the simplified assessment method for several column cross sections with flanges that are particularly sensitive to local buckling due to corrosion, listed in Table 5-1. Two independent analyses were conducted:

1. Assuming a maximum realistic flange section loss of 25%, as discussed in Section 5.4.1, to determine how accurately the proposed and CSA S16-09 methods can estimate the axial capacity of realistic deteriorated columns.
2. Assuming a more extreme maximum flange section loss of 50%-63%, to ensure the assessment method is sufficiently robust.

In both cases, the reduced axial capacities calculated using the proposed or CAN/CSA S16-09 methods are compared to those predicted using the FEA.

Table 5-2 shows the analysis results of columns with maximum flange deterioration of 25%. For the 17 cases examined, the ratio of the reduced axial capacity computed using the proposed simplified method to the axial capacity predicted by FEA,  $C_d / C_{FEA}$ , have a mean of 0.98 and a coefficient of variation of 3.6%. The ratios of the reduced axial capacity calculated using CSA S16-09 to that computed using the FEA ( $C_{S16} / C_{FEA}$ ) have a mean of 0.77 and a coefficient of variation of 7.1%. Clearly, the simplified assessment method is less conservative and has less variability than the CAN/CSA S16-09 criteria for determining the axial capacity of W-shape columns with deteriorated flanges.

Figure 5-7 illustrates the conservatism of the procedures in CAN/CSA S16-09, compared to the previously validated FEA. The vertical axis represents the ratio of the greater of



the axial capacities computed using the two methods given in CAN/CSA S16-09 ( $C_{S16}$ ), i.e. based on Eqs. [1.3] and [1.4], to the axial capacity determined using FEA ( $C_{FEA}$ ). The horizontal axis represents the slenderness ratio,  $kL/r$ , and the comparison is made for  $b/2t^*$  as large as  $614/\sqrt{F_y}$ . As the width-to-thickness ratio of the deteriorated region increases, the capacities determined using CAN/CSA S16-09 become increasingly conservative. As previously noted, it is unlikely that corrosion would be so severe in practice to cause  $b/2t^* > 300/\sqrt{F_y}$ . However, even given moderate section losses that cause  $b/2t^* = 205/\sqrt{F_y}$ , the CAN/CSA S16-09 procedures can yield axial capacities that are only 77% of those determined using the validated FEA.

Table 5-3 shows the analysis results of columns with more extreme cases of deterioration, where the flange section loss exceeds 25%. For the 16 cases examined  $C_d / C_{FEA}$  has a mean of 0.95 and a coefficient of variation of 6.2%. In contrast,  $C_{S16} / C_{FEA}$  has a mean of only 0.44 and a coefficient of variation of 34%. This further illustrates the inadequacy of the S16-09 methods to accurately estimate the reduced axial capacity of columns with severe localized flange deterioration.

Changes to the slenderness ratio, width-to-thickness ratio, or  $L^*/b$  do not significantly affect the accuracy of the simplified assessment method. The method becomes slightly more conservative, however, for slender members when  $L^*/b > 2.6$  because the method assumes uniform deterioration along the entire length of the member for these cases. Conversely, the S16-09 methods become significantly more conservative as the width-to-thickness ratio increases or  $L^*/b$  decreases.



While the proposed simplified assessment method is very accurate when compared to the FEA, it has some conservatism when used to evaluate the reduced axial capacity of corroded bridge members in practice. It is very unlikely that corrosive deterioration would occur uniformly in rectangular regions and symmetrically on both flanges, and the additional steel not accounted for in the simplified assessment method would increase the overall axial capacity of the column. Additionally, any end fixity of the bridge compression members being analyzed would further increase the conservatism of the proposed simplified method.

## **5.5 SUMMARY**

This chapter has presented research findings that justify the development and use of a simplified assessment method to determine the axial capacity of W-shape columns with corroded flanges that are susceptible to local buckling. The simplified assessment method uses two design charts that assist the evaluator in determining factors that account for the capacity reduction due to flange section loss and deteriorated length. A procedure for implementing the simplified assessment method is presented, and illustrated with example calculations. Finally, resistances computed using the method are compared with actual resistances computed using the validated FEA model and using the procedures in CAN/CSA S16-09 (CSA 2009).

In general, the simplified assessment method is markedly less conservative than the procedure given in CAN/CSA S16-09. For 17 columns with a realistic maximum flange section loss of 25%, the mean ratio of the axial capacity of the deteriorated column computed using the proposed simplified method to that predicted by FEA,  $C_d / C_{FEA}$ , is

0.98 with a coefficient of variation of 3.6%, indicating that the proposed assessment method is quite accurate when compared to the finite element analysis. For the same set of W-shapes with corroded flanges, the mean ratio of the axial capacity of the deteriorated column computed using the methods in CAN/CSA S16-09 to that predicted by FEA,  $C_{S16} / C_{FEA}$ , was only 0.77 with a coefficient of variation of 7.1%.

The conservatism in the CAN/CSA S16-09 method becomes even more apparent when examining more severe cases of deterioration. When examining 16 cases of more extreme flange section loss (>25%), the mean ratio:  $C_d / C_{FEA}$  was 0.95 with a coefficient of variation of 6.2%, while the mean ratio of  $C_{S16} / C_{FEA}$  was only 0.44 with a coefficient of variation of 34%.

Figure 8.1. Comparison of Proposed Method to FEA

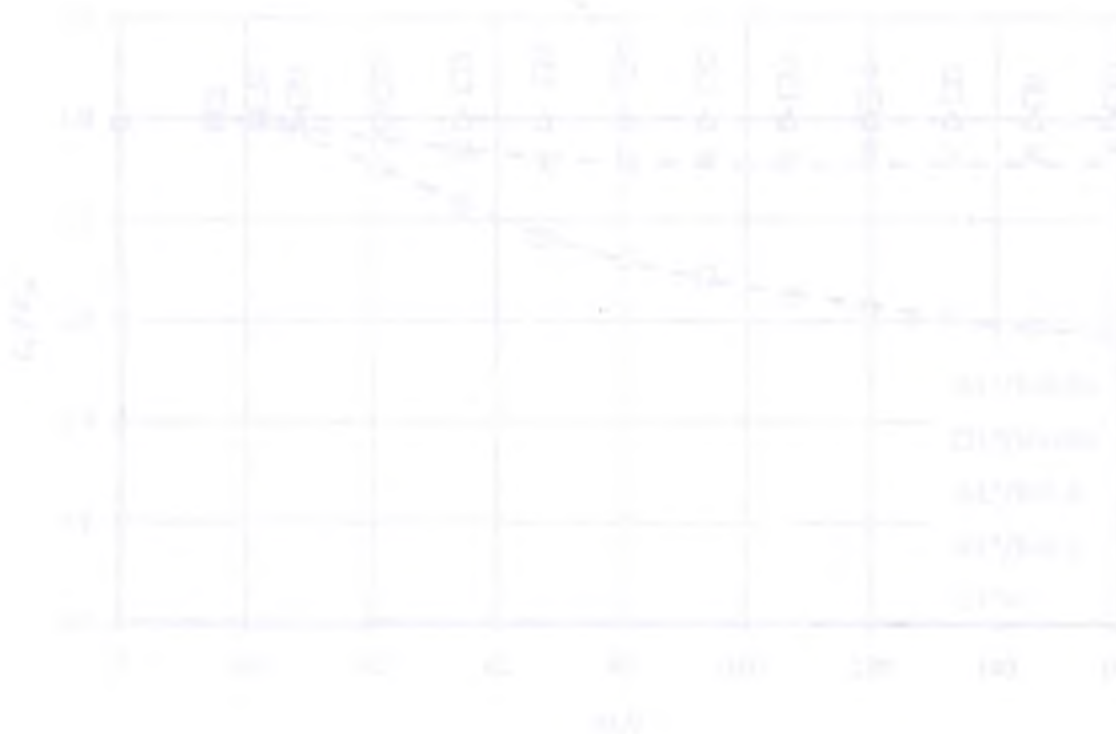


Figure 8.2. Comparison of Proposed Method to FEA for Severe Deterioration

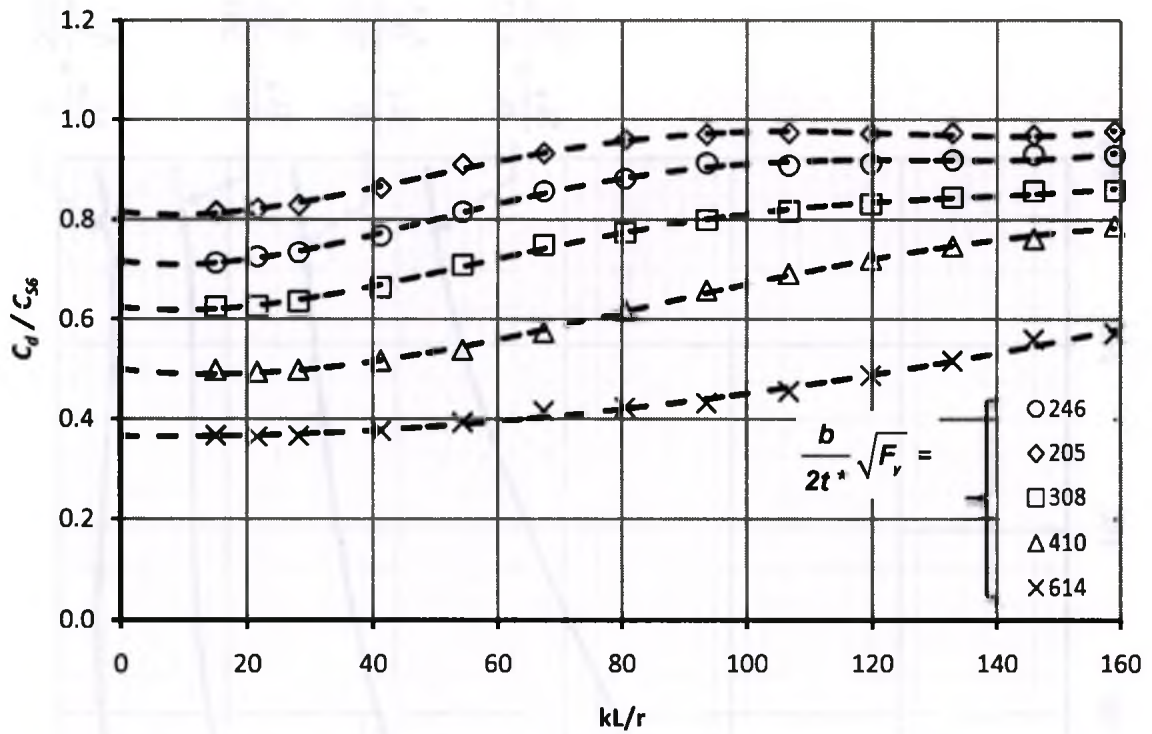


Figure 5-1: Deterioration Factor for Flange Loss ( $t^*$ )

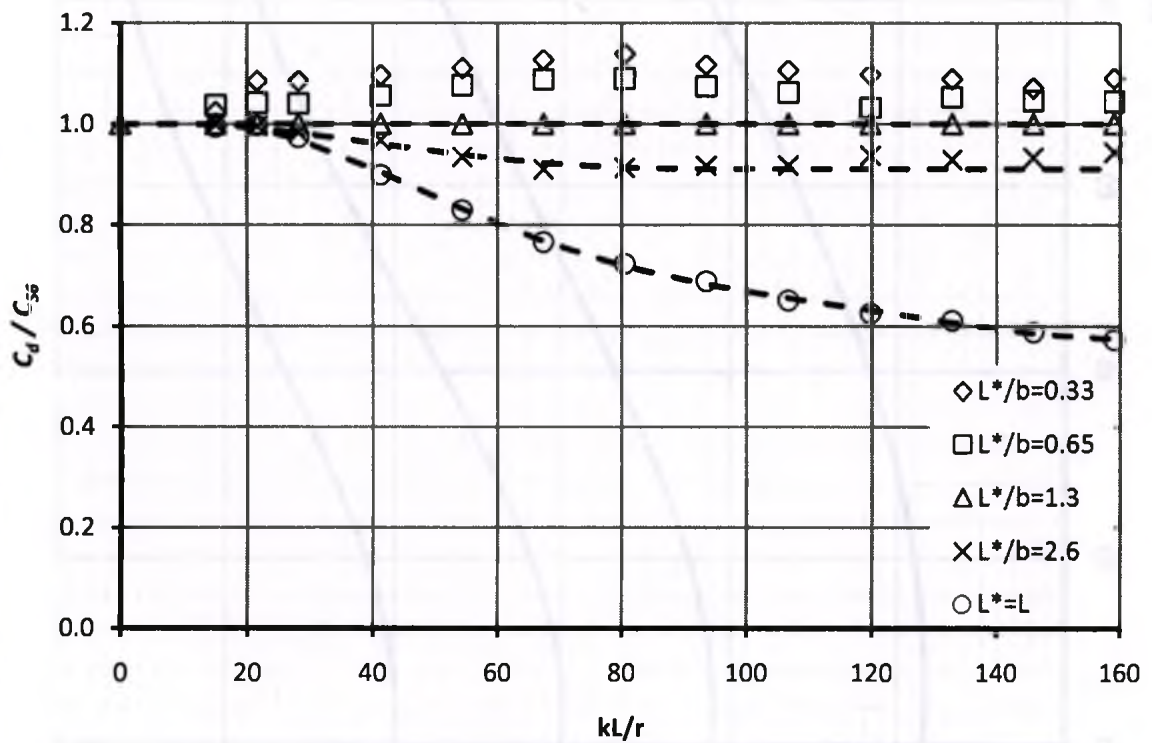


Figure 5-2: Deterioration Factor for Length of Deterioration ( $L^*$ ) Relative to Benchmark Case ( $t^*/t_o=0.5$ ,  $L^*/b=1.3$ )



Figure 5-3: Design Chart for Determining  $t^*$  Deterioration Factor,  $\Psi$

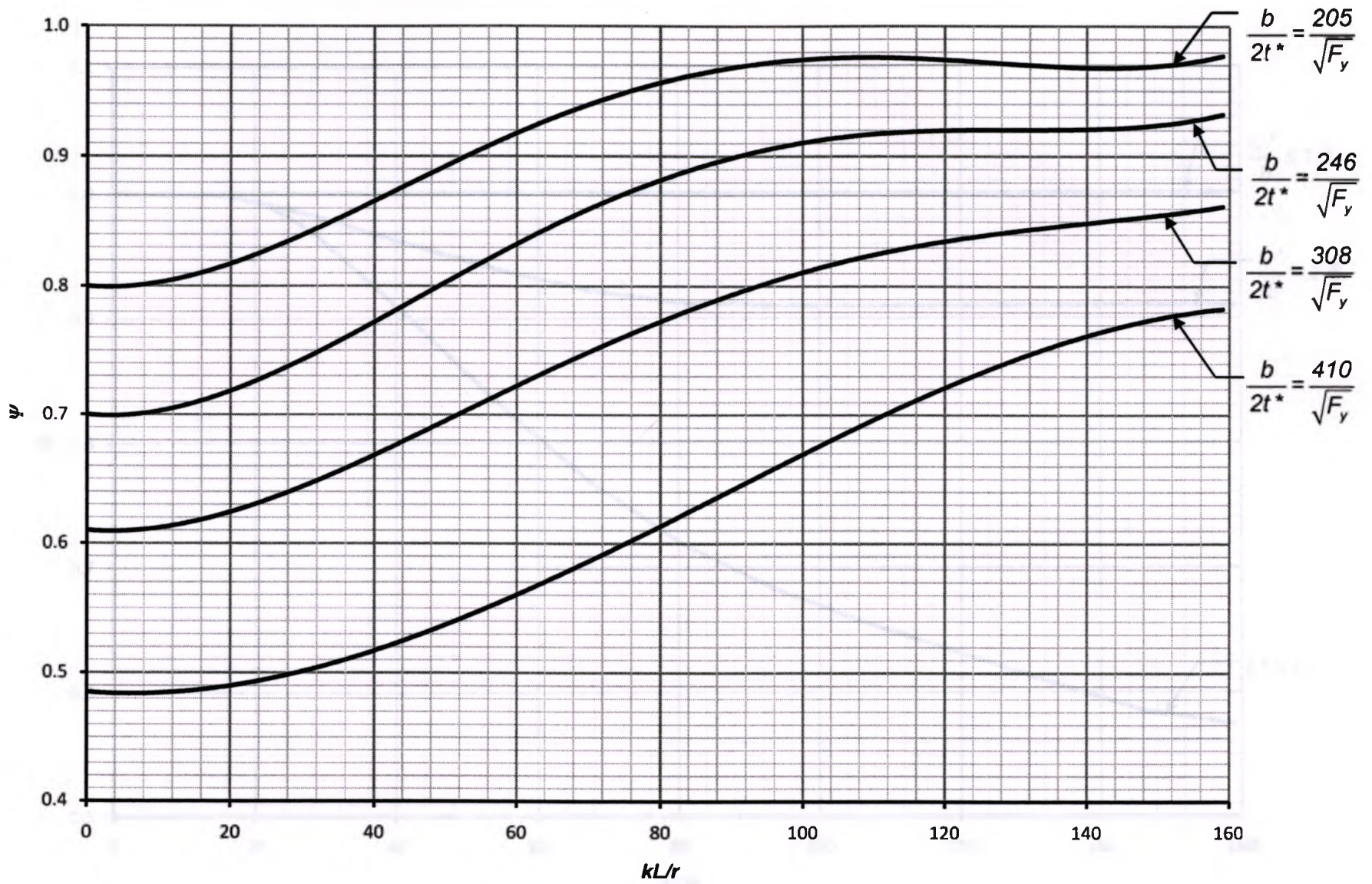
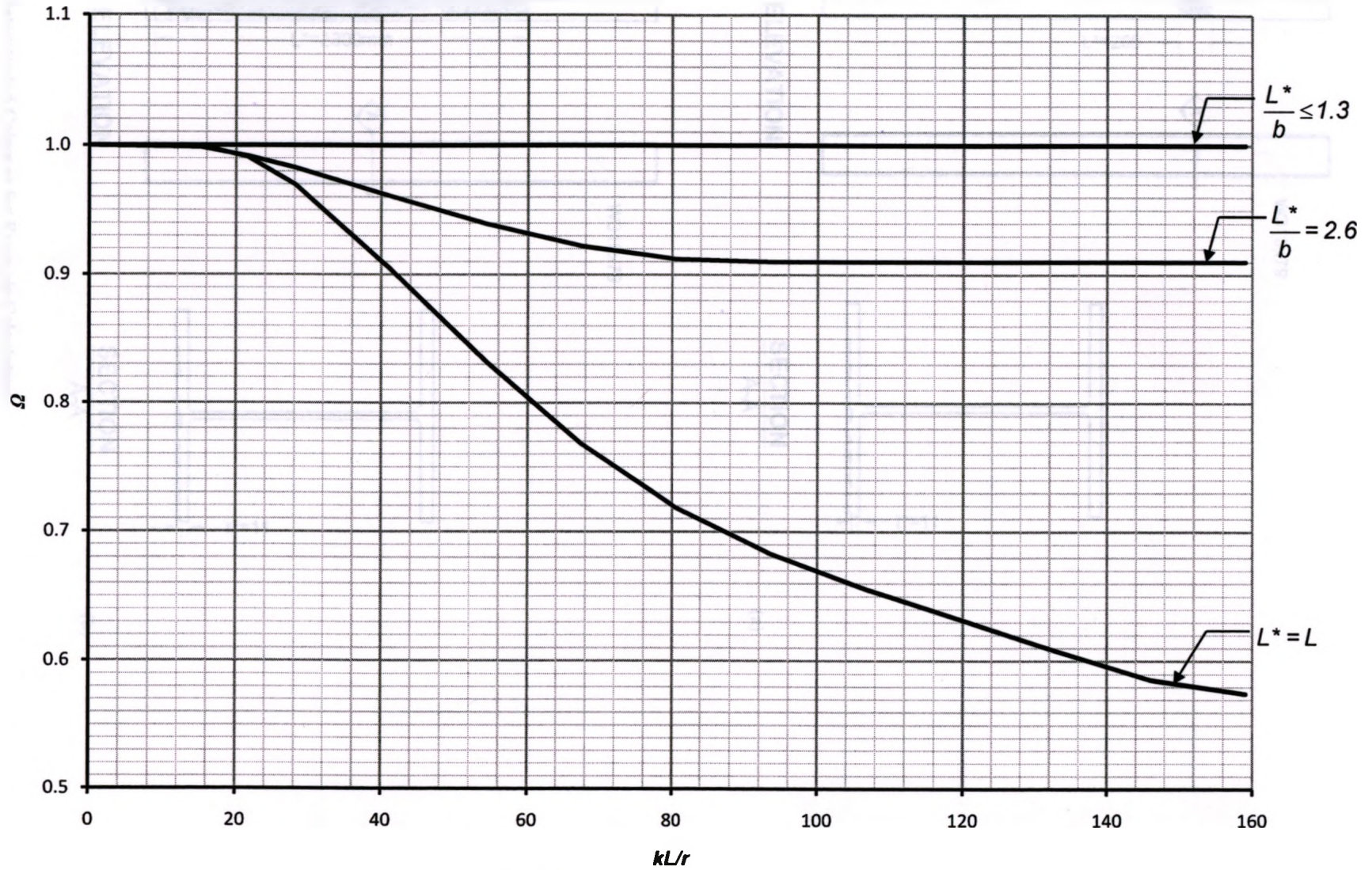
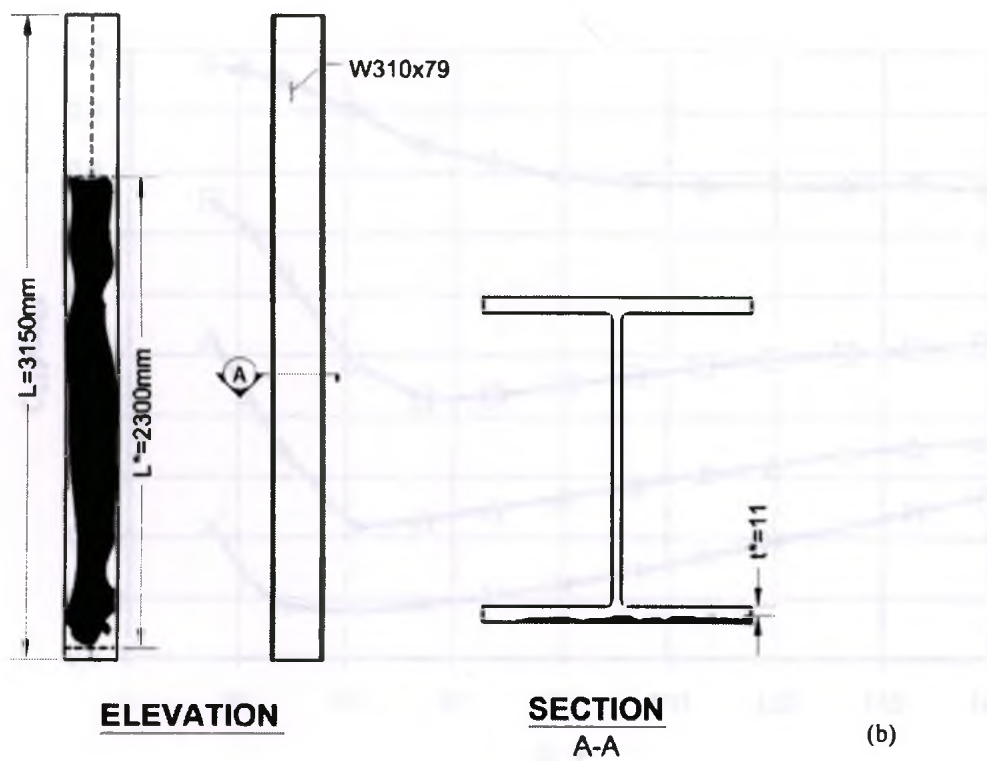
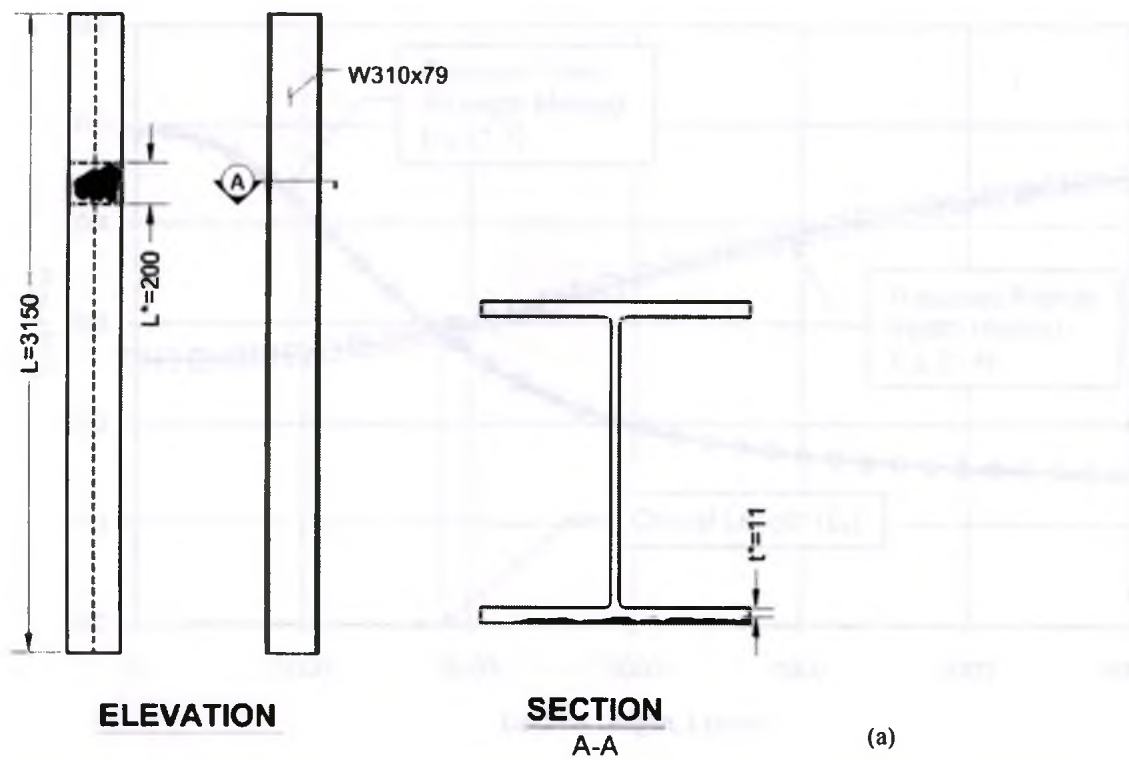




Figure 5-4: Design Chart for Determining  $L^*$  Deterioration Factor,  $\Omega$







**Figure 5-5: Deteriorated Columns for Example Calculations**

(a) Example 1 (W310x79,  $t^*=11$ ,  $L^*=200$ )

(b) Example 2 (W310x79,  $t^*=11$ ,  $L^*=2300$ )

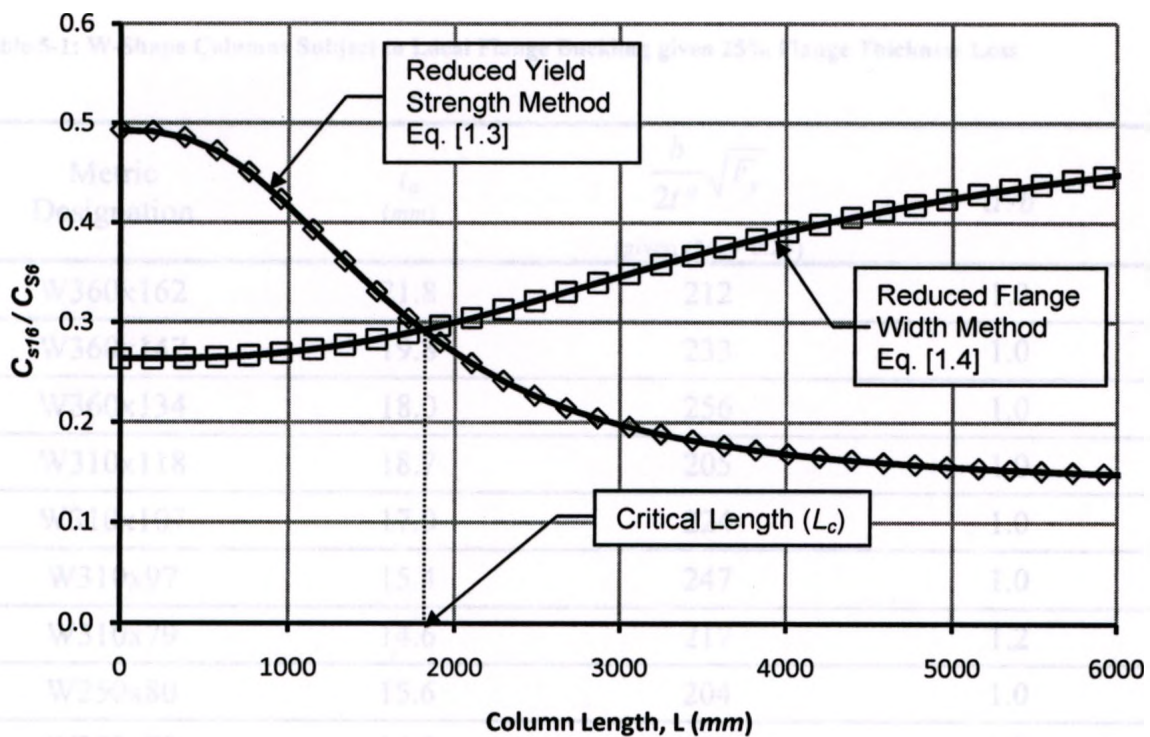


Figure 5-6: Comparison of Methods in CAN/CSA S16-09 (W150x30,  $t^*/t_o=0.5$ , Symmetric Deterioration)

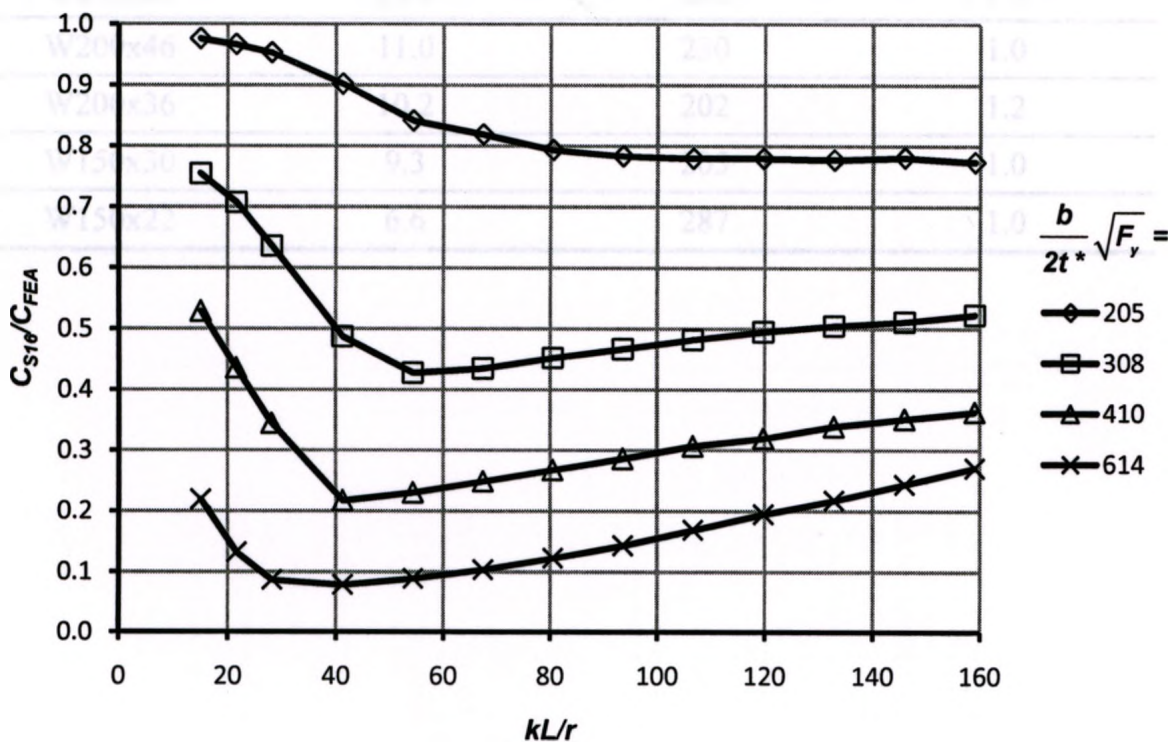


Figure 5-7: Conservatism of CAN/CSA S16-09 with Respect to FEA (W150x30,  $L^*=200$  mm, Symmetric Deterioration)

**Table 5-1: W-Shape Columns Subject to Local Flange Buckling given 25% Flange Thickness Loss**

Metric Designation	$t_o$ (mm)	$\frac{b}{2t^*} \sqrt{F_y}$ (given $t^*/t_o = 0.25$ )	$d/b$
W360x162	21.8	212	1.0
W360x147	19.8	233	1.0
W360x134	18.0	256	1.0
W310x118	18.7	205	1.0
W310x107	17.0	224	1.0
W310x97	15.4	247	1.0
W310x79	14.6	217	1.2
W250x80	15.6	204	1.0
W250x73	14.2	223	1.0
W250x49	11.0	229	1.2
W200x52	12.6	202	1.0
W200x46	11.0	230	1.0
W200x36	10.2	202	1.2
W150x30	9.3	205	1.0
W150x22	6.6	287	1.0



**Table 5-2: Analysis of Columns Sensitive to Corrosion (Realistic Cases)**

Cross Section	$kL/r$	$t^*/t$	$\frac{b}{2t}\sqrt{F_y}$	$L^*/b$	$C_{FEA}$ [kN]	$C_d$ [kN]	$C_d/C_{FEA}$	$C_{S16}$ [kN]	$C_{S-16}/C_{FEA}$
W150x30	80.5	0.75	205.2	0.3	735	702	0.96	564	0.77
W150x30	159	0.75	205.2	0.7	266	263	0.99	203	0.76
W360x162	50	0.75	212.3	0.1	5520	5111	0.93	4229	0.77
W360x162	50	0.75	212.3	1.1	5156	5111	0.99	4229	0.82
W360x162	50	0.75	212.3	1.3	5113	5111	1.00	4229	0.83
W360x162	159	0.75	212.3	1.3	1416	1405	0.99	1096	0.77
W360x162	159	0.75	212.3	1.2	1420	1405	0.99	1096	0.77
W310x79	50	0.75	217.0	0.2	2677	2478	0.93	1924	0.72
W310x79	50	0.75	217.0	1.3	2506	2478	0.99	1924	0.77
W310x79	50	0.75	217.0	0.8	2558	2478	0.97	1924	0.75
W310x79	50	0.75	217.0	3.1	2353	2106	0.90	1924	0.82
W310x79	159	0.75	217.0	0.2	697.5	696	1.00	456	0.65
W310x79	159	0.75	217.0	1.2	684.1	696	1.02	456	0.67
W310x118	50	0.75	204.8	0.2	3984	3764	0.94	3247	0.82
W310x118	50	0.75	204.8	1.1	3724	3764	1.01	3247	0.87
W310x118	159	0.75	204.8	1.1	1020	1034	1.01	801	0.79
W310x118	159	0.75	204.8	0.3	1047	1034	0.99	801	0.77
						Mean =	0.98		0.77
						Std. Dev. =	0.035		0.055
						CoV =	3.6%		7.1%

Table 5-3: Analysis of Columns Sensitive to Corrosion (Extreme Cases)

Cross Section	$kL/r$	$t^*/t$	$\frac{b}{2t}\sqrt{F_y}$	$L^*/b$	$C_{FEA}$ [kN]	$C_d$ [kN]	$C_d/C_{FEA}$	$C_{S16}$ [kN]	$C_{S-16}/C_{FEA}$
W150x30	61.5	0.38	408.9	2.0	634	539	0.85	153	0.24
W150x30	53.7	0.38	408.9	0.7	719	577	0.80	158	0.22
W150x30	159	0.38	410.1	1.3	212	211	1.00	79	0.37
W150x30	159	0.5	307.8	39.0	133	133	1.00	121	0.91
W360x162	50	0.5	318.4	0.3	4256	3891	0.91	1583	0.37
W360x162	50	0.5	318.4	1.2	3791	3891	1.03	1583	0.42
W360x162	159	0.5	318.4	2.2	1208	1145	0.95	642	0.53
W360x162	159	0.5	318.4	0.1	1373	1244	0.91	642	0.47
W310x79	50	0.5	325.5	0.8	1973	1908	0.97	757	0.38
W310x79	50	0.5	325.5	3.1	1778	1622	0.91	757	0.43
W310x79	159	0.5	325.5	0.2	662	610	0.92	274	0.41
W310x79	159	0.5	325.5	1.2	616	610	0.99	274	0.44
W310x118	50	0.5	307.1	0.7	2994	2918	0.97	1245	0.42
W310x118	50	0.5	307.1	2.6	2671	2743	1.03	1245	0.47
W310x118	159	0.5	307.1	0.3	962	917	0.95	476	0.49
W310x118	159	0.5	307.1	2.0	878	871	0.99	476	0.54
						Mean =	0.95		0.44
						Std. Dev. =	0.062		0.152
						CoV =	6.5%		34.1%



## **CHAPTER 6: SUMMARY, CONCLUSIONS, AND RECOMMENDATIONS FOR FUTURE WORK**

### **6.1 SUMMARY**

Localized and uniform corrosion in the flanges of steel bridge compression members adversely affect strength and can cause local buckling and sudden failure of the member. While CAN/CSA S6-06 (CSA 2006) requires that deterioration caused by corrosion be fully accounted for, no criteria are given to aid a bridge evaluator facing this problem. The two methods for calculating the axial capacity of Class 4 columns, given in CAN/CSA S16-09 (CSA 2009), do not give consistent results and are especially conservative for cases of localized deterioration which are common in steel truss bridge members. Thus, an investigation has been conducted to examine the effects of local and uniform flange deterioration on the local buckling of W-shapes to create an assessment procedure that more accurately predicts the axial capacity of deteriorated steel bridge compression members.

Solidworks Simulation, a full-featured finite element analysis (FEA) package used primarily for mechanical engineering applications, was used to accurately simulate Euler, intermediate and local buckling of steel compression members. Although the program lacks direct methods to implement imperfections common in rolled W-shapes, the built-in thermal analysis tools were manipulated to create realistic residual stress patterns and initial out-of-straightness.

After the finite element analysis model was validated for undeteriorated columns, an experimental testing program was undertaken to check the validity of its use in predicting the axial capacity of columns with flange deterioration. Five full scale column tests were conducted in the Structures Lab at The University of Western Ontario. One test column had no deterioration and was used as a control specimen to ensure end fixity and displacement in the load frame were minimal. The other four test columns each had varying degrees and patterns of localized flange deterioration. The deterioration patterns were idealized as rectangular regions at midheight that were machined out in predetermined patterns. Ancillary tests were conducted to determine material yield strength and maximum magnitude of the residual stresses.

Using the validated finite element model, an in-depth sensitivity analysis was conducted. The sensitivity of the compressive strength of deteriorated steel W-shape columns to several geometric parameters that define the flange section loss caused by corrosion was examined in detail. The dimensional variables examined that define corrosion geometry were: the extent of flange section loss, the distance of the corroded region from the column midpoint, and initial out-of-straightness. The cross-section aspect ratio, the ratio of the flange area to web area, and the effect of symmetric and non-symmetric flange loss were also examined. The range of parameters examined in the sensitivity analysis were exaggerated beyond realistic limits to explore the underlying mechanics behind the complex interaction between local and column buckling.

Using the data obtained in the sensitivity analysis, a simplified assessment method was developed to allow evaluators to quickly predict the axial capacity of deteriorated W-shape columns. The key variables identified in the sensitivity analysis, extent of flange

section loss and length of deterioration, were included in the assessment method as two reduction factors:  $\Psi$  and  $\Omega$ , respectively. These factors limit the original uncorroded column capacity such that localized and uniform deterioration is accounted for and can be obtained directly from provided design charts. Finally, the proposed simplified assessment method is compared with guidance given in CAN/CSA S6-06 as well as FEA predictions.

## 6.2 CONCLUSIONS

The major conclusions of this study are as follows:

1. To simulate accurately the response of W-shape columns in axial compression using finite element analysis, it is necessary to account for both residual stress and initial out-of-straightness. Using a linear residual stress pattern with a maximum magnitude of  $0.3F_y$ , and an initial out-of-straightness of  $L/1000$  effectively simulates the empirically based column curve given in CAN/CSA S6-06, for slenderness ratios,  $kL/r$ , between 0 and 160.
2. Solidworks Simulation can effectively simulate local buckling in steel bridge columns with deteriorated flanges, provided the maximum element dimension does not exceed the thickness of the deteriorated flange,  $t^*$  in these regions. The ratio of the failure loads observed in the test columns to those predicted by FEA had a mean of 1.01 and coefficient of variation of 3.8%.
3. The failure of columns with local deterioration observed in full-scale tests can be very sudden, especially if there is symmetric section loss on both flanges. The specimen with section loss on one flange experienced a post initial-buckling peak



- because stresses were able to redistribute to the undeteriorated flange, resulting in a less brittle failure.
4. The exact geometry of local buckles is difficult to predict using FEA but this does not significantly affect overall axial capacity.
  5. The axial capacity of columns with local deterioration is very sensitive to flange loss  $(1-t^*/t_o)$ , particularly for stocky and intermediate columns. Slender columns tend to be dominated by Euler buckling except when the flange section loss becomes particularly severe.
  6. For very stocky columns with local deterioration ( $kL/r < 15$ ), the difference between the theoretical crushing capacity of the deteriorated cross section and the failure load does not deviate significantly until the width-to-thickness ratio of the deteriorated flange exceeds  $380/\sqrt{F_y}$ . This implies that while local buckling deformation may occur, the axial capacity may not be significantly reduced until  $b/2t^* > 380\sqrt{F_y}$ .
  7. The axial capacity of columns with deteriorated flanges is also sensitive the length of deterioration,  $L^*$ , particularly if the length of deterioration approaches the length of the member.
  8. The worst location for deterioration is at the midheight of the column, but the axial capacity is not greatly increased as the deteriorated section is moved away from this location. Cross-section aspect ratio, initial out-of-straightness and ratio of the flange area to web area  $A_f/A_w$  do not significantly affect the axial capacity of columns with deteriorated flanges.

9. Columns with symmetric deterioration on both flanges are weaker than columns with the same flange loss on one flange only. The torsional rotations and large lateral deformations at failure of columns with non-symmetric deterioration on one flange only make the associated strength calculations less accurate. Therefore, it is recommended symmetric deterioration be conservatively assumed for all cases.
10. The proposed simplified assessment method provides evaluators with a means to quickly assess the reduced capacity of columns with deteriorated flanges that are prone to local buckling. It is accurate for W-shape columns with  $0 < kL/r < 160$  and is much less conservative than the methods given in CAN/CSA S16-09. For deteriorated columns with realistic maximum flange section loss of 25%, the mean ratio of the axial capacity of the deteriorated column computed using the proposed simplified method to that predicted by FEA is 0.98, with a coefficient of variation of 3.6%. The mean ratio of the axial capacity of the deteriorated column computed using the methods in CAN/CSA S16/09 to that predicted by FEA was only 0.77, with a coefficient of variation of 7.1%.

### 6.3 RECOMMENDATIONS FOR FUTURE WORK

Recommendations for future work are as follows:

1. The implications of web deterioration on local buckling should also be examined, even though it is less likely than flange deterioration.
2. Repair techniques for deteriorated bridge compression members with flanges that are prone to local buckling should be investigated.



3. The effect that changes in failure mode and ductility have on reliability should be further examined within the scope of guidance given in Clause 14 of the CHBDC (CSA 2006).
4. The applicability of conclusions obtained from the sensitivity analysis and the simplified assessment method should be examined for other typical rolled steel shapes and for built-up members.

## REFERENCES

- American Institute of Steel Construction (AISC) (1978). *Specification for the Design, Fabrication and Erection of Structural Steel for Buildings*, New York, NY: AISC.
- American Society of Civil Engineers (ASCE) (1971). *Plastic Design in Steel: A Guide and Commentary*, New York, NY: ASCE Manuals and Reports on Engineering Practice.
- American Society for Testing and Materials (ASTM) (2010). *ASTM A6/A6M-10 -- Standard Specification for General Requirements for Rolled Structural Steel Bars, Plates, Shapes, and Sheet Piling*. West Conshohocken, PA: ASTM International.
- American Society for Testing and Materials (ASTM) (2010a). *ASTM A370-10 -- Standard Test Methods and Definitions for Mechanical Testing of Steel Products*, West Conshohocken, PA: ASTM International.
- Bakht, B., Mufti, A. A., and Jaeger, L. G. (1996). *Bridge Superstructures: New Developments*, New York, NY: National Book Foundation.
- Bartlett, F.M. (2011). Private Communication. London, ON: The University of Western Ontario.
- Canadian Institute of Steel Construction (CISC) (2010). *Handbook of Steel Construction*, Willowdale, ON: Canadian Institute of Steel Construction.
- Canadian Standards Association (CSA) (2006). *CAN/CSA-S6-06 Canadian Highway Bridge Design Code (CHBDC)*, Mississauga, ON: CSA International.
- Canadian Standards Association (CSA) (2006a). *Commentary on CAN/CSA-S6-06, Canadian Highway Bridge Design Code*, Mississauga, ON: CSA International.
- Canadian Standards Association (CSA) (2009). *CAN/CSA-S16-09 Limit States Design of Steel Structures*, Mississauga, ON: CSA International.
- Dassault Systèmes. (2010). Solidworks Simulation Help Database, <<http://help.solidworks.com>>, accessed December 2009.
- Galambos, T.V. (1998). *Guide to Stability Design Criteria for Metal Structures*, New York, NY: John Wiley & Sons.
- Gardner, L. and Nethercot, D.A. (2004). "Experiments on stainless steel hollow sections - Part 2: Member behaviour of columns and beams", *Journal of Constructional Steel Research*, 60(9), 1319–1332.

- Jelinek, J. (2002). *Material Properties of New and Historical Bridge Steels*, London, ON: The University of Western Ontario.
- Kayser, J. R. and Nowak, A. S. (1989). "Capacity Loss Due to Corrosion in Steel-Girder Bridges", *Journal of Structural Engineering*, 115(6):1525-1537.
- Kennedy, D.J.L. and Gad Aly, M. (1980). "Limit States Design of Steel Structures: Performance Factors", *Canadian Journal of Civil Engineering*, 7:45-77.
- Kulak, G. (2006). *Limit States Design in Structural Steel*. Willowdale, ON: Canadian Institute of Steel Construction.
- Kulicki, J. M., Prucz, Z., Sorgenfrei, D. F., and Mertz, D. R. (1990). *NCHRP Report 333: Guidelines for Evaluating Corrosion Effects in Existing Steel Bridges*. Washington, DC: Transportation Research Board.
- van de Lindt, J. W. and Ahlborn, T. M. (2005). *Development of Steel Beam End Deterioration Guidelines*. Houghton, MI: Michigan Tech Transportation Institute Center for Structural Durability.
- van de Lindt, J. W. and Pei, S. (2006). "Buckling Reliability of Deteriorating Steel Beam Ends", *Electronic Journal of Structural Engineering*, 6:1-7.
- Logan, W. (2010). Private Communication. London, ON: The University of Western Ontario.
- Nakai, T., Matsushita, H., and Yamamoto, N. (2004). "Effect of Pitting Corrosion on Local Strength of Hold Frames of Bulk Carriers (2nd Report): Lateral-distortional buckling and local face buckling." *Marine Structures*, 17(8):612-641.
- Prucz, Z. and Kulicki, J. (1998). "Accounting for Effects of Corrosion Section Loss in Steel Bridges." *Transportation Research Record*, 1624(1):101-109.
- Shek, K. (2006). *Behaviour and Design of Strengthened Built-Up Hybrid Steel Columns*. London, ON: The University of Western Ontario.
- Tall, L. (1961). *Stub-Column Test Procedure*. Bethlehem, PA: Lehigh University.
- Tall, L. and Tebedge, N. (1970). *Procedure For Testing Centrally Loaded Columns*, Bethlehem, PA: Lehigh University.
- Timoshenko, S. and Gere, J. (1961). *Theory of Elastic Stability*. New York, NY: McGraw-Hill.





## **A1.1 INTRODUCTION**

This appendix presents the steel properties of the test columns used in the experimental validation presented in Chapter 3 that were determined from tensile coupon tests and stub column tests. Columns 1 and 4 were obtained from one original member and Columns 2 and 3 were obtained from a different original member. Thus, the strength properties only had to be determined once for each pair of columns. In general, the yield strength of the flanges and webs determined from the tensile coupon tests and the average cross-sectional yield strength determined from stub column tests were in good agreement.

## **A1.2 TENSILE COUPON DATA**

Figure A1-1, A1-2 and A1-3 show the tensile coupon test data for Columns 1 and 4 (Test Group A); 2 and 3 (Test Group B); and 5 (Test Group C), respectively. The tests were conducted in accordance with ASTM A370 (ASTM 2010). The coupons were loaded to failure at a constant load rate of approximately 175MPa/minute or a strain rate of approximately 15 $\mu\epsilon$ /sec.

For Test Group A (Columns 1 and 4), the flange and web yield strengths were nearly identical: the flange yield strength was calculated as 365MPa and the web yield strength was calculated as 364MPa.

For Test Group B (Columns 2 and 3), the flange yield strength was calculated as 368MPa and the web yield strength was calculated as 371MPa, a difference of only 0.8%.

For Test Group C (Column 5), the flange yield strength was calculated as 380MPa and the web yield strength was calculated as 394MPa, a difference of 3.6%.

### A1.3 STUB COLUMN TEST DATA

The stub column tests were conducted in accordance with the procedure recommended by Tall (1961) at McMaster University. The main objective of the stub column tests was to determine the maximum magnitude of the residual stresses in the cross section,  $\sigma_r$ , but the average yield strength of the full cross section was also obtained.

#### Columns 1 and 4 (Stub Column Test A):

Figure A1-4 shows the stress-strain response for Stub Column A. There results were favorable, and the slope of the elastic stress-strain curve is approximately equal to  $1/E$ . The maximum magnitude of the compressive residual stress,  $\sigma_r$ , was calculated as the difference between the average cross-sectional yield strength and the stress at which the slope of the stress-strain curve started to deviate from  $1/E$ :

$$\sigma_r = F_y - 330MPa = 40MPa, \text{ or } 0.11F_y.$$

#### Columns 2 and 3 (Stub Column Test B):

Figure A1-5 shows the stress-strain response for Stub Column B. The slope of stress-strain curve changed after the initial seating load was exceeded because there was a small hole in one of the bearing plates that went unnoticed. After the initial seating load had been overcome, the slope of the stress-strain curve was greater than  $1/E$ . It was assumed that deviation from linearity was indicated the presence of residual compressive stresses.

The maximum magnitude of the compressive residual stress,  $\sigma_r$ , was calculated as the difference between the average cross-sectional yield strength and the stress at which the

slope of the stress-strain curve started to deviate from linearity:

$$\sigma_r = F_y - 339 \text{ MPa} = 33 \text{ MPa}, \text{ or } 0.089F_y.$$

Column 5 (Stub Column Test C):

Figure A1-6 shows the stress-strain response for Stub Column C. Similar to Stub Column B, a small hole in the bearing plate caused the stress-strain curve to change slopes in the elastic region. The maximum magnitude of the compressive residual stress,  $\sigma_r$ , was calculated as the difference between the average cross-sectional yield strength and the stress at which the slope of the stress-strain curve started to deviate from linearity:

$$\sigma_r = F_y - 353 \text{ MPa} = 25 \text{ MPa}, \text{ or } 0.066F_y.$$

Figure A1-6. Typical Stress-Strain Data for Column 5 (Load 4)

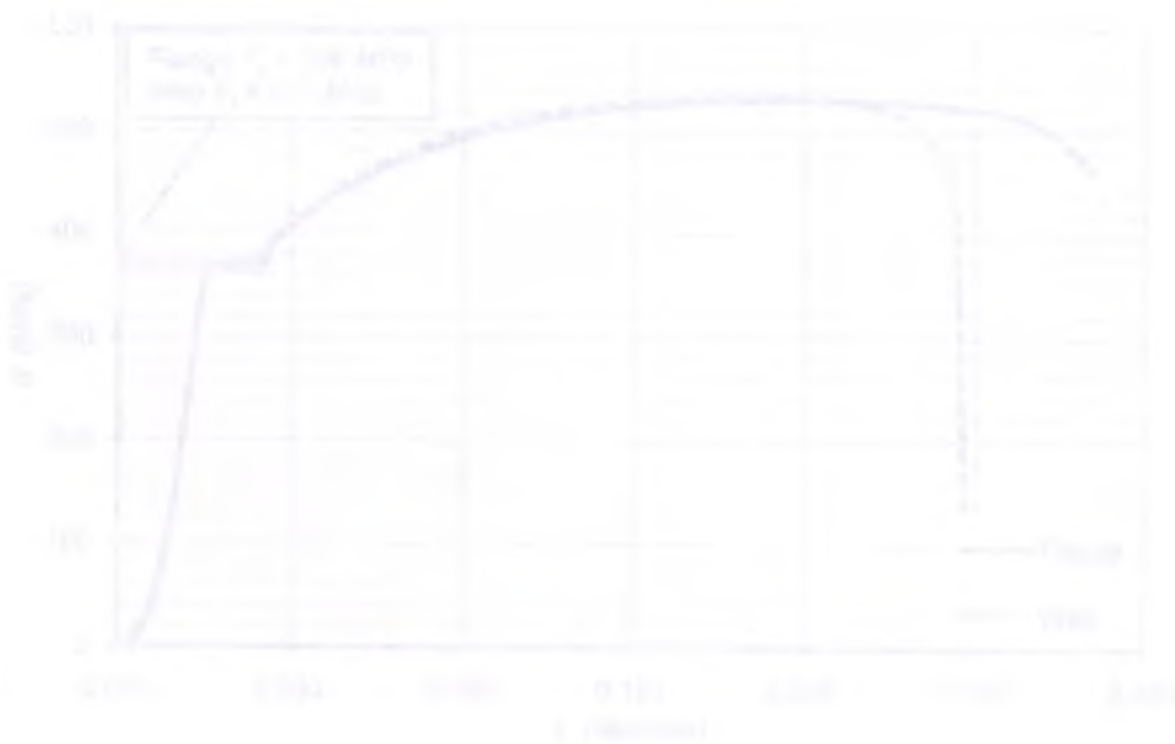


Figure A1-7. Typical Stress-Strain Data for Column 5 (Load 4)



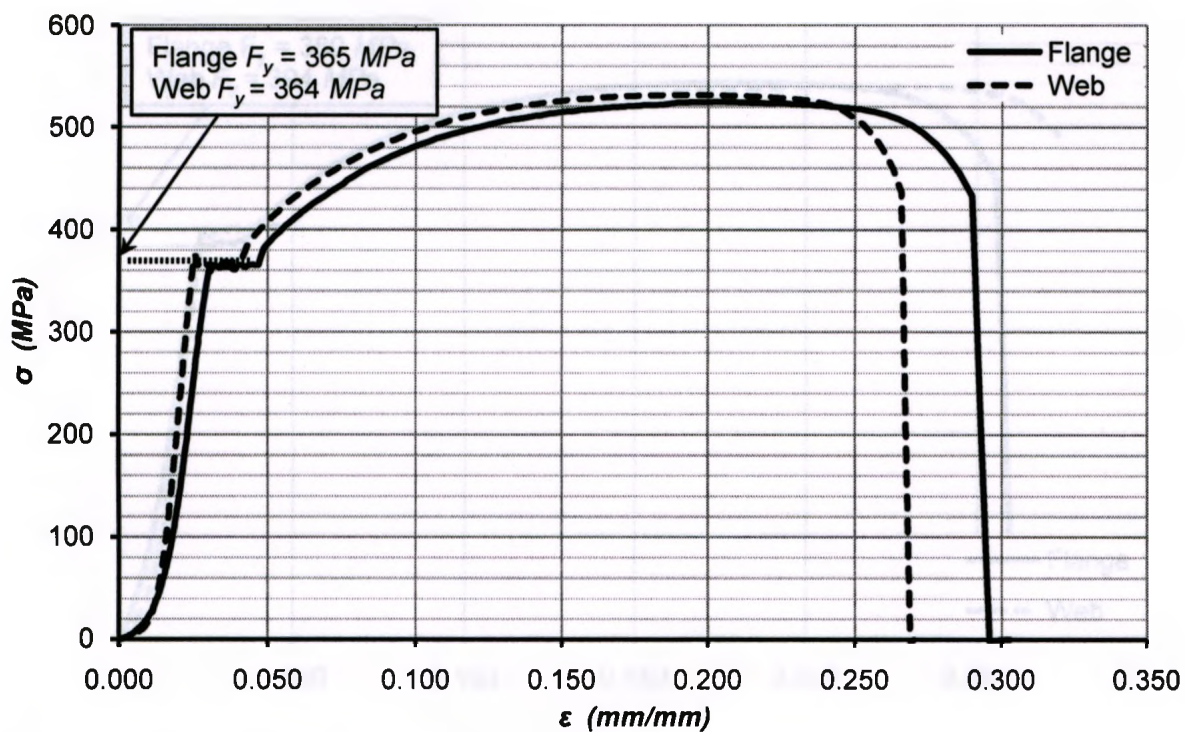


Figure A1-1: Tensile Coupon Test A for Columns 1 and 4

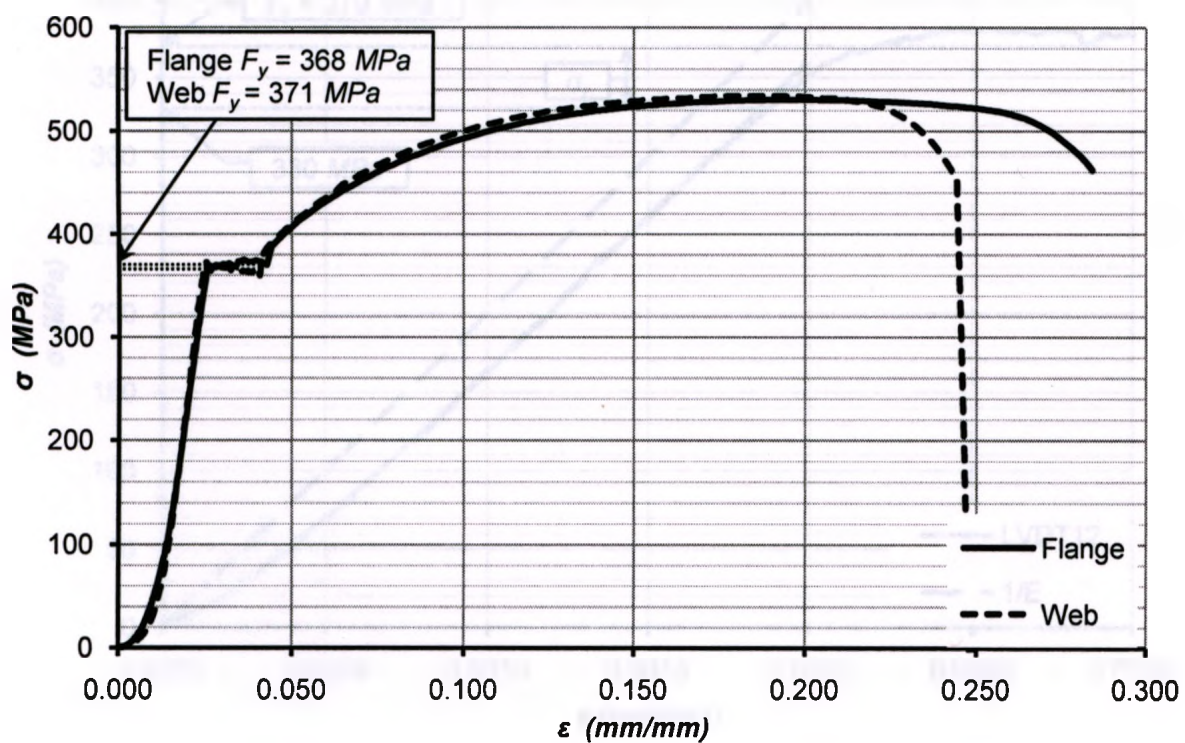


Figure A1-2: Tensile Coupon Test B for Columns 1 and 4



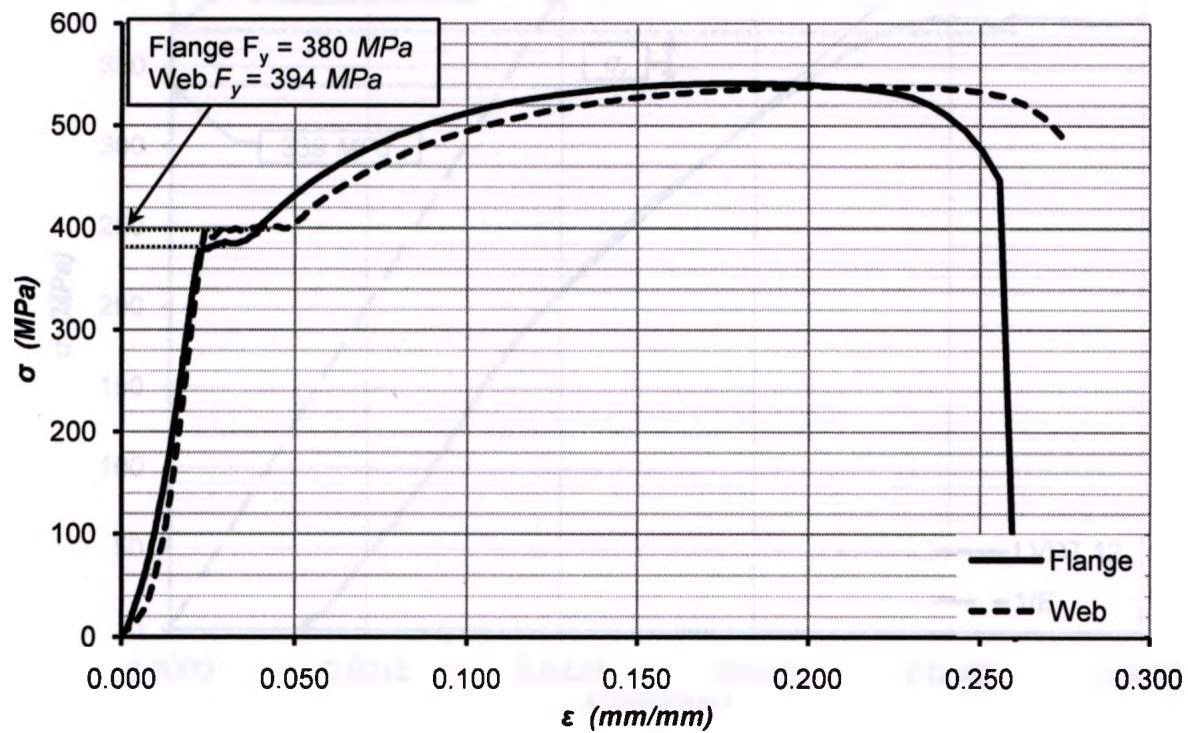


Figure A1-3: Tensile Coupon Test C for Column 5

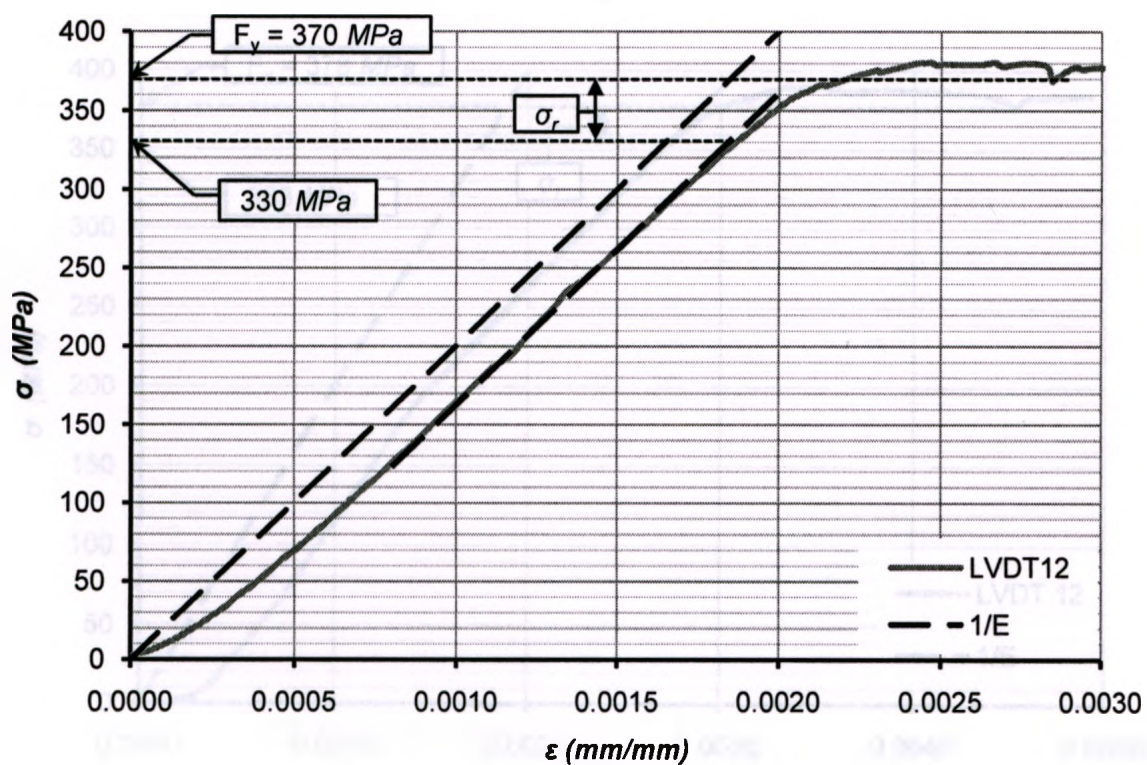


Figure A1-4: Stub Column Test A for Columns 1 and 4



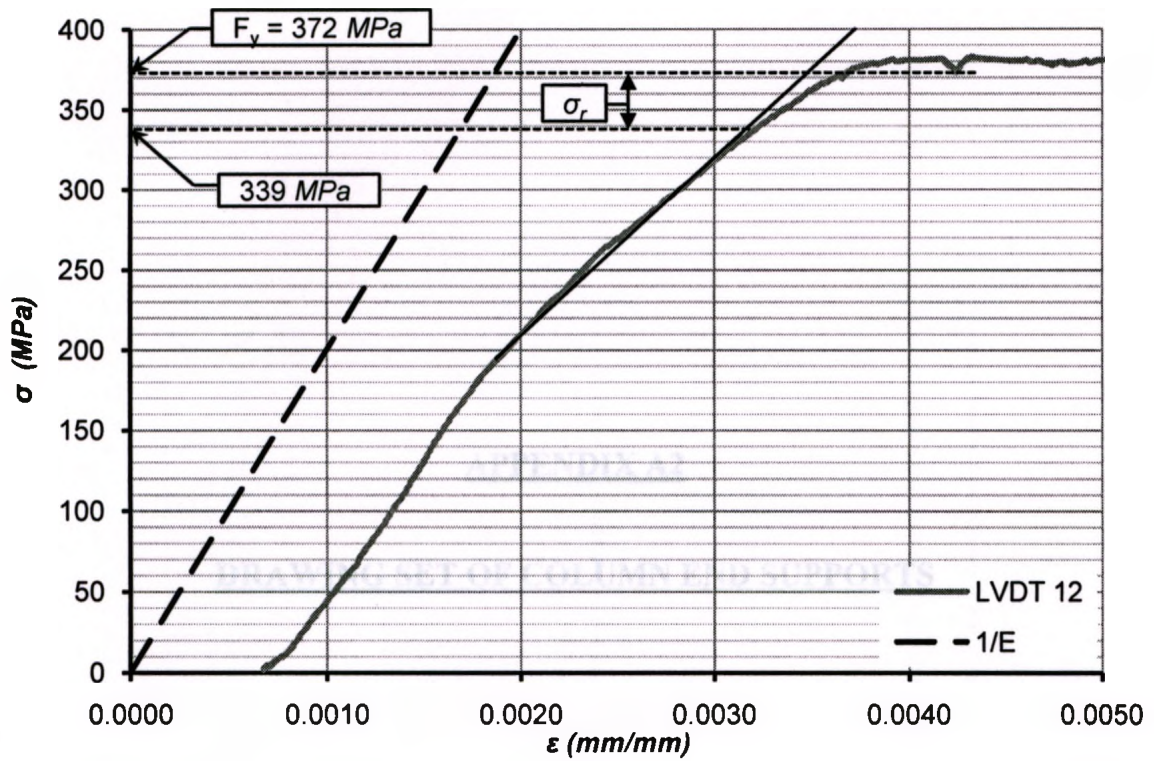


Figure A1-5: Stub Column Test B for Columns 2 and 3

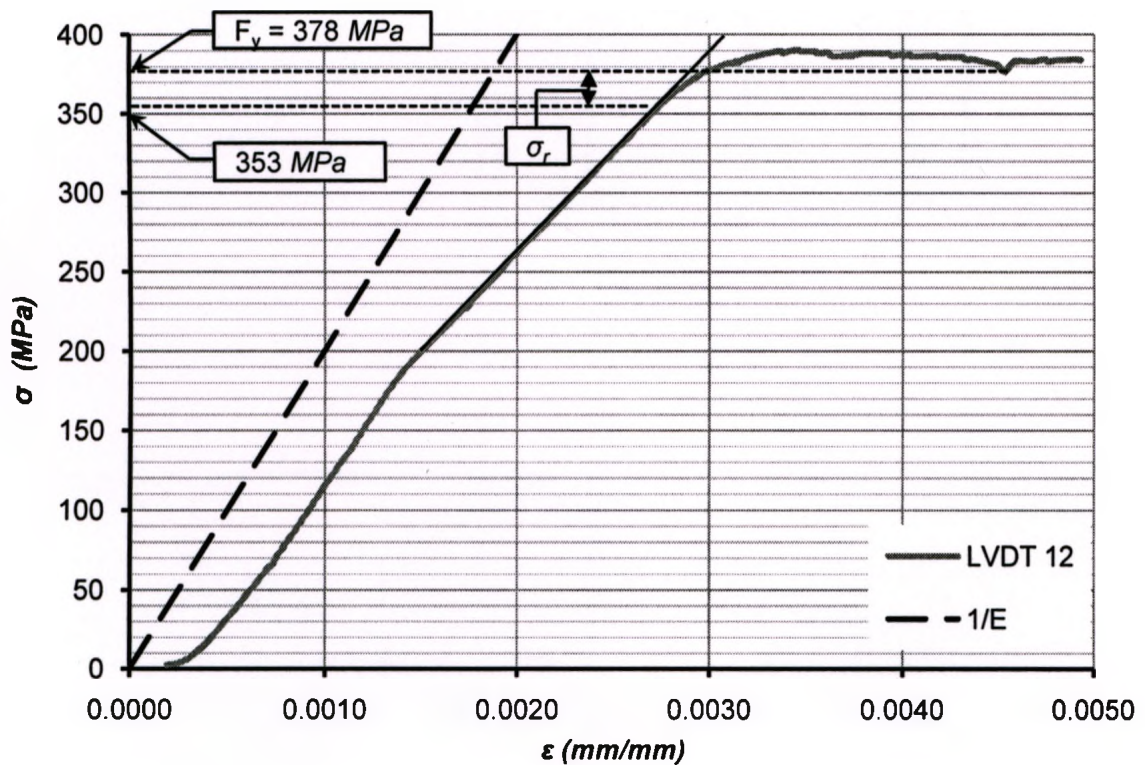
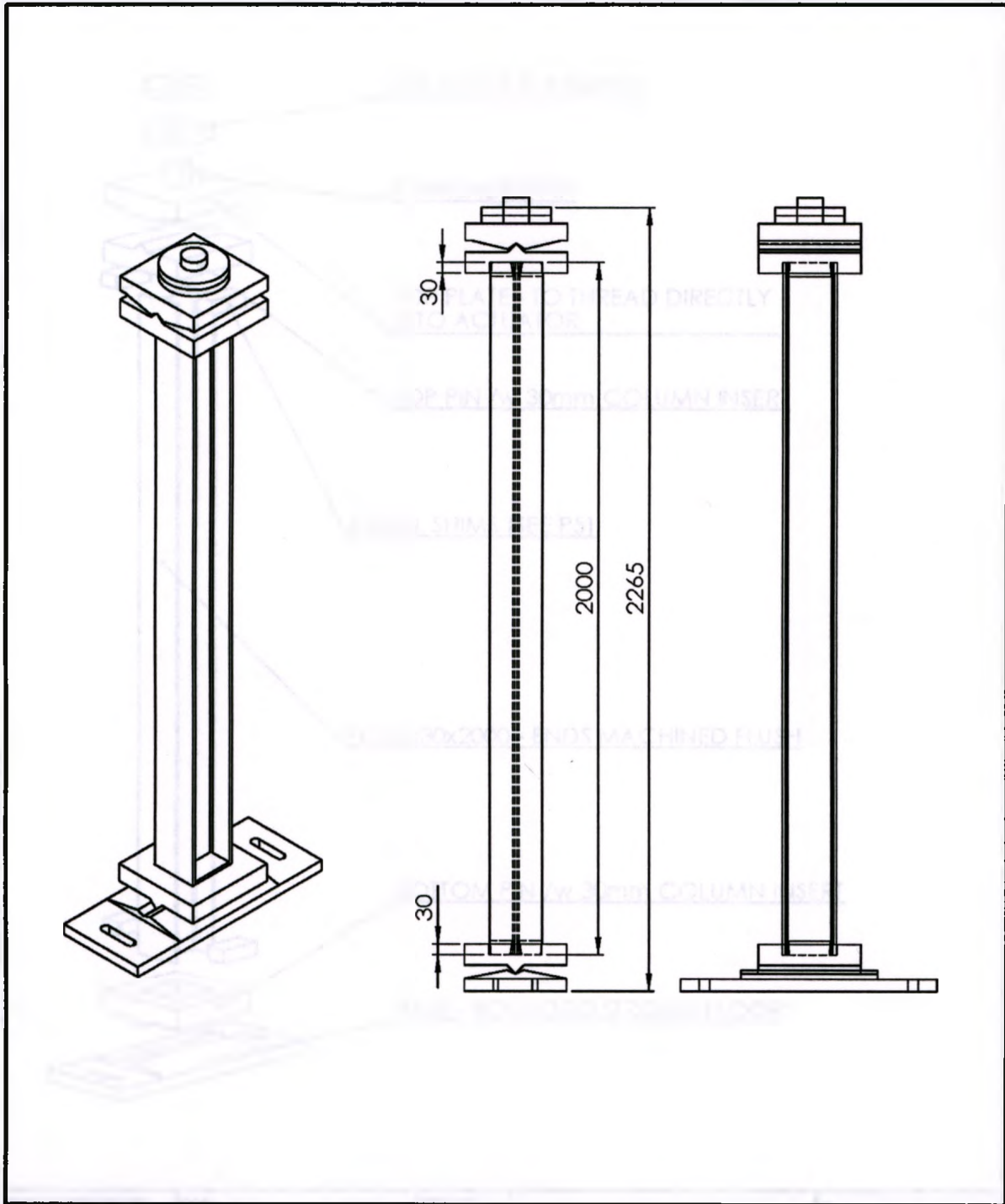


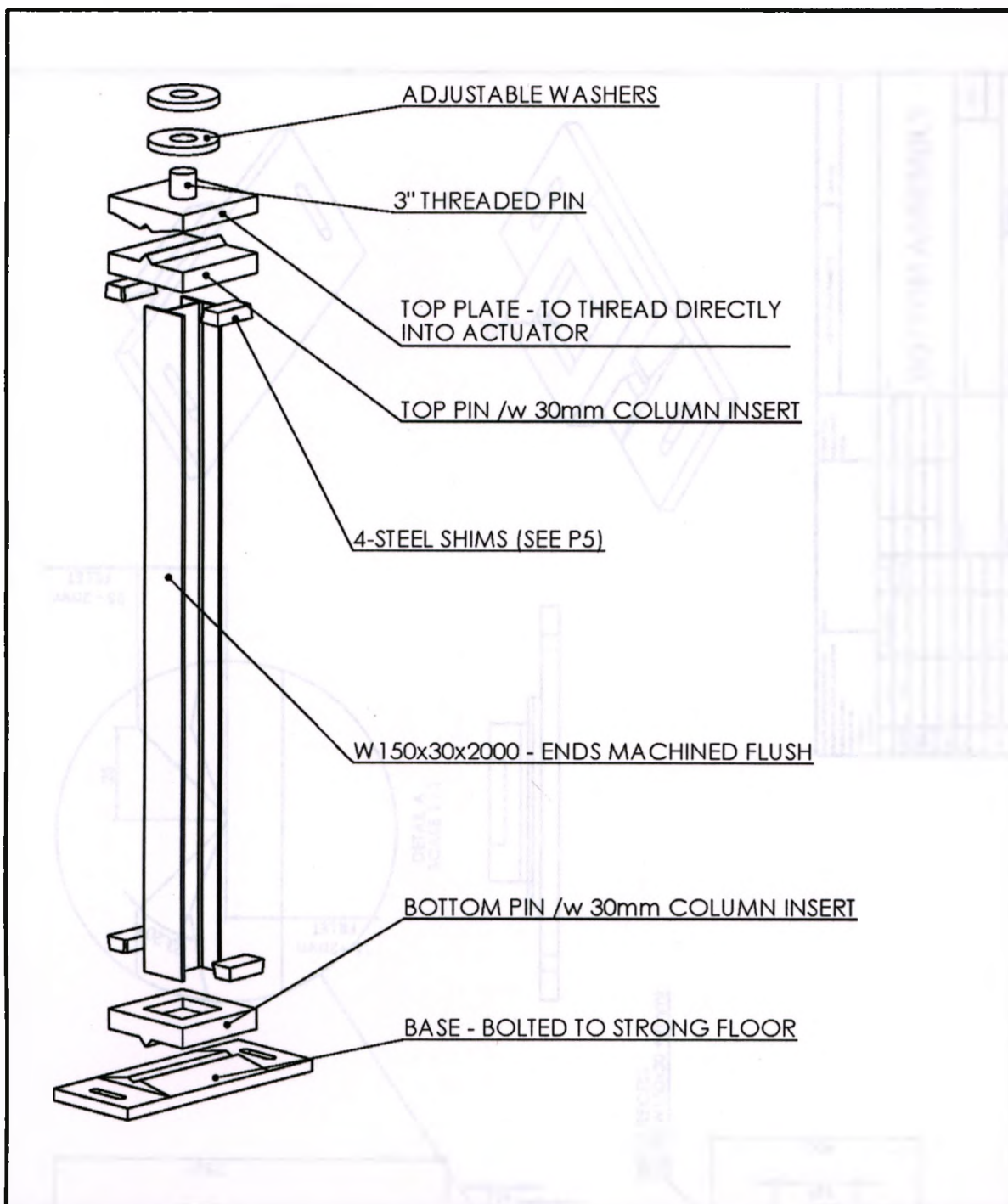
Figure A1-6: Stub Column Test C for Columns 5





UNLESS OTHERWISE SPECIFIED: DIMENSIONS ARE IN MILLIMETERS SURFACE FINISH: TOLERANCES: LINEAR: ANGULAR:		FINISH:		DEBUR AND BREAK SHARP EDGES		1:15		REVISION	
NAME	SIGNATURE	DATE				FILE:			
DRAWN	ARE	6/10/10				<b>GENERAL ARRANGEMENT</b>			
CHK'D									
APP'VD									
MFG									
Q.A.					MATERIAL:	DWG NO.		A4	
					WEIGHT:	SCALE: 1:1		SHEET 1 OF 4	



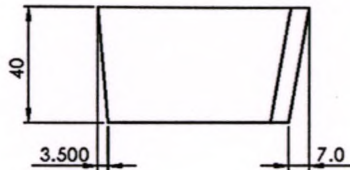


UNLESS OTHERWISE SPECIFIED: DIMENSIONS ARE IN MILLIMETERS SURFACE FINISH: TOLERANCES: LINEAR: ANGULAR:			FINISH:		DEBUR AND BREAK SHARP EDGES		DO NOT SCALE DRAWING		REVISION		
DRAWN: ARK			SIGNATURE		DATE: 6/10/10		TITLE: <b>EXPLODED VIEW OF ASSEMBLY</b>				
CHK'D:											
APP'VD:											
MFG:											
QA:											
					MATERIAL:		DWG NO.				
					WEIGHT:		SCALE: 1:1				
							SHEET 2 OF 5				
							A4				

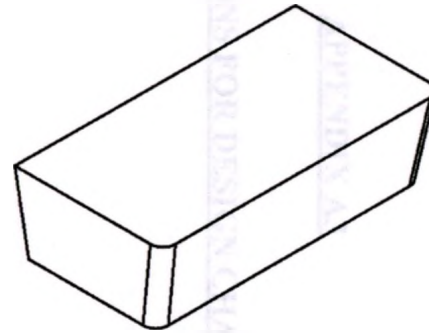
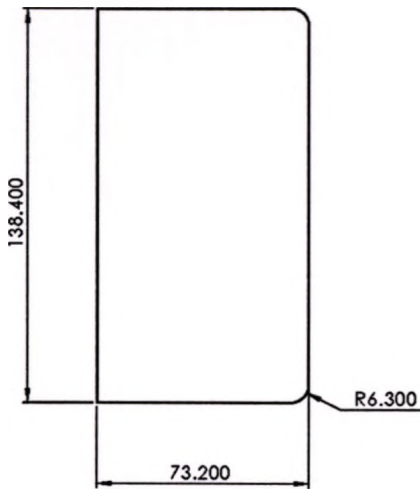








NOTE: STEEL SHIMS WERE OMITTED IN FINAL DESIGN AND REPLACED WITH A SET-SCREW CLAMP SYSTEM.



DIMENSIONS SPECIFIED DIMENSIONS ARE IN MILLIMETERS UNLESS OTHERWISE SPECIFIED DIMENSIONS LINEAR ANGULAR				SHEET NO.		DO NOT SCALE DRAWING		REVISION	
NAME DATE				SIGNATURE		FILE			
DRAWN DATE				CHECKED DATE		SHIM DETAIL			
DESIGNED DATE				APPROVED DATE		DWG NO.			
D.W.				APPROVED		A3			
WEIGHT				SCALE 1:1		SHEET 1 OF 1			



## APPENDIX A3

The design charts for the design of a beam-column joint are presented in Chapter 12. The design charts are based on the design of a beam-column joint with a rectangular cross-section and a square column. The design charts are based on the design of a beam-column joint with a rectangular cross-section and a square column.

The design charts for the design of a beam-column joint are presented in Chapter 12. The design charts are based on the design of a beam-column joint with a rectangular cross-section and a square column. The design charts are based on the design of a beam-column joint with a rectangular cross-section and a square column.

### APPENDIX A3

### EQUATIONS FOR DESIGN CHARTS

### A3.1 INTRODUCTION

This appendix presents the equations that define the curves in the design charts, presented in Chapter 5. The curves are 4th order polynomials fitted to data obtained in the sensitivity analysis, presented in Chapter 4.

The curve equations for the factor  $\Psi$  are presented in Table A3-1 and the curve equations for the factor  $\Omega$  are presented in Table A3-2.

Table A3-1: Design Curve Equations for  $\Psi$ 

Width-to-Thickness Ratio	Equation
$\frac{b}{2t^*} = \frac{205}{\sqrt{F_y}}$	$\Psi = 2.57 \times 10^{-9} (kL/r)^4 - 8.72 \times 10^{-7} (kL/r)^3 + 8.37 \times 10^{-5} (kL/r)^2 - 4.75 \times 10^{-4} (kL/r) + 0.80$
$\frac{b}{2t^*} = \frac{246}{\sqrt{F_y}}$	$\Psi = 2.54 \times 10^{-9} (kL/r)^4 - 8.94 \times 10^{-7} (kL/r)^3 + 9.05 \times 10^{-5} (kL/r)^2 - 5.50 \times 10^{-4} (kL/r) + 0.70$
$\frac{b}{2t^*} = \frac{308}{\sqrt{F_y}}$	$\Psi = 1.55 \times 10^{-9} (kL/r)^4 - 6.00 \times 10^{-7} (kL/r)^3 + 6.90 \times 10^{-5} (kL/r)^2 - 4.38 \times 10^{-4} (kL/r) + 0.61$
$\frac{b}{2t^*} = \frac{410}{\sqrt{F_y}}$	$\Psi = -8.19 \times 10^{-11} (kL/r)^4 - 1.17 \times 10^{-7} (kL/r)^3 + 3.50 \times 10^{-5} (kL/r)^2 - 4.05 \times 10^{-4} (kL/r) + 0.49$

Table A3-2: Design Curve Equations for  $\Omega$ 

Length to Width Ratio	Equation
$\frac{L^*}{b} = 1.3$	$\Omega = 1.0$
	For $kL/r \leq 15$ :
	$\Omega = 1.0$
$\frac{L^*}{b} = 2.6$	For $kL/r > 15$ :
	$\Omega = -2.35 \times 10^{-9} (kL/r)^4 + 7.67 \times 10^{-7} (kL/r)^3 - 6.99 \times 10^{-5} (kL/r)^2 + 7.93 \times 10^{-4} (kL/r) + 1.00$
	For $kL/r \leq 15$ :
	$\Omega = 1.0$
$L^* = L$	For $kL/r > 15$ :
	$\Omega = -3.35 \times 10^{-9} (kL/r)^4 + 1.21 \times 10^{-6} (kL/r)^3 - 1.28 \times 10^{-5} (kL/r)^2 + 4.97 \times 10^{-4} (kL/r) + 1.02$



## INTRODUCTION

The present study is concerned with the problem of the stability of a thin layer of liquid on a solid surface. The problem is of great importance in many practical situations, such as the coating of a surface by a liquid, the spreading of a liquid on a solid, and the flow of a liquid on a solid. The problem is also of interest in the theory of thin films and in the theory of capillarity.

## APPENDIX A4

### DERIVATION OF THE CRITICAL LENGTH

Let us consider a thin layer of liquid of thickness  $h$  on a solid surface.

$$h \ll \lambda$$

$$h \ll \frac{1}{k}$$

$$h \ll \frac{1}{\sqrt{k}}$$

Let us assume that the liquid is in equilibrium with the solid surface.

$$h = \frac{1}{\sqrt{k}}$$

$$h = \frac{1}{\sqrt{k}} \frac{\sqrt{R}}{\sqrt{R}}$$

Let us assume that the liquid is in equilibrium with the solid surface.

Let us assume that the liquid is in equilibrium with the solid surface.

Let us assume that the liquid is in equilibrium with the solid surface.

#### A4.1 INTRODUCTION

This chapter presents the derivation of the critical length at which both the reduced yield strength method and the reduced flange width method (CSA 2009) give the same axial capacity for Class 4 columns. Eqs. [5.8] and [5.12] were first derived by Bartlett (2011). Figure A4.1 idealizes the cross-sectional dimensions of a W-shape in compression. In this method the web is assumed to extend into the top and bottom flange by  $t/2$  and thus the area of steel is overestimated by  $t \times w$ . However, this simplification is offset by the fillet radius where the flanges and web intersect is not being accounted for in the cross-sectional area.

Given these assumptions, the following variables can be derived:

$$\alpha = b/2t = b'/t$$

$$\beta = (d - 2t)w/t^2 = h'w/t^2$$

$$\gamma = 200/\sqrt{F_y}$$

The axial capacity of a steel column is computed by CAN/CSA S16-09 (CSA 2009) as:

$$C = AF_y (1 + \lambda^{2n})^{1/n}$$

$$\text{where: } \lambda = \frac{kL}{r} \sqrt{\frac{F_y}{\pi^2 E}}$$

S16-09 gives two methods for calculating the axial capacity of Class 4 columns. The reduced yield strength method,  $[C_{S16}]_1$ , is a function of  $(F_y)_{eq}$  and the reduced flange width method,  $[C_{S16}]_2$ , is a function of  $b_{eq}$  or  $b'_{eq}$ :

$$(F_y)_{eq} = \left( \frac{400}{b/t} \right)^2$$

and

$$b_{eq} = \frac{400t}{\sqrt{F_y}}$$

and

$$b'_{eq} = \frac{200t}{\sqrt{F_y}}$$

To simplify calculations,  $b'_{eq}$  will be used throughout this derivation.

#### **A4.2 CROSS SECTIONAL PROPERTIES**

The cross section properties of for each method can be calculated as follows:

$[C_{S16}]_1$

Cross-sectional area:

$$\begin{aligned} A &= 2(2b't) + h'w \\ &= 4\alpha t^2 + \beta t^2 \\ &= (4\alpha + \beta)t^2 \end{aligned}$$

Second moment of area and radius of

gyration about the weak axis:

$$\begin{aligned} I_y &= 2 \left[ \frac{(2b'^3 t)}{12} \right] \\ &= 16\alpha^3 t^4 / 12 \\ &= 4\alpha^3 t^4 / 3 \end{aligned}$$

$[C_{S16}]_2$

Cross-sectional area:

$$\begin{aligned} A &= 2(2b'_{eq} t) + h'w \\ &= 4\gamma t^2 + \beta t^2 \\ &= (4\gamma + \beta)t^2 \end{aligned}$$

Second moment of area and radius of

gyration about the weak axis:

$$\begin{aligned} I_y &= 2 \left[ \frac{(2b'_{eq}{}^3 t)}{12} \right] \\ &= 16\gamma^3 t^4 / 12 \\ &= 4\gamma^3 t^4 / 3 \end{aligned}$$

$$\begin{aligned}
 r_x &= \sqrt{\frac{I_x}{A}} \\
 &= \sqrt{\frac{4\alpha^3 t^4}{3(4\alpha + \beta)t^2}} \\
 &= t \sqrt{\frac{4\alpha^3}{3(4\alpha + \beta)}}
 \end{aligned}$$

Second moment of area and radius of gyration about the strong axis:

$$\begin{aligned}
 I_x &= [2b't(h'/2)^2]2 + h^3 w/12 \\
 &= \alpha t^2 h^2 + \beta t^2 h^2 /12 \\
 &= (\alpha + \beta/12)t^2 h^2
 \end{aligned}$$

$$\begin{aligned}
 r_x &= \sqrt{\frac{I_x}{A}} \\
 &= \sqrt{\frac{(\alpha + \beta/12)t^2 h^2}{(4\alpha + \beta)t^2}} \\
 &= h' \sqrt{\frac{(\alpha + \beta/12)}{(4\alpha + \beta)}}
 \end{aligned}$$

### A4.3 WEAK-AXIS CRITICAL LENGTH

For the **reduced yield strength method**, the slenderness parameter is calculated as:

$$\lambda_y = \frac{kL_y}{r_y} \sqrt{\frac{F_y}{\pi^2 E}}$$

if  $k = 1.0$ :

$$\begin{aligned}
 r_x &= \sqrt{\frac{I_x}{A}} \\
 &= \sqrt{\frac{4\gamma^3 t^4}{3(4\gamma + \beta)t^2}} \\
 &= t \sqrt{\frac{4\gamma^3}{3(4\gamma + \beta)}}
 \end{aligned}$$

Second moment of area and radius of gyration about the strong axis:

$$\begin{aligned}
 I_x &= 4b'_{eq} t (h'/2)^2 + h^3 w/12 \\
 &= \gamma t^2 h^2 + \beta t^2 h^2 /12 \\
 &= (\gamma + \beta/12)t^2 h^2
 \end{aligned}$$

$$\begin{aligned}
 r_x &= \sqrt{\frac{I_x}{A}} \\
 &= \sqrt{\frac{(\gamma + \beta/12)t^2 h^2}{(4\gamma + \beta)t^2}} \\
 &= h' \sqrt{\frac{(\gamma + \beta/12)}{(4\gamma + \beta)}}
 \end{aligned}$$



$$\begin{aligned}\lambda_y &= \frac{L_y}{t} \sqrt{\frac{3(4\alpha + \beta)}{4\alpha^3}} \sqrt{\frac{(F_y)_{eq}}{\pi^2 E}} \\ &= \frac{L_y}{t} \sqrt{\frac{3(4\alpha + \beta)}{4\alpha^3}} \left( \frac{200}{\pi\alpha\sqrt{E}} \right) \\ &= \frac{L_y}{t} \sqrt{\frac{3(200)^2(4\alpha + \beta)}{4\pi^2\alpha^5 E}}\end{aligned}$$

Axial capacity for the **reduced yield strength method**, Eq. [1.3], is calculated as:

$$\begin{aligned}[C_{S16}]_1 &= AF_y (1 + \lambda_y^{2n})^{-1/n} \\ [A4.1] \quad [C_{S16}]_1 &= (4\alpha + \beta)t^2 \left( \frac{200}{\alpha} \right)^2 \left\{ 1 + \left[ \frac{L}{t} \sqrt{\frac{3(200^2)(4\alpha + \beta)}{4\pi^2\alpha^5 E}} \right]^{2n} \right\}^{-1/n}\end{aligned}$$

For the **reduced flange width method**, Eq. [1.4], the slenderness parameter is calculated as:

$$\lambda_y = \frac{kL_y}{r_y} \sqrt{\frac{F_y}{\pi^2 E}}$$

if  $k = 1.0$ :

$$\begin{aligned}\lambda_y &= \frac{L_y}{t} \sqrt{\frac{3(4\gamma + \beta)}{4\gamma^3}} \sqrt{\frac{F_y}{\pi^2 E}} \\ &= \frac{L_y}{t} \sqrt{\frac{3F_y(4\gamma + \beta)}{4\pi^2\gamma^3 E}}\end{aligned}$$

Axial capacity for the **reduced flange width method** is calculated as:

$$[C_{S16}]_2 = AF_y (1 + \lambda_y^{2n})^{-1/n}$$

$$[A4.2] \quad [C_{S16}]_2 = (4\gamma + \beta)t^2 F_y \left\{ 1 + \left[ \frac{L}{t} \sqrt{\frac{3F_y(4\gamma + \beta)}{4\pi^2\gamma^3 E}} \right]^{2n} \right\}^{-1/n}$$

Equating Eqs [A4.1] and [A4.2] to solve for  $L$ :

$$\begin{aligned} (4\alpha + \beta)t^2 \left( \frac{200}{\alpha} \right)^2 \left\{ 1 + \left[ \frac{L}{t} \sqrt{\frac{3(200^2)(4\alpha + \beta)}{4\pi^2\alpha^5 E}} \right]^{2n} \right\}^{-1/n} \\ = (4\gamma + \beta)t^2 F_y \left\{ 1 + \left[ \frac{L}{t} \sqrt{\frac{3F_y(4\gamma + \beta)}{4\pi^2\gamma^3 E}} \right]^{2n} \right\}^{-1/n} \end{aligned}$$

Dividing both sides by  $F_y$  and simplifying:

$$\left[ \frac{\alpha^2}{\gamma^2(4\alpha + \beta)} \right]^n + \left( \frac{1}{\gamma^2} \right)^n \left[ \frac{3(200^2)}{4\pi^2\alpha^3 E} \right]^n \left( \frac{L}{t} \right)^{2n} = \left[ \frac{1}{4\gamma + \beta} \right]^n + \left[ \frac{3F_y}{4\pi^2\gamma^3 E} \right]^n \left( \frac{L}{t} \right)^{2n}$$

Multiplying both sides by  $F_y$  and rearranging to solve for  $L_c/t$ :

$$[5.8] \quad \frac{L_c}{t} = 2\pi \sqrt{\frac{E}{3F_y}} \left[ \frac{\left( \frac{\alpha^2}{4\alpha + \beta} \right)^n - \left( \frac{\gamma^2}{4\gamma + \beta} \right)^n}{\left( \frac{1}{\gamma} \right)^n - \left( \frac{\gamma^2}{\alpha^3} \right)^n} \right]^{\frac{1}{2n}}$$

#### A4.4 STRONG-AXIS CRITICAL LENGTH

For the **reduced yield strength method**, Eq. [1.3] the slenderness parameter is calculated

as:

$$\lambda_x = \frac{kL_x}{r_x} \sqrt{\frac{F_y}{\pi^2 E}}$$

if  $k = 1.0$ :

$$\begin{aligned}\lambda_x &= \frac{L_x}{h'} \frac{200}{\pi \alpha \sqrt{E}} \sqrt{\frac{4\alpha + \beta}{\alpha + \beta/12}} \\ &= \frac{L_x}{h'} \sqrt{\frac{(4\alpha + \beta) 200^2}{(\alpha + \beta/12) \pi^2 \alpha^2 E}} \\ &= \frac{L_x}{h'} \sqrt{\frac{(4\alpha + \beta) \gamma^2 F_y}{(\alpha + \beta/12) \pi^2 \alpha^2 E}}\end{aligned}$$

Axial capacity for the **reduced yield strength method**, Eq. [1.3], is calculated as:

$$\begin{aligned}[C_{S16}]_1 &= AF_y (1 + \lambda_x^{2n})^{-1/n} \\ [A4.3] \quad [C_{S16}]_1 &= (4\alpha + \beta) t^2 \frac{\gamma^2}{\alpha^2} F_y \left\{ 1 + \left[ \frac{L}{h'} \sqrt{\frac{(4\alpha + \beta) \gamma^2 F_y}{(\alpha + \beta/12) \pi^2 \alpha^2 E}} \right]^{2n} \right\}^{-1/n}\end{aligned}$$

For the **reduced flange width method**, Eq. [1.4], the slenderness parameter is calculated

as:

$$\lambda_x = \frac{kL_x}{r_x} \sqrt{\frac{F_y}{\pi^2 E}}$$

if  $k = 1.0$ :

$$\begin{aligned}\lambda_x &= \frac{L_x}{h'} \sqrt{\frac{4\gamma + \beta}{\gamma + \beta/12}} \sqrt{\frac{F_y}{\pi^2 E}} \\ &= \frac{L_x}{h'} \sqrt{\frac{(4\gamma + \beta) F_y}{(\gamma + \beta/12) \pi^2 E}}\end{aligned}$$

Axial capacity for the **reduced flange width method**, Eq. [1.4], is calculated as:

$$[C_{S16}]_2 = AF_y (1 + \lambda_y^{2n})^{-\frac{1}{n}}$$

$$[A4.4] \quad [C_{S16}]_2 = (4\gamma + \beta)t^2 F_y \left\{ 1 + \left[ \frac{L}{h'} \sqrt{\frac{(4\gamma + \beta)F_y}{(\gamma + \beta/12)\pi^2 E}} \right]^{2n} \right\}^{-\frac{1}{n}}$$

Equating Eqs [A4.3] and [A4.4] to solve for  $L$ :

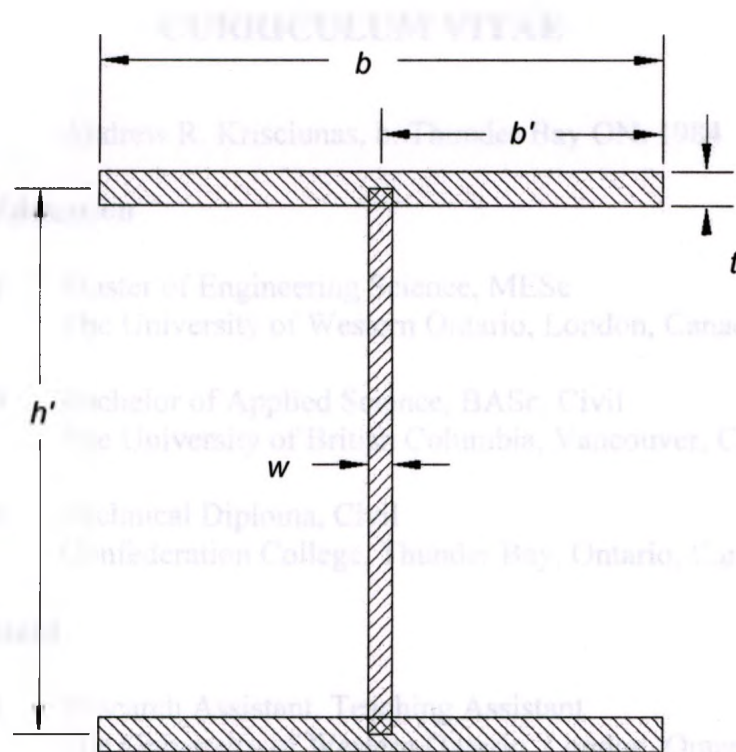
$$(4\alpha + \beta)t^2 \frac{\gamma^2}{\alpha^2} F_y \left\{ 1 + \left[ \frac{L}{h'} \sqrt{\frac{(4\alpha + \beta)\gamma^2 F_y}{(\alpha + \beta/12)\pi^2 \alpha^2 E}} \right]^{2n} \right\}^{-\frac{1}{n}}$$

$$= (4\gamma + \beta)t^2 F_y \left\{ 1 + \left[ \frac{L}{h'} \sqrt{\frac{(4\gamma + \beta)F_y}{(\gamma + \beta/12)\pi^2 E}} \right]^{2n} \right\}^{-\frac{1}{n}}$$

Simplifying and rearranging to solve for  $L_c / h'$ :

$$[5.12] \quad \frac{L_c}{h'} = \frac{\pi}{\gamma} \sqrt{\frac{E}{F_y}} \left[ \frac{\left( \frac{\alpha^2}{4\alpha + \beta} \right)^n - \left( \frac{\gamma^2}{4\gamma + \beta} \right)^n}{\left( \frac{1}{\gamma + \beta/12} \right)^n - \left( \frac{1}{\alpha + \beta/12} \right)^n} \right]^{\frac{1}{2n}}$$





**Figure A4.1: Idealized Cross-Sectional Dimensions for a W-Shape**